ABSTRACT

Title of Thesis:	INVESTIGATION OF THE EFFECT OF FLUCTUATING/DECREASING HEATING LOADS ON TEMPERATURE SENSITIVE PAINT MEASUREMENTS IN AEDC TUNNEL 9
	John David Juliano, Master of Science in Aerospace Engineering, 2018
Thesis Directed By:	Professor Ken Yu, A. James Clark School of Engineering, Aerospace Engineering Department.

An investigation was done on the effect of fluctuating or rapidly decreasing heating loads on the response of temperature sensitive paint (TSP). An experiment was designed and carried out in the University of Maryland Advanced Propulsion Research Laboratory's Vitiated Heater with sudden changes in heat flux over time. The results of the experiment showed that the accuracy of the discrete instrumentation under a thin layer of TSP is dependent on the thickness of the paint layer and magnitude of the heating load. It also showed that the accuracy of a TSP measurement with a sudden change in heat flux decreases as the paint thickness or heating magnitude increases when the current data reduction methodology is applied. Finally, a novel dual-calibration data reduction method was utilized to improve the calculated heat transfer accuracy for an experiment with a sudden change in heat flux.

INVESTIGATION OF THE EFFECT OF FLUCTUATING/DECREASING HEATING LOADS ON TEMPERATURE SENSITIVE PAINT MEASUREMENTS IN AEDC TUNNEL 9

by

John David Juliano

Thesis submitted to the Faculty of the Graduate School of the
University of Maryland, College Park, in partial fulfillment
of the requirements for the degree of
Master of Science
2018

Advisory Committee:
Dr. Kenneth Yu, Chair
Dr. Christopher Cadou
Dr. Stuart Laurence

Acknowledgements

I would like to first extend my gratitude to Dr. Ken Yu, who has given me a unique opportunity to work with AEDC Tunnel 9 over the years. I would like to thank Dr. Ken Yu and Jason Burr who opened their facility at the Advanced Propulsion Research Laboratory to me and assisted me in conducting this research.

Next, I would like to acknowledge the workforce at AEDC Hypervelocity Wind Tunnel 9, with special thanks to Inna Kurits, Joe Coblish, John Lafferty, and the TSP team including Arnold Collier and AJ Spicer. Without their assistance this research would not have been possible.

Finally, I would like to give special thanks to my family and friends who have supported me and continue to support me in all of my academic and professional endeavors.

Table of Contents

List of Tables

List of Figures

List of Abbreviations

AEDC	Arnold Engineering Development Complex
APRL	University of Maryland Advanced Propulsion Research Laboratory
BOLT	Applied Physics Laboratory Boundary Layer Transition Experiment
CCD	Charge-Coupled Device
DARPA	Defense Advanced Research Projects Agency
IR	Infrared
LaRC	Langley Research Center
LED	Light Emitting Diode
NASA	National Aeronautics and Space Administration
NIST	National Institute of Standards and Technology
PH	Precipitation-Hardened
sCMOS	Scientific Complementary Metal-Oxide-Semiconductor
SB	Schmidt-Boelter Direct Read Heat Flux Sensor
TC	Thermocouple
TSP	Temperature Sensitive Paint
UMD	University of Maryland
UV	Ultra-Violet

Chapter 1: Introduction

Hypersonic ground test facilities are seeing a large increase in demand in recent years. This is due to increased capabilities in hypersonic aerodynamics, the push to increase hypersonic warfare capabilities, and the rise of commercial space flight companies such as SpaceX, Blue Origin, The Boeing Company, and the Sierra Nevada Corporation.

Arnold Engineering Development Complex (AEDC) Hypervelocity Wind Tunnel 9 has not been excluded from this increase in demand. Tunnel 9 was developed in the early 1970's as part of the Naval Surface Warfare Center in White Oak, Maryland. Tunnel 9 has played a leading role in hypersonic ground testing by constantly expanding its capabilities, and consistently improving its measurement systems to improve data quality. Currently, Tunnel 9 is a branch of the Arnold Engineering and Development Complex. The main mission of Tunnel 9 is to provide aerodynamic and aerothermodynamic test data to a multitude of customers including government and private entities[1]. An image of Tunnel 9, with a Mach 10 nozzle

attached is seen in Figure 1[1].

Figure 1: Image of the Test Section of AEDC Hypervelocity Wind Tunnel 9

Aerothermodynamic test data are often critical in the design of a hypersonic vehicle. The surface heat transfer on a vehicle tends to be one of the main driving factors influencing the design of a hypersonic vehicle. Specifically, the heat transfer seen on the surface of a hypersonic body drives the size and weight of the thermal protection system needed. The heating rate of a hypersonic vehicle scales as a function of the cube of the velocity[2]. Therefore, hypersonic vehicles, flying at speed over Mach 5, see large heating rates, especially on blunt surfaces and leading edges simply due to the speed of the vehicle.

The characterization of heat flux on a hypersonic vehicle is extremely important, and Tunnel 9 is built to measure this by using flow with high total enthalpy. Tunnel 9 uses a large gas heater to supply high pressure, high temperature

nitrogen gas at total pressures up to 20,000 psi and total temperatures up to 3000°F depending on testing condition.

Global Thermal Measurement Systems

Because the heating rates on the surface of a vehicle are one of the main drivers for the design of hypersonic vehicles, it is extremely important to create an accurate representation of the heat transfer rates on the surface of an entire hypersonic body. This can be quite difficult due to complex flow structures that cannot be fully characterized using common discrete instrumentation or computations. One example of these flow structures is shock-boundary layer interactions.

Shock-boundary layer interactions occur when a shock wave impinges on a boundary layer creating a large adverse pressure gradient in the boundary layer. The large adverse pressure gradient causes the boundary layer to locally separate from the body. This separation creates a second shock wave at the detachment point, upstream from the impinging shock. A third shock is then created at the point of re-attachment of the boundary layer, further downstream. The boundary layer is quite thin at the re-attachment point, causing low pressures and high heating on the surface of the body[2].

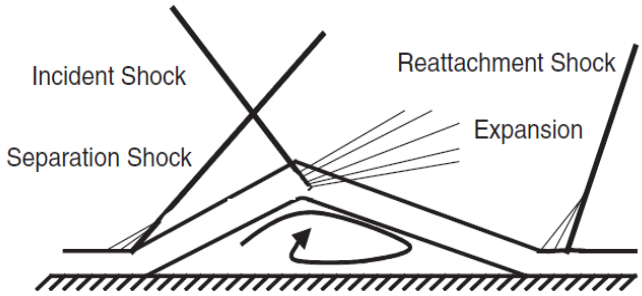

Figure 2: Example Shock Wave Boundary Layer Interaction

An example of a shock-boundary layer interaction from Hamner et.Al[3] is seen in Figure 2.

Shock-boundary layer interactions can have devastating effects on hypersonic bodies. An example of this is the failure of the X15 hypersonic test aircraft. During a flight at an altitude of 100,000 ft. and Mach 6.72 a shock impinged on a pylon in the aircraft's ramjet engine. The increased heating from this impingement burned a hole through the pylon, and ultimately a hole in the aircraft allowing high energy air into the aircraft's interior[2].

Another example proving the need for global thermal measurement is the investigation of the catastrophic failure of the Columbia Space Shuttle in February 2003. The Columbia failed during reentry, due to a hole in the thermal protection system, which allowed high energy air to flow into the interior of the vehicle.

Immediately following the failure, an investigation was completed to determine the cause. During this testing, a two-color phosphor thermography technique, as well as an Infrared-thermography technique was employed in the NASA Langley Research Center's 20in. Mach 6 Wind Tunnel to investigate the effect of damaged thermal protection systems on the surface of the vehicle[4]. Once again, a global thermal measurement system was key in the investigation of a complex body shape and flow interaction.

The effects of shock-turbulent boundary layer interactions, boundary layer transition and other complex flow phenomena are therefore quite complex and are extremely difficult to characterize with discrete instrumentation methods such as flush-mounted thermocouples and Schmidt-Boelter direct read heat flux sensors. To fully characterize the flow, a global measurement system is needed that can create a map of the heat transfer for the entire surface.

Tunnel 9 Global Thermal Measurement System

Tunnel 9 accomplishes global thermal measurements on the surface of a wind tunnel test article using a two-color intensity-based temperature sensitive paint (TSP) system. The system was designed roughly a decade ago and has been utilized ever since to create quantitative measurements of heat flux on the surface of a wind tunnel test article[5]. The TSP system was developed at Tunnel 9 and after several recent improvements to the Tunnel 9 capabilities, all steps of the data collection and reduction can be completed in-house[6]. Paint for the system is mixed and applied in the new Tunnel 9 Paint Application Lab and data are reduced using a data reduction method which was developed at Tunnel 9 and is consistently upgraded to improve capability and accuracy.

The Tunnel 9 TSP system has been utilized for nearly every test in Tunnel 9 for more than 5 years.

Tunnel 9 TSP Shortfalls

One specific area has been noted that results in poor performance by the TSP system. In cases where the heat transfer rate suddenly changes during a single tunnel run, the accuracy of TSP is greatly reduced. This is obvious due to poor agreement

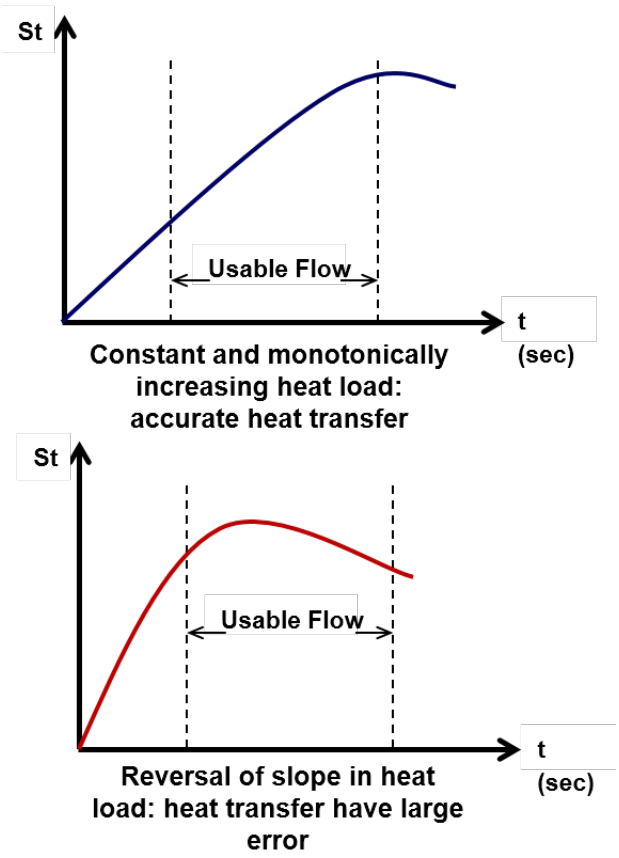

Figure 3: Example Heating Loads that Produces Accurate (top) and Inaccurate (bottom) TSP Measurements

between the TSP measurements, and measurements made using coaxial thermocouples mounted on the surface of the test article.

A sudden change in heat flux in Tunnel 9 is typically seen on the leeside of a test article during a tunnel run in which the model is dynamically pitched during the run. Figure 3 shows two examples of heating rates seen during a typical Tunnel 9 run. The top image shows a monotonically increasing heating load. The measurement made using TSP in this case is historically very accurate and shows good agreement with coaxial thermocouples on the test article surface. The bottom case shows a heating load with a sudden reversal of heat transfer slope during the usable flow period. A TSP measurement of this type of heating load has historically yielded poor results shown by poor agreement with surface coaxial thermocouple and poor calibrations.

Research Focus

Tunnel 9 is constantly upgrading its facility and methods to improve the quality of data produced for each run. This research will focus on the characterization and improvement of temperature sensitive paint measurements in cases where a sudden change in heating is present.

The underlying physical issue which causes the poor TSP measurements in certain heating situations is likely related to the heat capacity and heat storage in the thin TSP layer. During a sudden change in heat flux, the heat stored in the paint likely does not react in a uniform manor to that of the steel substrate of a wind tunnel test article causing the discrepancy between the TSP heat flux measurement and the coaxial thermocouple heat flux measurement.

However, the material properties and local paint thickness of the Tunnel 9 TSP have proven difficult to obtain, and analysis using the material properties of the paint has been avoided at Tunnel 9 in an effort to reduce uncertainty in calculated heat transfer[6]. Therefore, this experiment will seek to find a way to mitigate the error related to sudden changes in heat transfer slope using experimental results using the current data reduction and calibration for Tunnel 9 TSP.

A test was designed and completed that subjected an instrumented test article to a sudden change in heat flux, with several varying parameters. The research will attempt to characterize the response of TSP to a sudden change in heating load as a function of the magnitude of the heating load and the thickness of the TSP paint layer. It will also seek to propose a correction to the current Tunnel 9 TSP calibration method to increase the accuracy of TSP in these cases.

Research Objectives

Primary Objectives

1. Characterize the response of TSP to a sudden change in heating load as a function of heating magnitude and paint thickness
2. Develop a correction that can be applied to the TSP setup, or data reduction method that improves the accuracy of TSP in cases of a heating load reversal

Secondary Objectives

1. Investigate the effect, if any, that the application of TSP has on discrete instrumentation on the surface of a wind tunnel test article

Research Scope

This research will focus on the testing of the Tunnel 9 TSP system in a Vitiated Heater. It will seek to characterize the response of TSP and a coaxial thermocouple to heating inputs from a vitiated heater with varying heating magnitudes and TSP paint thickness. It will also seek to provide suggestions for alternative data reduction methods that may reduce errors in heat transfer measurements made using Tunnel 9's TSP system.

For this research, heat fluxes between 10 and 30 BTU/ft^2-s, and paint thicknesses between .00165 inches and .00275 will be considered.

Research Outline

This thesis will begin by looking into some background topics of relevance to this issue, including the capabilities and operation of Tunnel 9 and the Tunnel 9 TSP

system. Other discrete thermal measurements utilized in Tunnel 9 and this research will also be introduced.

Next, an in-depth look at the experimental setup for this research will be discussed, including the physical setup as well as the data collection and data reduction methods.

Finally, the results of testing will be presented as well as analysis of the results and conclusions that can be drawn.

Chapter 2: Background

AEDC Tunnel 9 Facility Description

The U.S Air Force AEDC Hypervelocity Wind Tunnel 9 is a blowdown wind tunnel located in Silver Spring, Maryland. It is regularly used as a testing site for several Department of Defense agencies, including the U.S Air Force, Army, Navy, Missile Defense Agency, DARPA, as well as NASA and several industry members.

Tunnel 9 has been one of the foremost centers for hypersonic testing for nearly the last 40 years because it has a unique combination of Mach and Reynolds numbers, with relatively long run times. Tunnel 9's primary mission is to provide aerodynamic and aerothermal test data for customers[1].

Facility Infrastructure

Tunnel 9 has a large vacuum sphere on the downstream side that is evacuated by Tunnel 9's vacuum compressor plant, which is a 4-stage compressor plant that can pump the vacuum sphere and Tunnel 9's test section to pressures of less than 1mmHg. On the upstream side, Tunnel 9's gas heater heats nitrogen gas to the desired total temperature and pressure for a given Mach and Reynolds number. A set of diaphragms separates the high pressure and low-pressure sides until the diaphragms are ruptured and flow is initiated. At this point, the high-pressure nitrogen is driven out of the heater by a set of three drivers, which are kept at a pressure much higher than the pressure in the heater[1].

Figure 4 shows the infrastructure at Tunnel 9 including the location of the Vacuum sphere, heater, and driver vessels[1].

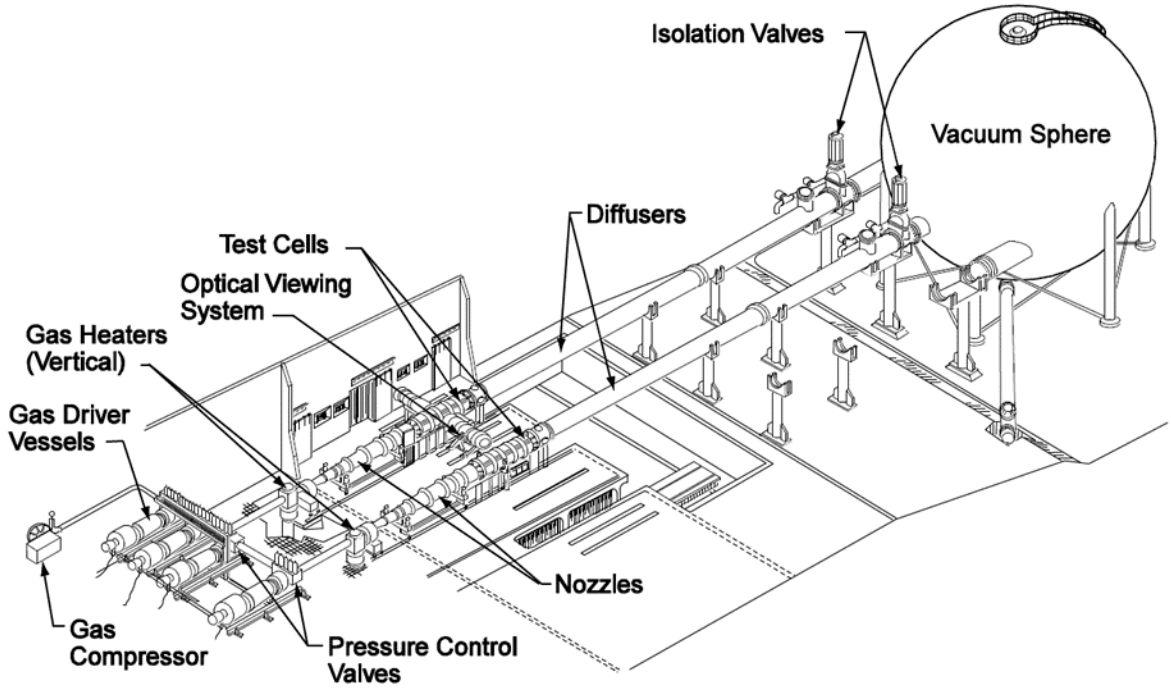

Figure 4: AEDC Tunnel 9 Infrastructure

Mach Numbers

Tunnel 9 can run at discrete Mach numbers of 7, 8, 10, and 14. Each Mach number has a unique nozzle, that connects the Tunnel 9 heater to the test section. The nozzles for Mach 8, 10, and 14 are most commonly used, and are each 40 ft. in length. The Mach 10 and 14 nozzles have a 60 in. diameter circular exit, matching the diameter of the test section. The Mach 8 nozzle has a 35 in. diameter exit and operates as a free-jet in the 60 in. diameter test section[1].

Instrumentation is available on the side walls of each test section along with nozzle supply measurements of pressure and temperature, to assist in measurement and calculation of tunnel conditions at the nozzle exit.

Test Section

The Tunnel 9 test section is 12 ft. long and 60in. diameter. It has multiple window stations in different axial locations, with windows on both sides and the top of the tunnel. Any of these window stations can be used, allowing for large or small test articles[1].

Several different windows can be utilized at Tunnel 9, including different sizes, shapes and material, so optical techniques are not limited to optics in the visible spectrum.

The test article support system can also complete a 50 deg pitch sweep at a pitch rate of 80 deg/sec. The pitch system, coupled with Tunnel 9's long test times mean that a test article can be pitched dynamically through a full angle of attack sweep during a single run, increasing the run efficiency of Tunnel 9[1].

Tunnel 9 Data Systems

Tunnel 9 has a state-of-the-art data acquisition system, EDAPS, which can sample upwards of 100 channels at a time at a 16-bit resolution. All data are

amplified and fed through an analog filter, with user programable cutoff frequencies that can change depending on the test requirements.

For a standard Tunnel 9 test, most data is taken at 500 samples/second with analog filters set to 30-Hz to eliminate the typical 60-Hz noise[1].

Tunnel 9 Typical Test Articles

Typical test articles in Tunnel 9 are manufactured out of 15-5PH or 17-4PH steel[1]. This is necessary because of the high structural and thermal loading that can be seen in Tunnel 9. Also, the material properties of 15-5PH and 17-4PH steel closely match the material properties of the coaxial thermocouples, which is necessary for data reduction of the thermocouples. This is discussed more in later sections. Test articles range in size from 20 in. to 60 in. in length.

Tunnel 9 Conditions

Tunnel 9 can run at 4 discrete Mach numbers of 7, 8, 10, and 14. For each Mach number, there is a range of Reynolds numbers that can be tested, with the overall range going from 0.05×10^6/ft to 48×10^6/ft. The range supplied by Tunnel 9 can provide useful high-altitude simulations, important for studying viscous interactions. It can also

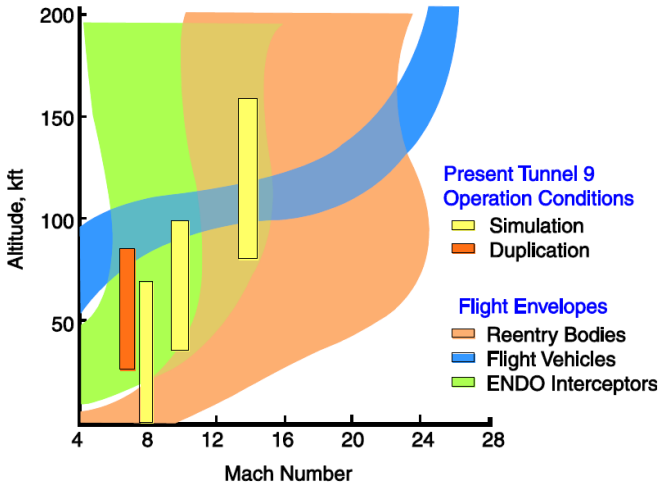

Figure 5: Tunnel 9 Operating Conditions

provide duplication of flight conditions at high Reynolds numbers. Runs can last anywhere from 0.25 sec. to 15 sec, depending on the Mach and Reynolds number combination[7]. A diagram of the Tunnel 9's current operating conditions in relation to current hypersonic bodies is given in Figure 5[1].

Run Procedure

To begin a run day, Tunnel 9 technicians address the test article and perform any applicable test article changes, including setting any deflectable surfaces to the correct location, setting the test article angle of attack and sideslip angle, checking out all installed instrumentation on the test article, and cleaning the test article and test cell.

After the test article and test cell are prepared, the Tunnel is closed and locked, and the set of 4 vacuum compressors in the vacuum compressor plant evacuate the vacuum sphere to a pressure near 1 mmHg. After the vacuum sphere is brought to near vacuum, the test cell (and test article support system) are incrementally evacuated to less than 1 mmHg. Pulling a vacuum incrementally allows for all pressure sensors to be calibrated prior to each tunnel run.

After the test cell and vacuum sphere are evacuated to less than 1mmHg, the heater is powered on, and nitrogen gas is heated. When the gas in the heater reaches the desired pressure and temperature, a pair of diaphragms are ruptured. The nitrogen gas is then driven out of the heater by high pressure nitrogen in 3 driver vessels, which are pressurized significantly higher than the pressure in the heater. The cold gas from the driver vessels drives the hot nitrogen out of the top of the heater in a

piston-like fashion, which maintains the supply conditions during the tunnel run providing a relatively constant Mach and Reynolds during the good flow section. The hot nitrogen from the heater is expanded through a contoured nozzle and reaches its desired conditions in the test section.

Heat Transfer Measurements in AEDC Tunnel 9

An in-depth knowledge of the heat transfer on the surface of a hypersonic body is extremely important. The heat transfer rate on the leading edge of a hypersonic vehicle scales by the velocity cubed[2], so at high Mach numbers it is often critical to know the heating rates to correctly determine the necessary size of the thermal protection system of the vehicle.

There are many methods to quantify the heat transfer rate on a wind tunnel test article ranging from discrete point sensors, such as thermocouples and Schmidt-Boelter sensors, to global measurements, such as Infrared thermography, and temperature sensitive paint. This section will seek to introduce some examples of instrumentation and other methods used to quantify the heat transfer on the surface of a wind tunnel test article.

Coaxial Thermocouples

The main source of heat transfer measurements at Tunnel 9 are coaxial thermocouples. Coaxial thermocouples have been used extensively in Tunnel 9 starting in the early 1980's. Coaxial thermocouples are particularly useful as instrumentation for test articles due to their small size (about 1/32 – 1/16 in. diameter), fast response durability, and ability to match the outer mold line of a test article.

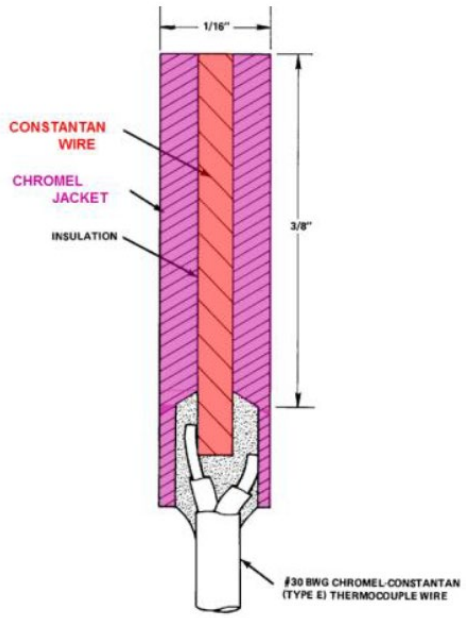

Figure 6: Type-E Coaxial Thermocouple Diagram

Thermocouples only measure temperature at the surface, but the temperature history during a tunnel run can be used to calculate the heat transfer. In Tunnel 9 it is assumed that the convective heating input is equivalent to the one-dimensional heat conduction at the surface. It is also assumed that the material properties of the thermocouple do not differ appreciably from the material properties of the 17-4 or 15-5 stainless steel test article. A second order, Euler-explicit finite difference numerical solution of the one-dimensional heat conduction equation is solved to give the heat transfer at the surface of the thermocouple[8].

For the greatest sensitivity, Tunnel 9 uses type E coaxial thermocouple, manufactured by the Medtherm Corporation[8]. A type E thermocouple is composed of a Chromel and Constantan junction. A coaxial thermocouple is different from a typical beaded thermocouple because the junction is created by surrounding a

Constantan wire in a Chromel jacket. Figure 6 shows a diagram of a type-E coaxial thermocouple, like the ones used in Tunnel 9[8].

Coaxial thermocouples can be sanded at the surface to match the outer mold line (OML) of a test article. This means that they cause very little disturbance to the flow in the area around the thermocouple. For a facility like Tunnel 9, with high Reynold number capabilities, this is very important in order to reduce disturbances in the flow, which could trip the boundary layer from laminar to turbulent.

Thermocouples are also very simple devices, and are durable, reliable, and easy to troubleshoot. The simplicity of the sensors is important in Tunnel 9 since they can play a key role in increasing testing efficiency.

While reliable and accurate, thermocouples are still physical, discrete sensors, and must be designed into the test article. Sensors must be secured into drilled holes in the test article. Further, for the heat transfer calculation, described below, the wall of the test article must be sufficiently thick, and have similar thermal properties to that of the thermocouple. The use of thermocouples is often limited space considerations on the test article surface, and inside the test article cavity.

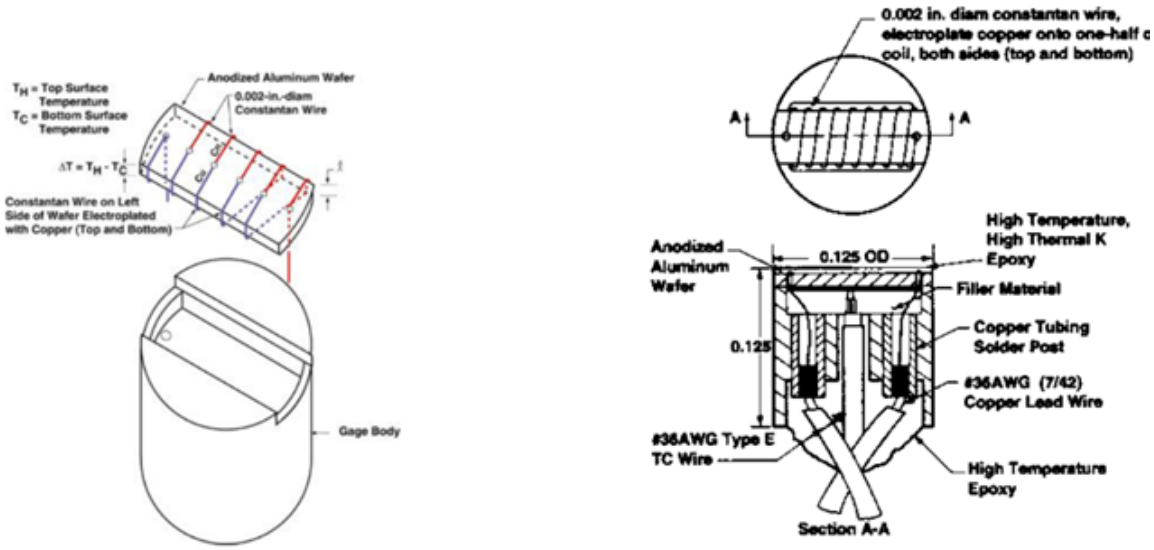

Figure 7: Diagram of Schmidt-Boelter Direct Read Heat Flux Gage[1]

Another type of sensor used in Tunnel 9 to measure heat transfer is a Schmidt-Boelter sensor, which is a direct read heat flux sensor, whose output is directly proportional to the incident heat flux on the gage. Tunnel 9 utilizes small fast-response Schmidt-Boelter gages which are manufactured internally at AEDC Arnold AFB[1]. A diagram of a Schmidt-Boelter gage commonly found in Tunnel 9 is given in Figure 7.

Schmidt-Boelter sensors have several key advantages and disadvantages when compared to a coaxial thermocouple. They read heat flux directly using a calibration, which means that they do not need to be installed in a specific substrate, allowing for more flexibility in test article design. They are also very good in low heating situations because they do not depend on a 1D inverse calculation, which is necessary for coaxial thermocouples, as will be discussed in more detail in later chapters.

Schmidt-Boelter sensors are considerably larger than a coaxial thermocouple (about twice the diameter), and typically not as reliable. They also cannot be shaped to the contour of the test article as well as a coaxial thermocouple, limiting their placement to relatively flat areas on a test article with low expected heat transfer rates.

Global Thermal Measurement Systems

Discrete measurements using sensors like thermocouples, or Schmidt-Boelter gages are the most common types of heat transfer measurements in wind tunnel application in Tunnel 9. Discrete measurements however struggle to accurately characterize interactions on the surface of the body, such as boundary layer transition, flow separation, and shock-boundary layer interactions due to the highly local phenomenon that occurs as in these types of flow structures[6].

To better characterize common flow phenomenon, several wind tunnel facilities have begun making global thermal measurement a standard form of measurement in the last few decades. Global thermal measurement systems can create a surface map of temperature and, with calculations, the heat transfer on the surface of a wind tunnel test article. This method obtains more data on the surface of a wind tunnel test article than discrete measurements that can assist in better understanding flow field phenomena.

Common global thermal measurement systems will be described below.

Temperature Sensitive Paint

One type of global thermal measurement is temperature sensitive paint (TSP). TSP is usually comprised of luminescent molecules suspended in a polymer binder, which is applied to a wind tunnel test article. These luminophores become excited when illuminated with light of the appropriate wavelength (normally ultra-violet or blue light). The intensity of the excitation of the luminophores can be measured using a scientific grade camera such as a CCD camera or a sCMOS camera[3].

The florescence from the luminophores is inversely proportional to temperature, which means that a calibration can be applied to convert intensity values from a camera to temperature using a reference temperature[6]. This is the method applied in AEDC Tunnel 9, and Tunnel 9's temperature sensitive paint system will be described in more detail below in Section 4.

Phosphor Thermography

Phosphor thermography is similar to TSP because it involves a temperature sensitive phosphor sprayed onto a test article, which can be calibrated to measure temperature using a camera to acquire intensity data from the surface. Phosphor thermography is the main global thermal measurement for the wind tunnels at the NASA Langley Research Center (LaRC)[9].

The phosphors used at NASA LaRC are excited using an Ultra-Violet (UV) light and are imaged using a color camera. In order for the 1-D heat transfer assumptions used at NASA LaRC to hold, test articles must be made from a material with low thermal diffusivity. Therefore the test articles being investigated with

phosphor thermography are made using a silica ceramic[9]. NASA LaRC has been using this technique since about 1999.

Infrared Thermography

Infrared (IR) thermography uses an IR camera to measure the radiative intensity on the surface of the wind tunnel test article. This is then converted to temperature using a calibration. IR camera technology has greatly improved in the last 10 years, making these measurements in a hypersonic wind tunnel feasible.

One example of IR measurements on a wind tunnel test article is the boundary layer transition locations measurements made on The Johns Hopkins University Applied Physics Laboratory Boundary Layer Transition (BOLT) Flight Experiment. IR and TSP measurements were taken simultaneously on the surface of a scaled wind tunnel test article to assist in the determination of the locations of boundary layer transition on the BOLT test article in the The Boeing/AFOSR Mach-6 Quiet Tunnel at Purdue University[10].

Tunnel 9 Temperature Sensitive Paint

Tunnel 9 has been utilizing an intensity-based temperature paint system during wind tunnel tests for nearly 10 years. Tunnel 9 presents some unique challenges, that force its TSP system to differ slightly from other TSP systems and has gone through several iterations.

Fundamentals of Tunnel 9 TSP

Tunnel 9 utilizes a two-color intensity-based TSP system during wind tunnel testing. During test article installation, Tunnel 9 technicians instrument the test article with coaxial thermocouples to obtain discrete measurements. After these sensors are installed, TSP technicians prepare the test article for paint application, and apply the paint. Figure 8 shows an example wind tunnel test article in AEDC Tunnel 9 with the two-color TSP paint applied.

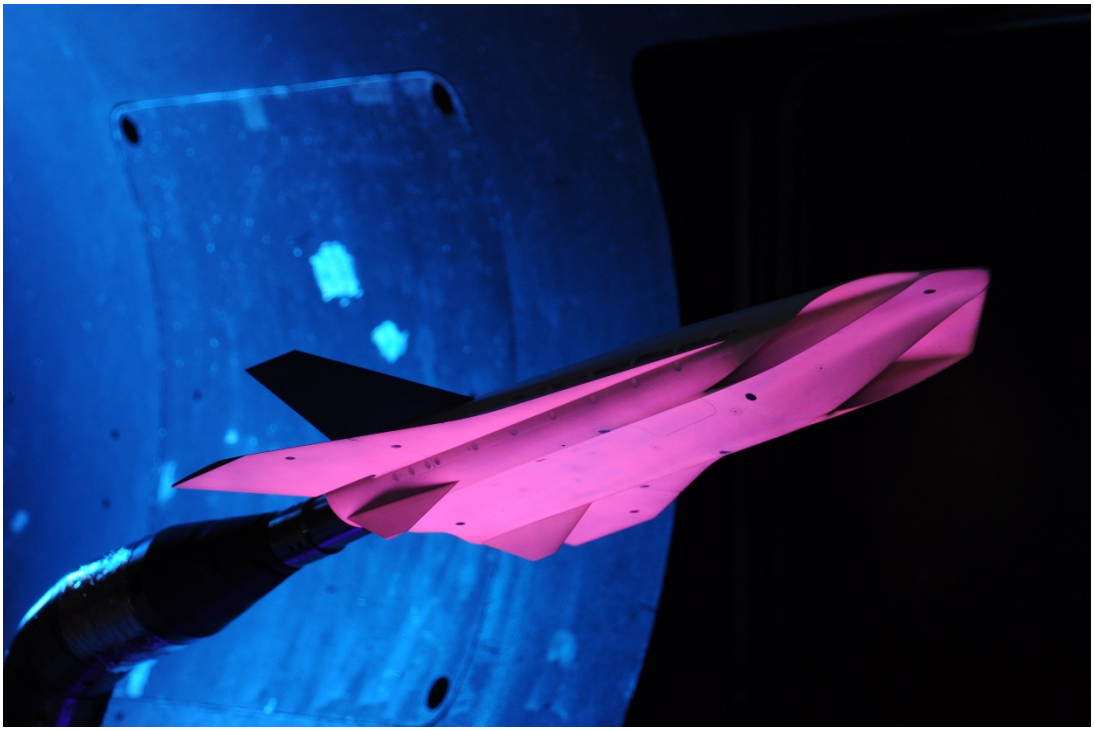

Figure 8: Example Wind Tunnel Test article with TSP Applied in AEDC Wind Tunnel 9

After the thermocouple installation is completed, the test article is cleaned, and a white basecoat is applied using a spray application. The basecoat serves two purposes. First, it helps the TSP active layer stick to the test article. Second, it serves to reflect UV light back through the active layer. This effectively doubles the path

length the UV light takes through the active layer, increasing the fluorescence of the active layer.

After the base coat sets, the active layer is sprayed onto the test article. Finally, the test article receives any final detailing and returns to the Tunnel 9 instrumentation shop to have the remaining sensors installed.

After painting, any remaining instrumentation including Schmidt-Boelter sensors are installed on the test article, and then the test article is installed into the test section for testing.

Test articles in Tunnel 9 typically remain installed for the duration of a test program. This means the TSP must be durable enough to last for an entire test program without peeling off the test article or losing its fluorescence.

During testing, the TSP is illuminated using Tunnel 9's 365 nm ultraviolet LED systems, which excite the particles in the paint, causing them to fluoresce. The intensity of the fluorescence is captured on scientific grade CCD or sCMOS cameras, with filters on the front. Each camera captures only one color.

After all data tares are taken, all image sets are transferred from the camera control computers to the data reduction computers, where the TSP data reduction process is performed.

All data are mapped to a 3-dimensional grid of the test article. This allows multiple camera systems to be used and accounts for different positions of each camera in the data reduction. It also allows for the pitching of a test article, and accounts for the movement of a test article in the image sensor of each camera. After data are mapped onto the grid, the temperature is computed using a calibration that

will be discussed later, and using the time history of the temperature, the heat flux and Stanton number are computed.

Reduced TSP data are then post-processed to create useful plots and images for a Tunnel 9 customer. This includes comparison plots between heat transfer computed using TSP data, and heat transfer computed using thermocouples.

Ratio of Ratios Equation

As mentioned earlier, Tunnel 9 TSP operates using two color intensity-based TSP. An intensity-based system measures the temperature on the surface of the model by measuring the ratio of the intensity of the fluorescence of the paint compared to a reference temperature and intensity. Thermal quenching is the driving method behind the temperature dependence. Further, the binder used in the paint is made of an oxygen impermeable binder. For a thermal quenching TSP with an oxygen impermeable binder, it can be shown from Liu and Sullivan[11] that the intensity output seen by the camera is a function of only the change in temperature from a reference temperature:

$$\frac{I(T)}{I(T_{ref})} = f\left(\frac{T}{T_{ref}}\right)$$

For Tunnel 9. The TSP intensity is a linear function of temperature or:

$$\frac{\mathrm{T}}{\mathrm{T_{ref}}} = \frac{\mathrm{I}}{\mathrm{I_{ref}}}$$

The intensity of the light fluorescing from the paint is a function of the paint chemical makeup, the paint thickness, the temperature, and the intensity of the incoming excitation source. During a run, the chemical makeup and paint thickness

are constant. However, Tunnel 9's normal mode of operation includes pitching the model through an angle of attack during the run, which makes the illumination field inconsistent during a typical run. The LED's that make up the illumination field for the excitation light are affixed to the tunnel wall and do not move with the pitch system. Therefore, as the test article pitches, it moves through the illumination field creating non-temperature-induced spatial-temporal variations.

The second color in the two-color TSP system is used to account for changes in illumination intensity during a run. For the paint currently used in Tunnel 9 the excitation wavelength is centered at 365 nm (ultraviolet), with two emission wavelengths centered at 614 nm and 450 nm which correspond to red and blue light respectivly[12].

The red luminophore fluorescence is dependent on both temperature and excitation intensity due to the chemical makeup of the luminophore chosen. The fluorescence intensity is inversely proportional to temperature. The blue luminophore fluorescence intensity is nearly independent of the temperature, but it is dependent on the excitation intensity. This allows the use of the ratio of the intensities of the red to blue paint to effectively eliminate non-temperature-induced spatial-temporal variations from the results. The generalized temperature sensitive paint equation then becomes what is known as the ratio of ratios (RofR):

$$\frac{T}{T_{ref}} = \frac{\left(I_{red}/I_{red,ref}\right)}{\left(I_{blue}/I_{blue,ref}\right)}$$

The paint used at Tunnel 9 is applied in house by trained technicians in the new Tunnel 9 Paint Application Lab. The coaxial thermocouples installed under the paint on a test article are necessary for TSP calibration, which will be discussed later.

Excitation System

The excitation required for Tunnel 9 TSP is centered at 365 nm which is in the ultraviolet spectrum. Custom made LED's are used in Tunnel 9 and a band-pass filter centered at 365 nm is also added to eliminate other wavelengths that may be produced by the LED's.

The LED's are controlled by a dedicated control system in the Tunnel 9 control room. They can be monitored and adjusted remotely during a run cycle, while the tunnel room is secured for safety reasons. They are triggered by the tunnel control system and turn on just before a tunnel run begins. This guarantees that they have sufficient time to warm up before the tunnel flow period begins.

The LED's remain powered on for the duration of the test and automatically turn off after the cameras stop taking images at the end of the run.

Imaging System

TSP imaging at Tunnel 9 is accomplished using either scientific grade CCD or sCMOS cameras. Two cameras are used for data collection to maximize system dynamic range. Each camera is fitted with a bandpass filter centered around the emission wavelength of either the "blue" or "red" lumiphores. The cameras are positioned as close to each other as is physically possible. The result is a set of images of the test article, from roughly the same angle, at two different wavelengths

Since the mapping process maps the images to a 3D grid of the test article, and all ratios and calculations are done on this grid, it is not necessary to image the test article at the same location for the blue and red. As a result, the camera pair does not need the same image plane, which simplifies the camera setup positions.

It is also possible to image the test article from multiple angles. The current system can utilize up to 4 pairs of cameras to image the test article from the top, bottom and both sides. If desired, a temperature and heat transfer map of the entire test article surface can be created.

Each camera pair is connected to a stand-alone computer system that controls exposure time, number of images to be collected, and image recording modes. All computer inputs are wired into the Tunnel 9 control room, and the computers are controlled in the control room during a test.

The Tunnel 9 control system supplies a trigger that begins image collection on all cameras simultaneously. They begin data collection when the total pressure in the tunnel rises to a pre-determined value. Also, the cameras output the time of each exposure to the Tunnel 9 data collection system, allowing each frame to be matched up with the correct tunnel conditions and the correct angle of attack, which are computed after the tunnel run ends.

Typical Run Day Procedure

A typical run at T9 that includes TSP operates in the following fashion:

1. Dark image collection

a. Images are taken with the test article in run position and all lights (including UV lights and tunnel room safety lights) powered off.

2. Reference Image data collection
    a. Images are taken during the dynamic tare where the test article completes the same angle of attack sweep that will be completed during the run. This set of images is taken with the UV lights, and the test article fluorescing, but the tunnel is not running.
3. Run data collection
    a. As the tunnel operates, data is taken with UV lights on, and the test article completes the same angle of attack sweep that was done during the dynamic tare
4. Data reduction
    a. TSP data reduction is completed, which will compute the ratio of ratios, temperature, heat flux and Stanton number on the surface of the test article.

Tunnel 9 Data Reduction

After each run, a TSP engineer analyzes data using codes that were created at Tunnel 9 and have evolved as the system has evolved over the years. Data reduction requires a set of dark images, a set of dynamic tare images, and a set of run images from each camera, along with a 3D structured grid to map images onto, and reduced data from Tunnel 9's primary data system. All data reduction at Tunnel 9 is done using MathWorks MATLAB.

TSP Data reduction in Tunnel 9 is done in 5 steps

1. Raw Data Preparation and mapping all images onto a 3D grid
2. Calculating a ratio of mapped images to obtain the ratio of ratios at each grid point
3. Calibrating TSP, and computing temperature at all grid points
4. Computing heat transfer at all grid points
5. Post processing data

The following sections will detail these steps:

Raw Data Preparation and Mapping

Before mapping, all data must be loaded into MATLAB. First, the set of "dark" images is loaded into the software. All images in a single set are averaged. This gives the average "dark" image, which will be subtracted from all corresponding reference or run image sets. Subtracting "dark" images eliminates any bias in the camera intensity measurement that could be caused by any remaining ambient light outside the test cell, or by any other optical diagnostic technique (like a Schlieren light source).

After all images have been imported into the software, and all dark offsets have been subtracted, all images are mapped to a grid. The grid used is a 3D structured grid of the outer mold line of the test article.

Mapping is done at Tunnel 9 by finding the location of all cameras relative to the test article and projecting the images from each camera onto the grid. This is done

using a set of optical targets with known location, drawn on the surface of the test article.

Mapping is done at every frame, so that the correct projection can be done as the test article dynamically pitches through each image frame.
For this experiment, only one point in the center of the test article was used. That point was manually determined for each run, which eliminates the need to include a mapping algorithm.

Calculating the Ratio of TSP Images

Once TSP images are mapped onto the grid, a ratio of ratios can be calculated at each grid point. Because all images are added to a grid, this can simply be done by using the ratio of ratio formula to find the value at each point on the mapped grid. This value will then be used to perform the calibration and calculate the temperature on the test article.

At the end of this step, a qualitative TSP image is available for temperature, as the ratio of ratios is roughly inversely proportional to temperature.

Calibration

During initial iterations of the Tunnel 9 TSP system, the calibration was performed a priori on a sample of the paint to be used on the test article. Currently, a separate, in situ calibration is done for each tunnel run.

The thermal properties of the TSP used in Tunnel 9 are not currently known with high accuracy. Because the calculation of heat flux is highly sensitive to the material thermal properties, a method was designed to calculate the heat flux without

using the material properties of the TSP. To do this, it is assumed that the temperature gradient through the TSP layer is linear[6]. The use of this assumption for a Tunnel 9 run was shown to have very little effect on the calculated heat flux by Kurits[6].

In order to calculate the heat flux assuming that the temperature gradient in the paint layer is linear, the temperature history at the surface of the steel test article (under the paint layer) must be known.

The calibration comes from a polynomial fit of the test article surface temperature vs. the ratio of ratios. A separate curve can be created at each location of a coaxial thermocouple coated in TSP. The ratio of ratio values are extracted from the TSP data at the location of each thermocouple. The thermocouple data is extracted at the time of each camera exposure, and then compared to the TSP value at that location.

Once all data is extracted, a calibration curve can be plotted, and a polynomial curve fit can be completed. In an ideal TSP setup, the calibration is linear and identical for all points. At times this varies, and a TSP calibration can have a slight curve that can be modeled better with a third-order polynomial.

Once the calibration is completed, a simple polynomial can describe the relationship between the TSP ratio of ratio value and the temperature at the surface of the steel test article, under the paint layer. The temperature is then calculated for all mapped 3D grid points on the test article, giving a full map of the temperature on the surface of the test article for each camera frame.

Calibrations of TSP are typically assumed to be linear, but in these cases of sudden heat flux change caused by dynamic pitching of a test article the calibrations

no longer appear linear. An example of the calibrations can be seen in Figure 9. The typical calibration on the left shows a nearly linear calibration, which would produce good accuracy when applied to TSP data. The calibration on the right shows a nearly linear calibration until about 150°F in which a large non-linearity is seen. This non-linearity would cause poor accuracy in TSP.

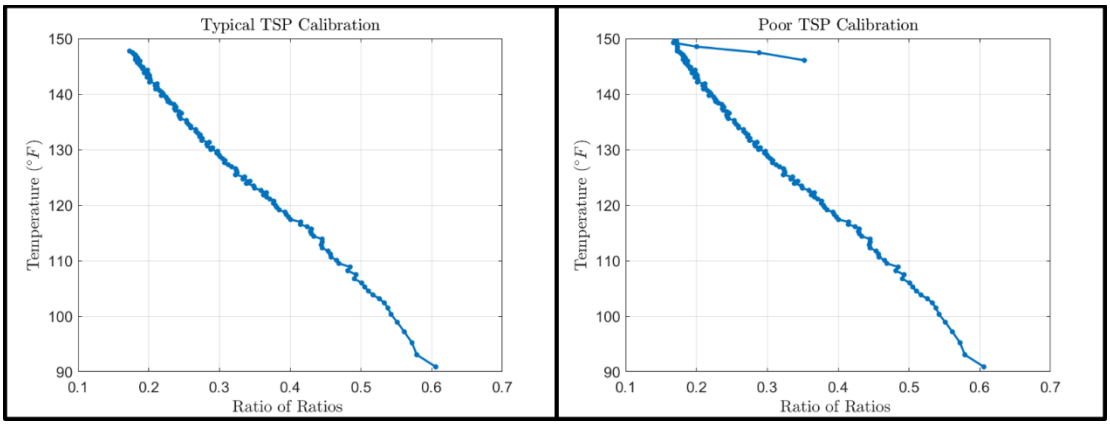

Figure 9: Typical TSP Calibration (left) and Poor TSP Calibration (right) indicating Poor TSP Accuracy

Calculation of Heat Flux

As the temperature that is calculated from the calibration is the temperature on the surface of the steel test article and not the temperature on the surface of the TSP, the same assumptions that were used in the calculation of heat flux for a thermocouple can be used[6].

The main assumptions are that the material properties are defined using the material properties for the steel used in the test article production, that the heat transfer is one-dimensionally moving into the test article wall, and that the back face of the test article wall is adiabatic[8].

The calculations will be described in more detail in the next chapter.

Challenges of TSP in Tunnel 9

Several other global thermal measurement systems used in wind tunnel testing make a series of assumptions that greatly simplify solving the heat equation, to determine heat transfer rate from temperature data. The NASA LaRC wind tunnels for example inject their test articles into the flow, which effectively creates a step heat transfer input[9]. Also, it is common for TSP and thermographic phosphor systems to use a large insulating layer, or use ceramic test articles, to assume there is no heat transfer into the test article wall

Tunnel 9 test articles face a high dynamic loading environment, both thermally and mechanically. This means that for the test articles to be robust, they must be made from stainless steel. When developing the Tunnel 9 TSP system, it was desired to be able to use the same steel test articles for testing with TSP. This means the TSP in Tunnel 9 was designed to be used on a stainless-steel test article, and withstand the high dynamic loading that would be seen on a typical Tunnel 9 test article[13].

Further, the test articles in Tunnel 9 see temperature rises between a few degrees Fahrenheit, to a few hundred degrees Fahrenheit. This large increase in temperature causes a temperature rise on the backside of the paint layer. This means that even with a thick insulative layer, a semi-infinite wall assumption is invalid, which greatly increases the complexity of the data analysis.

Finally, Tunnel 9 does not inject test articles into the flow. Injecting test articles into the flow allows for a step input of heating to be assumed. Instead, a test

article in Tunnel 9 will experience a non-negligible startup time, and will see heating during this time that cannot be ignored[13].

Chapter 3: Experimental Setup

To investigate the response of TSP to sudden heat flux changes, a test was designed that closely matched the data collection and data reduction techniques utilized in Tunnel 9 in a separate facility capable of producing large, sudden changes in heat flux.

Experimental Conditions

To investigate sudden changes of incident heat flux on a test article surface with TSP applied, a heat flux profile was chosen that includes a sudden increase in heating, and a sudden decrease in heating. An example of this profile is seen in Figure 10. This profile will be discussed in length in Chapter 4.

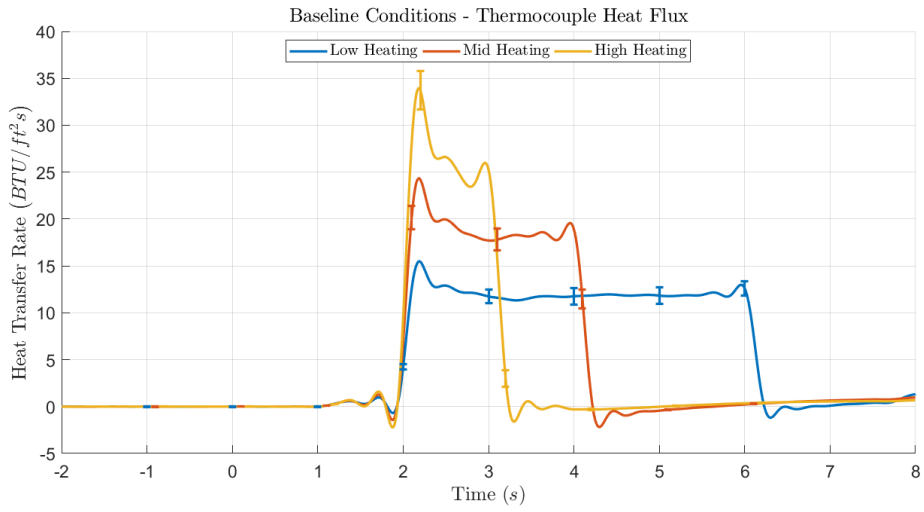

Figure 10: Example Heating Input Used in Investigation of TSP Response to Sudden Heat Flux Changes

To fully characterize the response of TSP to a fluctuating or decreasing heating load in Tunnel 9, the magnitude of the heating load and the thickness of the TSP paint layer was varied.

Heating Load Magnitude Conditions

To attempt to quantify the response difference due to the change of heating rates, three heating magnitudes were selected to approximate a range of heating conditions typically seen in Tunnel 9. An example of these heating loads is shown in Figure 10. The target heating conditions were 10, 20 and 30 BTU/ft^2-s.

During testing, these target conditions were nearly, but not exactly met. The actual values and trends of the baseline conditions are discussed in depth in Chapter 4.

Paint Thickness

Paint thickness was also varied, because during the operation of TSP in Tunnel 9 the paint thickness has proven to influence the measurement made by TSP. Three paint thicknesses were targeted that approximately bound the range of the paint thicknesses seen in Tunnel 9.

The target paint thicknesses for this experiment were 1.0 mil, 1.3mil, and 2.0mil. This roughly covers the empirically determined range of acceptable paint thicknesses on a Tunnel 9 test article.

Like the actual magnitude, the actual paint thicknesses varied from the target thicknesses. The actual paint thicknesses tested will be discussed later in this section.

Testing Methodology

Testing Series

The combination of three paint thicknesses, a baseline series with no paint applied and three heating magnitudes gives a total of 12 heating magnitude-paint thickness combinations. These cases were then split in testing series based on paint thickness, and all cases in a test series were grouped and tested together. The organization of cases is shown in Table 1 in the order they were tested.

Table 1: Testing Series of All Cases

Paint Thickness	**Low Heating**	**Mid Heating**	**High Heating**
Unpainted - Baseline	S100 - LH	S100 - MH	S100 - HH
Thin Paint	S200 - LH	S200 - MH	S200 - HH
Thick Paint	S300 - LH	S300 - MH	S300 - HH
Middle Paint	S400 - LH	S400 - MH	S400 - HH

Each case was tested a minimum of 10 times to calculate statistics and uncertainty of each case. Then, the nine cases where paint was applied were compared to the three cases without any paint application. All analysis was done using the result of these comparisons.

Control Sensors

The test article was designed such that not all sensors would be painted over. This means that the arrangement of multiple sensors remained constant for each test

series regardless of the paint thickness. These control sensors were used to normalize the readings of the painted tests to the baseline test series. This facilitated a one to one comparison between testing series.

Test Facility Description

The test facility chosen for this experiment was the University of Maryland Advanced Propulsion Research Lab's (APRL) vitiated heater. The heater facility was originally designed to test Scramjet propulsion systems, and match the total enthalpy at Mach 4.6 at an altitude of roughly 63,000 feet[14]. Our experiment seeks to test representative heat transfer rates that would be seen in Tunnel 9, and this facility has proven capable of producing similar heating rates on a representative test article.

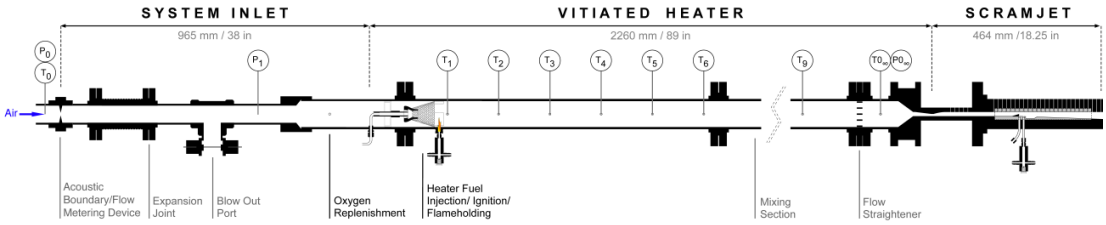

Figure 11: Flow Path Schematic of the APRL Vitiated Heater facility with scramjet test section attached[14]

High pressure air for the test facility is generated using an Atlas Copco GA75 Type Compressor, and dried using a Hankinson HPRP400-460 dryer. The airflow enters the vitiated heater through a 0.4 in. orifice which is used as a flow measurement device. After the orifice, the flow travels through an expansion joint, past a blowout port, and an expansion section[14] and into the heater. This is shown in Figure 11.

Ethylene and oxygen are added in an ignitor section downstream and are ignited using an AC Delco D585 ignition coil. Hydrogen fuel is used as the main fuel and is added just upstream of the ignitor.

Figure 12: Fuel and Oxidizer Supply for Vitiated Heater

All fuels are fed from regulated pressurized bottles shown in Figure 12. The bottles are located in the control room and plumbed through the ceiling and into the testing bay. Flow passes through a manual valve in the control room, followed by a large section of pipe into the testing bay. Once in the testing bay, flow goes through a solenoid valve controlled by the heater control system, followed by a check valve. After the check valve, the flow goes through a section of flexible tubing and a choked flow orifice which ensures that the flowrate is determined entirely by the upstream pressure. The orifice sizes can be changed but were left constant for this experiment.

Flame holding is achieved using an inverse cone just upstream of the ignitor. Following ignition, there is roughly 90 in. of 3 in. diameter pipe to contain the hydrogen flame. The exhaust flows out of the pipe and through an open test section, over the test article. In Figure 11, the scramjet assembly on the far right of the image

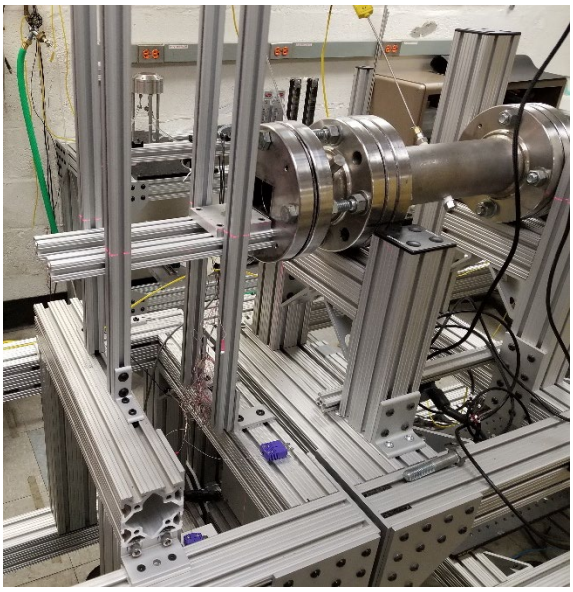

Figure 13: Heater outlet and open test section

is replaced with the test section, which will be discussed in more detail in future sections. The heater outlet and test section are shown in Figure 13.

After the test section, the exhaust is collected in a vent, and vented out of the testing bay.

The facility is controlled by a National Instruments cRIO-9022. The cRIO, and all data collection systems are controlled in a separate control room.

Facility Capabilities

The facility conditions are determined by the supply pressure of the main hydrogen fuel, the ignitor oxygen and ethylene supply pressure, and the test times. The ignitor conditions (ignitor oxygen pressure, and ignitor ethylene pressure) were proven to have little effect on the heating at the test section, and so were kept constant for the experiment.

The operating conditions were chosen to give heat flux values on the surface of the test article that are representative of what would be seen in Tunnel 9. To achieve different heat fluxes, the supply pressure of the main hydrogen fuel was adjusted. To adjust the main hydrogen fuel supply pressure (and the ignitor fuel and oxidizer pressures) the heater air flow is turned on, and all valves for the fuel are opened. The regulator for the gas is then adjusted until the static pressure downstream

of the check valve reads the target pressure. Once all pressures are set, they do not have to be reset unless the condition is changed, or the bottle pressure becomes insufficient and cannot supply the pressure to the heater.

Facility Standard Operation Procedure

During operation, the supply air is constantly flowing. It is not controlled by the control system, but instead is controlled by a hand valve in the testing bay. To begin a test, the supply air valve is opened and is not typically closed between tests. Next, if necessary the supply pressures of all fuels and oxidizers are adjusted. Once all supply pressures are correct, the testing bay is closed.

All data acquisition systems are then armed to collect data, and the heater control system is armed. Once all systems are armed, the manual valves for all fuels and oxidizers are opened, and the system is placed into remote control.

When computer control of the system starts, the ignitor fuel and oxidizer solenoid valves are opened, and the spark plug is activated. This creates the initial flame that will ignite the main fuel. After approximately one second the main fuel solenoid valve is opened. The main fuel ignites using the ignitor flame. Once ignition is achieved the spark plug is turned off. This generally happens one second after the main fuel turns on. After main fuel flame holding is achieved, the main fuel valve is held open for the duration of the test. At the end of the test the main fuel solenoid valve is closed. Some fuel remaining in the length of flexible tubing between the solenoid valve and the heater then bleeds out.

When the main fuel solenoid valve is opened, the heater control system sends a 5V rising step trigger signal to all data collection systems, to begin data collection. All data collection systems are triggered using the same trigger, which guarantees all systems are collecting in unison.

Testing Order

Because the input heating condition is set by a hand valve and includes human error an ideal test setup would include test condition randomization to attempt to remove any bias from the results. However, setting the regulator pressures while setting the heating input consumes a large amount of the available hydrogen. Typically, setting the pressure uses more gas than a set of 10 runs would use in this experiment. Therefore, to reduce the amount of hydrogen tank refills needed, all tests for a certain case were run at one time. The control sensors were used to normalize the heating input of all cases to the heating input of the baseline cases.

Facility Advantages over Tunnel 9

The vitiated heater facility has some key advantages over Tunnel 9 that makes it ideal for this type of testing. The main advantages are the maximum rate of testing and low cost. It is possible to run the vitiated heater upwards of 30 times in an 8-hour day. In contrast, Tunnel 9 can only complete a maximum of two run cycles per 8-hour run day[1]. Also, operation of the vitiated heater only requires two trained operators, while the operation of Tunnel 9 requires upwards of 25 engineers and technicians. For this study, it was important to repeat each test multiple times to develop statistics and increase confidence in the results. Each test was completed a minimum of 10 times in

order to gather enough data to calculate statistics on the results, resulting in over 150 tests. This would be time consuming, and very expensive to complete in Tunnel 9. The vitiated heater could complete the testing rapidly and cheaply.

Second, the vitiated heater facility is more versatile than Tunnel 9. Because Tunnel 9 is pumped down to near-vacuum for each run, the facility is closed, and test hardware tends to be quite complex and expensive. Last-minute adjustments are often not possible in Tunnel 9 because of the time it takes to evacuate the air from the facility. The vitiated heater facility is open, and versatile. The supporting structure of the facility is made from a T-slotted aluminum frame, which is quite common in engineering applications and easy to add structures to. Also, the test section can remain open, which allows for easier optical access, and easier test article design.

Because the vitiated heater facility can generate similar heat transfer rates on a test article as Tunnel 9 (because of similar flow total enthalpy) and it is a more versatile and simpler facility, it is an ideal choice for testing the TSP on a representative test article.

Test Article

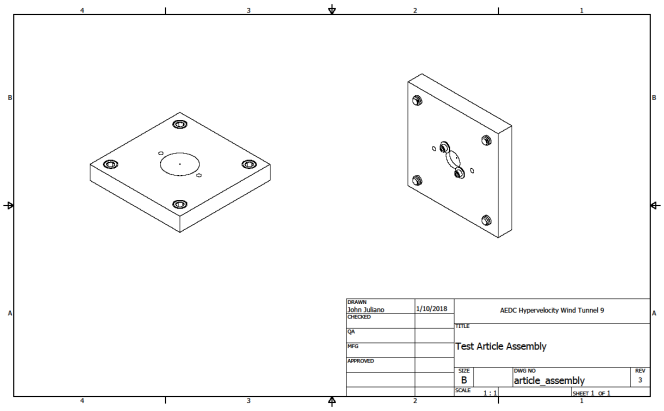

Figure 14: Test Article Assembly Drawing

The test article for this experiment was designed to be representative of a section of a test article in Tunnel 9. A drawing of the test article is seen in Figure 14. The test article is a two-piece assembly, and dimensioned drawings of those two pieces are shown in Figure 15 and Figure 16.

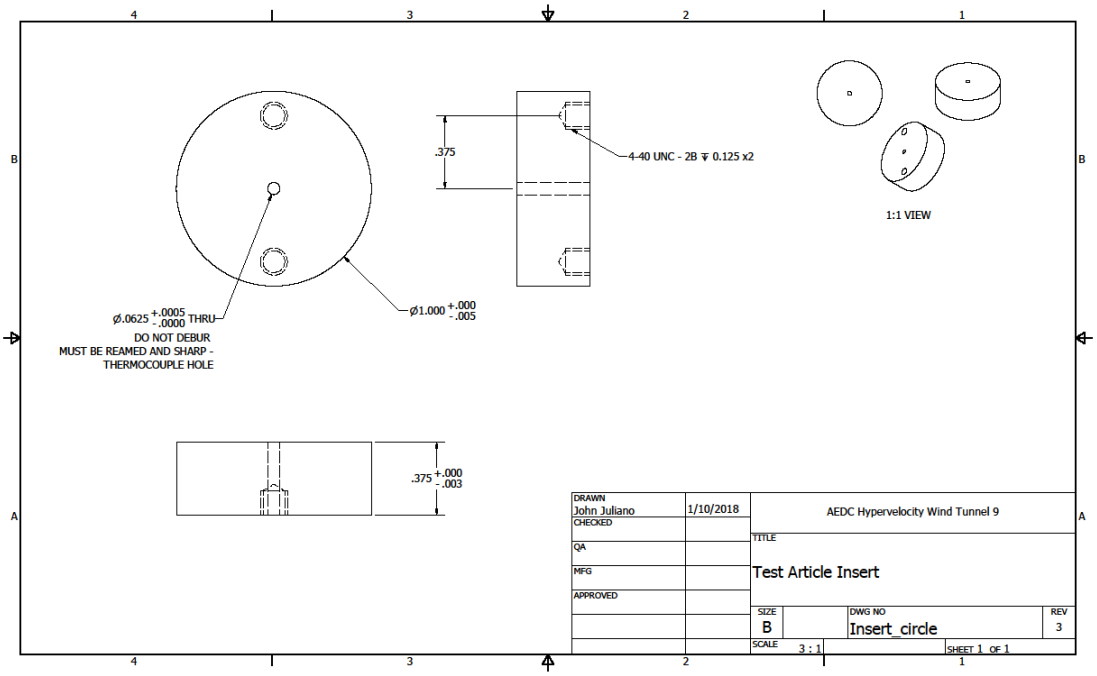

Figure 15: Dimensioned drawing of test article insert

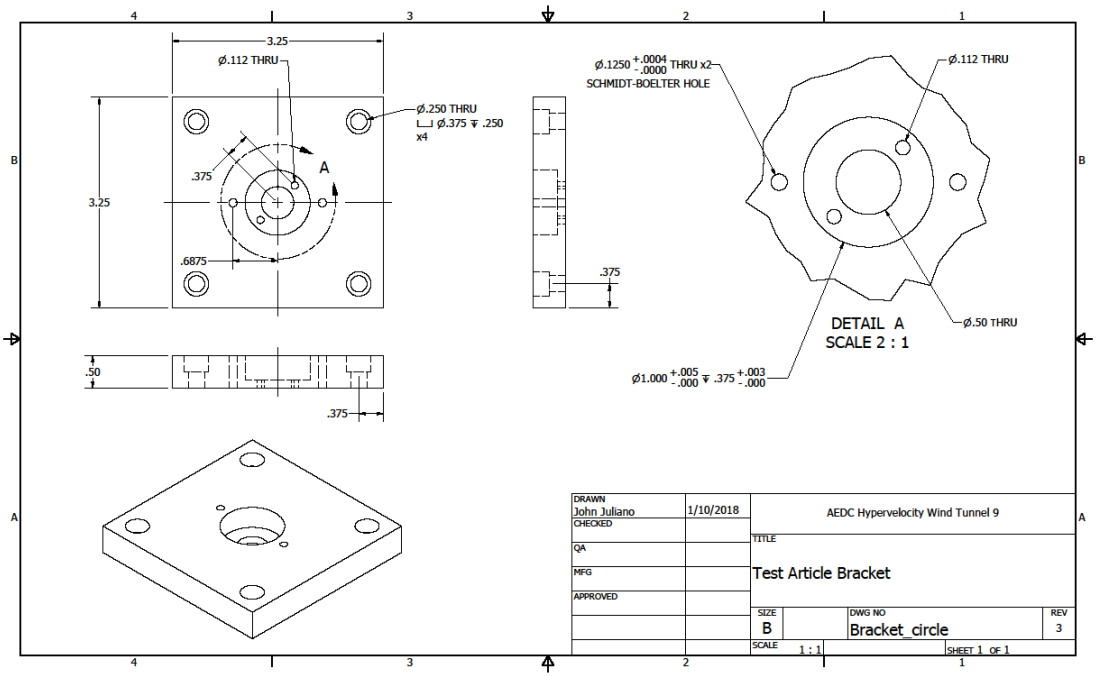

Figure 16: Dimensioned drawing of test article bracket

Test Article Insert

The main piece of the assembly is a steel insert at the center of the test article. The article is made from 17-4 PH stainless steel. Test articles in Tunnel 9 are almost entirely made from 17-4 PH or 15-5 PH stainless steel[8]. The test article is 1 in. in diameter to give enough space to image TSP. It is also 0.375 in. thick to imitate a general wall thickness used in Tunnel 9.

The insert is instrumented with a single .061 in. outer diameter Type E coaxial thermocouple, which was supplied by Tunnel 9. This is an identical sensor to ones that are used in Tunnel 9.

The gage is affixed into a slip-fit hole using a Loctite adhesive. Again, this is consistent with the method used to install coaxial thermocouples into a Tunnel 9 test article[8] and was completed by the Tunnel 9 Test article Technician.

The insert is affixed to the bracket using 4-40 screws. The threaded holes for these screws are shallow, to not affect the wall thickness and heat transfer on the insert.

Test Article Bracket

The test article bracket is made from aluminum. It does not hold any coaxial thermocouples and therefore does not need to match (or nearly match) the thermal properties of the thermocouple. The bracket was designed to hold the test article insert and attach to the test frame. It is a square piece that is 3.25 in. on each side. This is slightly larger than the outlet of the vitiated heater.

The bracket has a 1 in. pocket in the center where the insert sits. The center of the pocket is drilled through to allow the thermocouple wire to pass through. There are also two other holes in the pocket to secure the insert to the bracket.

On the surface of the bracket are four countersunk holes used to bolt the bracket to the test frame. The holes are countersunk to keep the bolt heads out of the flow, protecting the structural integrity of the bolts, and the ensuring little effect on the flow.

The bracket is instrumented with two Schmidt-Boelter sensors located 3/16 in. from the edge of the steel insert. They are also affixed into a slip-fit hole using a Loctite adhesive. All three sensors on the plate are located on a line. Because the plate is symmetric, this line of sensors can either be placed perpendicular to the flow direction or streamwise. The test article was machined in the Tunnel 9 machine shop and instrumented in the Tunnel 9 instrumentation shop.

Test Article Instrumentation Positions

An image of the test article with all part locations and sensor locations is shown in Figure 17.

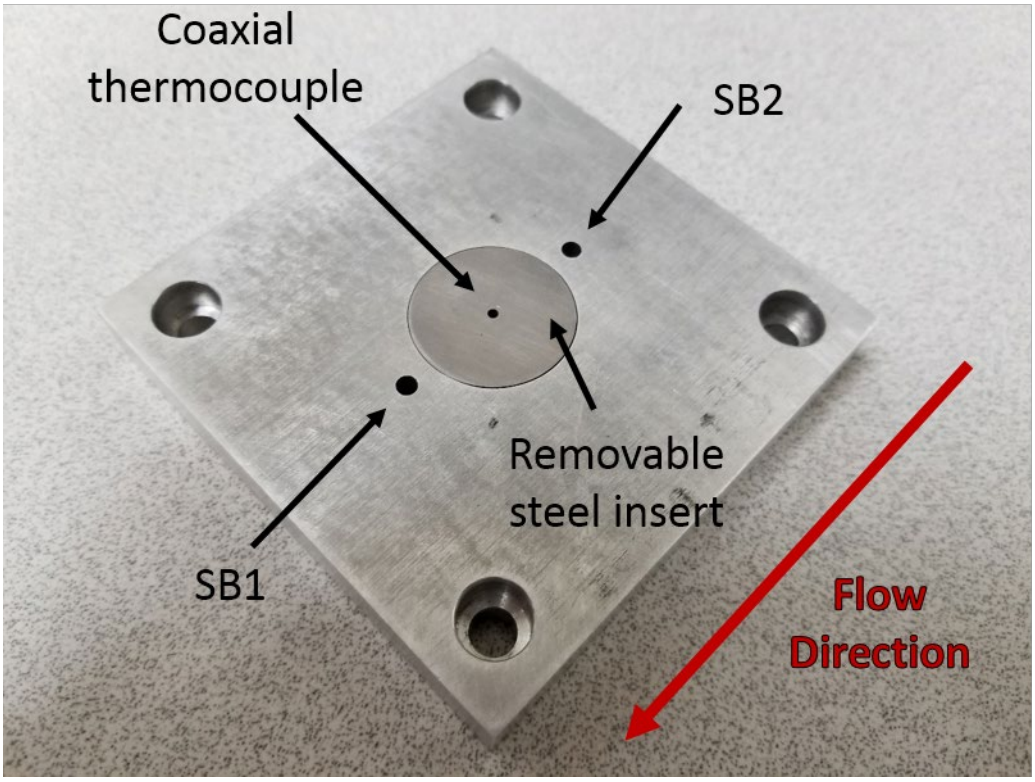

Figure 17: Diagram of Test Article with All Parts and Sensors Called Out

During preliminary testing, the optimal test article orientation was determined. The test article was designed such that the sensors were always co-linear. The line connecting all sensors could either be parallel to the flow or perpendicular to the flow due to the symmetry of the test article.

It was determined during preliminary testing that to get the most repeatable results the sensor line must be parallel to the flow. With the sensors perpendicular to the flow, the Schmidt-Boelters were outside the core flow of the heater and did not produce repeatable results.

For testing, SB2 was located upstream of the coaxial thermocouple, and SB1 was located downstream of the thermocouple. The notation SB1 and SB2 was based on the serial number of the sensors, and not the sensor locations.

Schmidt-Boelter Control Sensors

As shown in Figure 17, the two Schmidt-Boelter sensors are not located on the test article insert. The insert was the only part that was painted, making the 2 Schmidt-Boelter sensors the control sensors. The arrangement of the Schmidt-Boelter sensors did not change for each test series once a final arrangement was determined.

Test Section

The test section was affixed to the structure for the vitiated heater, and a diagram can be seen in Figure 18.

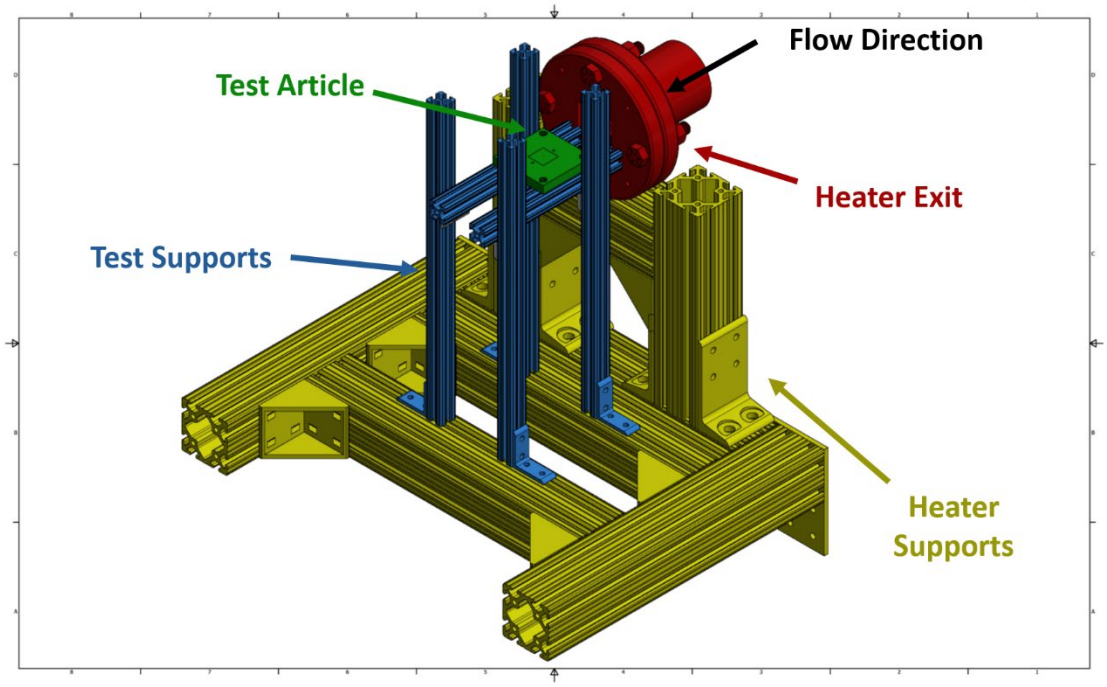

Figure 18: Test section assembly diagram

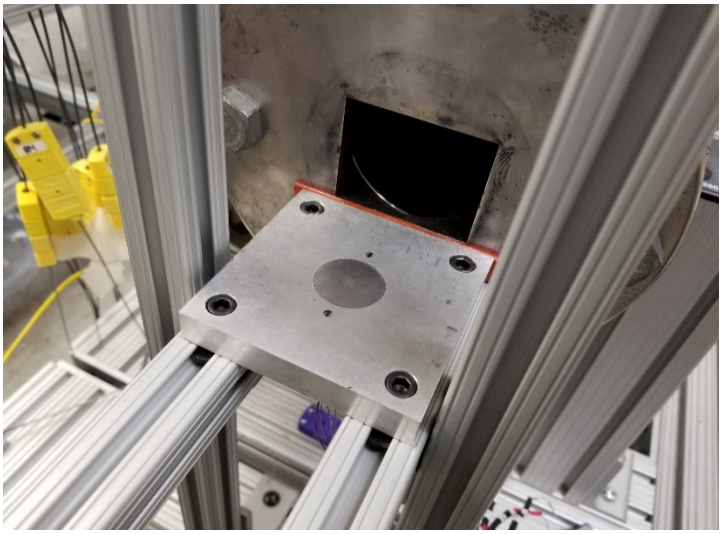

Figure 19: Test article placement and seal mechanism

The test section is open, and preliminary tests showed that this can give us a repeatable result, so no additional pieces were needed to close the test section. The test section was designed as an open test section for the ease of construction and installation, as well as the ease of optical access.

The top of the test article was co-planar with the bottom of the heater outlet. The test article was placed flush with the front face of the heater outlet, and a gasket seal was used to make sure no cold flow from below the test article comes up and is entrained with the hot flow. A picture of the test article placement is seen in Figure 19.

TSP Application

For this experiment, temperature sensitive paint was applied to the steel insert shown in Figure 15, but not the aluminum bracket shown in Figure 16. The paint was applied to the entire surface of the steel insert, including the exposed surface of the coaxial thermocouple.

All paints were mixed in the application lab on the day of painting, and the active layer used in this experiment is the same formulation used for a typical Tunnel 9 test.

The insert was painted in the Tunnel 9 TSP Application Lab by a trained paint technician. The paint was applied in two parts. First a base layer was applied using a pneumatic spray gun and allowed to set. Then the active TSP layer was applied onto the base layer using a clean pneumatic spray gun. The painted insert was then allowed to cure for at least 24 hours prior to testing. A comparison image of a painted vs. unpainted steel insert is seen in Figure 20.

Painting a sample typically takes 2-3 days or longer depending on the availability of the Tunnel 9 paint application lab. Because of this, each test series was completed on different weeks. Again, the control Schmidt-Boelter sensors were used to normalize all heating input conditions to the baseline heating conditions and did not change throughout the testing.

Figure 20: Comparison of Unpainted (left) vs. Painted (right) Test article plate

Paint Thickness Measurements

Paint thickness measurements were completed using a Fischer MP40 E-S Dual scope magnetic induction probe which was calibrated to the sample before any paint was applied. It was more difficult to obtain the target paint thicknesses than anticipated, and the paint thicknesses tested differed from the test plan. The actual paint thicknesses tested are shown in Table 2.

Table 2: Actual Paint Thicknesses Tested in Testing Order

Testing Series	**Paint Thickness (mil)**	**Standard Deviation (mil)**
100	0	0
200	1.65	0.09
300	2.75	0.23
400	1.98	0.21

The test plan included one paint thickness that was representative as an average paint thickness used in Tunnel 9, one thinner paint layer and one thicker paint layer. The thinner paint layer was not obtained for use in this experiment.

Analog Data Acquisition

Data collection was done using 2 separate systems: a data acquisition system for all analog signals and a TSP 2-camera system.

Analog data was captured using an HBM Genesis 5i High Speed Data Acquisition System. All discrete instrumentation, trigger information, and camera frame information were captured on the HBM for this experiment.

All data was recorded at 10,000 samples per second and down-sampled in post processing. All gage information (Schmidt-Boelters and thermocouples) used a 100 mv span, and all triggers and frame information used a 20 V span. Data was analog filtered with a low pass filter at 1 kHz, and further filtered in data reduction.

Thermocouple Data Acquisition

There are 3 total thermocouples on the test which include one coaxial thermocouple on the insert, and two thermocouples (as a part of a Schmidt-Boelter sensor) on the bracket. All thermocouples are type E. The two thermocouples on the bracket were connected to the HBM using Omega Reference Junctions. The coaxial thermocouple was not connected to a reference junction. The thermocouple leads were soldered to copper wires, and then wired into the HBM. As shown later, the coaxial thermocouple was referenced to the thermocouples on the Schmidt-Boelter sensors to obtain the referenced temperature measurement.

Schmidt-Boelter Data Acquisition

Each Schmidt-Boelter has two outputs, one direct read heat transfer sensor, and one thermocouple. The thermocouples, as mentioned above, were wired through reference junctions to the data acquisition system. The direct-read heat transfer gages are analog sensors and were wired directly to the data acquisition system.
Two Schmidt-Boelter sensors were used, and the calibration constants for those sensors are given in Table 3.

Table 3: Schmidt-Boelter Calibration Constants

Gage Name	**Serial #**	**SF Absorbed**	**Tau***

SB1	2582	4.234	0.0154
SB2	3363	2.690	0.0123

The calibration constants will be used to calculate the heat transfer on the gage, and to correct the temperature output. That will be described in more detail below.

Trigger Data Acquisition

The vitiated heater control system outputs a 5V rising step trigger when the main fuel solenoid valve is opened. This trigger is input into the HBM data acquisition system and the TSP cameras. It was used to begin data collection on both devices. The HBM uses a buffer to collect data, and therefore begins data collection two seconds before the trigger.

TSP Frame Information Data Acquisition

The TSP cameras emit an analog output related to the state of the electronic shutter. When the shutter is open, and the camera is exposing, the output reads 5V, and when the shutter is closed the output reads 0V. The camera exposure data was connected directly to the HBM and used in TSP data reduction to synchronize the time of the camera exposure to the HBM thermocouple data time.

TSP Data Acquisition

Cameras

TSP Data collection was done using a pair of Princeton Instruments ProEM 512B EMCCD Cameras. The cameras are operated, and the data is collected using a

single desktop computer, running Princeton Instruments Lightfield software. The camera is connected to the computer for data transfer and camera control using a gigabit ethernet data interface.

Both cameras were mounted on tripods and pointed towards the sample in the test section. Each camera had a 25 mm c-mount lens attached, which was manually focused and locked prior to the runs. Camera apertures were set as open as possible (f\1.4) to allow as much signal as possible into the camera. One lens had a red filter, centered at 614 nm, and the other lens had blue filtered, centered at 450 nm.

Illumination

The sample was illuminated using a Tunnel 9 UV-LED. The LED was designed at AEDC and is a similar version to the one used in Tunnel 9. A 365 nm UV filter was affixed to the light, to block any blue-light emitted by the LED. The light cannot be controlled remotely in this setup, so it was powered on before the testing bay was secured for testing.

To reduce noise, and increase the usable signal recorded by the cameras, the lights in the testing bay and the control room were dimmed. This reduced the number of reflections that could affect camera measurements[7].

An image of the experimental setup including both cameras and the UV-LED is shown in Figure 21.

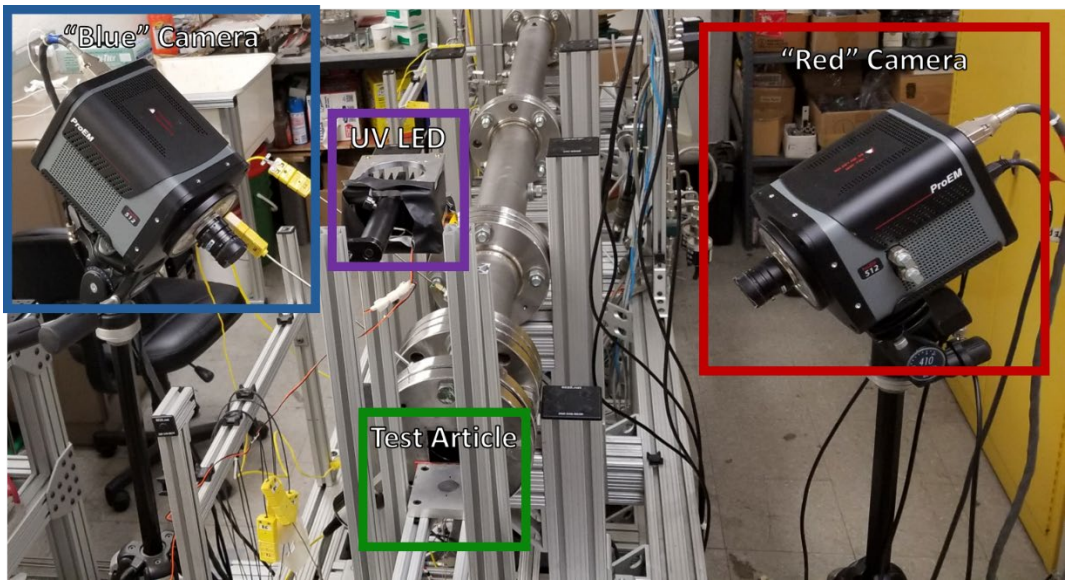

Figure 21: TSP Experimental Setup Including Both Cameras and the Illumination System

Data Sets

To fully reduce TSP 3 data sets are needed[15]:

1. Dark Image Set: A set of images with the UV-LED and all room lights turned off. This data set only contains any stray light that could not be eliminated, and background offset inherent to the sensor that could be picked up by the camera and can be subtracted from the data.
2. Reference Image Set: A set of reference images with the UV-LED powered on, but no heating. A reference intensity and temperature are needed to complete a TSP calibration
3. Run Image Set: A set of run data. This data is one where the UV-LED is on and the test sample is heated. This data will be compared to the reference image to determine the ratio-of-ratios, and the temperature calibration

A set of dark images were taken at the beginning of each day of testing. A set of reference images were taken before each run because the initial temperature of the sample could vary by a few degrees during a single day.

Discrete Sensor Data Reduction

Raw Data Preparation

The raw data was sampled at 10k S/s. However, to match the data reduction at Tunnel 9, this was first down sampled to 500 S/s. The trigger responses were not down sampled, to ensure accuracy.

After down-sampling, all data were filtered using a 6th order Butterworth filter applied in forward and reverse directions for a zero-phase shift. All down-sampled data were digitally filtered to 3 Hz.

Temperature Calibration

The temperature calibration was done using a similar data reduction method to the one used for a Tunnel 9 test[16]. To compute the temperature at all thermocouples, we first find the average pre-run tare in mV. The pre-run tare is the average raw output of the sensors for the first 0.2 seconds of data collection, before the main fuel solenoid valve is opened. It is assumed that the test article hardware was isothermal prior to each test.

$$\mathrm{MV}_{\mathrm{thermocouple,PRT}} = \sum_{t=0}^{0.2} \mathrm{MV}_{\mathrm{thermocouple}}$$

The tared value of each thermocouple can then be found by subtracting the pre-run tare (PRT) from the filtered raw reading.

$$\mathrm{MV_{thermocouple,tared}} = \mathrm{MV_{thermocouple}} - \mathrm{MV_{thermocouple,PRT}}$$

Now, the average tare value of each thermocouple with a reference junction is found[16].

$$\mathrm{MV_{RJ,PRT}} = \frac{\mathrm{MV_{RJ1,PRT}} + \mathrm{MV_{RJ2,PRT}}}{2}$$

The average reference junction tare is now added to each tared thermocouple, to give a value that can be entered into a typical thermocouple table.

$$\mathrm{MV_{thermocouple,referenced}} = \mathrm{MV_{thermocouple,tared}} + \mathrm{MV_{RJ,PRT}}$$

Finally, using the NIST International Temperature Standard of 1990 (ITS 90) lookup table[17], we can calculate the temperature in degrees Fahrenheit for all thermocouples.

$$\mathrm{T_{thermocouple}} = \mathrm{ITS90}\left(\mathrm{MV_{thermocouple,referenced}}\right)$$

Schmidt-Boelter Temperature Correction

Schmidt-Boelter sensors have a temperature correction to the raw value (before using the ITS 90 tables to look-up temperature values). The temperature correction factor, $\mathrm{TC_{SB}}$, can be written as:

$$\mathrm{TC_{SB}} = 4.799 \times \mathrm{SF_{absorbed}}$$

And the corrected temperature can then be calculated as:

$$\mathrm{T_{SB,corr.}} = \mathrm{T_{SB}} + \mathrm{MV_{SB,tared}}\mathrm{TC_{SB}}$$

The equations for the reduction of Schmidt-Boelter Data are given by the AEDC Heat Lab.

Thermocouple Heat Flux Calculation

The heat flux for thermocouples is calculated in the same way for this experiment as it would be for a test in Tunnel 9. It is generally assumed that the convective heat input at a location is equivalent to the one-dimensional heat conducted at the surface of the test article wall.

The heat transfer of the thermocouples is completed using a solution of the transient one-dimensional heat conduction equation which is given by[8]:

$$\frac{\partial \mathrm{T}}{\partial \mathrm{t}} = \alpha \frac{\partial^2 \mathrm{T}}{\partial \mathrm{x}^2} = \left(\frac{\mathrm{k}}{\rho \mathrm{C_p}}\right) \frac{\partial^2 \mathrm{T}}{\partial \mathrm{x}^2}$$

Heat flux can then be given by:

$$\dot{Q} = k \frac{\partial T}{\partial x}\Big|_{x=0}$$

The heat flux was calculated using a MATLAB function (QCALC96.m) that is used at Tunnel 9.

For this calculation, the material properties are known. It is assumed that the material properties of the coaxial thermocouple do not appreciably differ from the material property of the steel substrate, and the material properties of steel are used in the calculation. The material properties of the 17-4PH steel used in this experiment are given in Table 4[8].

Table 4: Thermal Material Properties of 17-4PH Stainless Steel

Property [units]	**Value or Equation**

Density [lbm/in^3]	0.315
Thermal Conductivity [BTU/(in.-s-°F)]	$1.13 \times 10^{-7}T + 2.08 \times 10^{-4}$
Specific Heat [BTU/(lbm-°F)]	$4.45 \times 10^{-8}T^2 + 3.38 \times 10^{-5}T + 1.04 \times 10^{-1}$

Schmidt-Boelter Heat Flux Calculation

The calculation of heat flux from the Schmidt-Boelter data is also done in the same way as it is in Tunnel 9[16]. The reduction uses the calibration data given in Table 3. The equation is given as

$$\dot{q} = \left(MV_{SBA} + \tau^* \frac{dMV_{SBA}}{dt}\right) \times SF_{ABSORBED}$$

where MV_{SBA} is the raw sensor reading of the Schmidt-Boelter A channel, τ^* is the calibration time constant from Table 3 and $SF_{ABSORBED}$ is the absorbed scale factor from Table 3.

TSP Data Reduction

TSP Data reduction has five main steps:

1. Prepare Raw Data
2. Ratio raw data to create ratio of ratios
3. Create calibration from raw data and reduced thermocouple data
4. Calibrate TSP data to obtain temperature
5. Calculate heat flux from TSP temperature history

The data reduction method used here is similar to the one used by Kurits and Norris for a two color TSP system in Tunnel 9[7].

Raw Data Preparation

First, the dark images are averaged and subtracted from the reference image sets and the run image sets. This removes artifacts from the data by subtracting any features that are constant and not related to the TSP system. The dark images are averaged in the following manner:

$$I_{dark,color}(x,y) = \frac{1}{(t_2 - t_1)} \sum_{t=t_1}^{t_2} I_{dark,color,raw}(t,x,y)$$

Then the set of reference data and run data can be calculated as:

$$I_{ref,color,sub}(t,x,y) = I_{ref,color,raw}(t,x,y) - I_{dark,color}(x,y)$$

$$I_{run,color,sub}(t,x,y) = I_{run,color,raw}(t,x,y) - I_{dark,color}(x,y)$$

Next, the reference data can be averaged over time. As the test article is static, the reference images should all be relatively equal, and an average is done to eliminate any major outliers.

$$I_{ref,color,avg}(x,y) = \frac{1}{(t_2 - t_1)} \sum_{t=t_1}^{t_2} I_{ref,color,sub}(t,x,y)$$

For each run and each camera, a region was manually selected around the center of the test article (at the location of the coaxial thermocouple). The emission intensity in that region was averaged for each frame, creating a single temporally varying value of light intensity for each camera and each run. Spatially varying data was collected for each run, but as the focus of this research is at a single point, it was

not analyzed as part of this research. The equations for the spatial averaging for all three data sets are shown below, where x_1, x_2, y_1, and y_2 are determined manually, and I is the intensity recorded by the camera. There is one for each color (red and blue).

$$I_{ref,color} = \frac{1}{(x_2 - x_1)(y_2 - y_1)} \sum_{x=x_1}^{x_2} \sum_{y=y_1}^{y_2} I_{ref,color,avg}(x, y)$$

$$I_{run,color}(t) = \frac{1}{(x_2 - x_1)(y_2 - y_1)} \sum_{x=x_1}^{x_2} \sum_{y=y_1}^{y_2} I_{run,color,sub}(t, x, y)$$

At this point, all raw data has been prepared for the next step of the data reduction, and there are two reference sets of images (one for each color) and two run sets of images.

Calculation of Ratio of Ratios

Now using the values of the reference intensity, and the run intensity over time, we can calculate the ratio of ratios for all times. The ratio of ratios (RR) is calculated in the following way

$$RR(t) = \frac{I_{run,R}(t)/I_{ref,R}}{I_{run,B}(t)/I_{ref,B}}$$

Where R stands for the red images, and B stands for the blue images.

Calculation of Temperature

It is assumed that the temperature gradient through the paint layer is linear. Because of this, the heat flux at the surface of the TSP layer and the heat flux at the surface of the steel test article are assumed to be identical[6]. Therefore, the

temperature that will be used for the calibration is the temperature at the surface of the steel test article, recorded by the coaxial thermocouple.

Using the TSP frame information that was collected on the HBM, the exact time that each frame was exposed is known. This can be used to extrapolate the temperature data from the coaxial thermocouple at those exact times. The temperature can then be plotted vs. the recorded ratio of ratios at a similar time. An example calibration for this is seen in Figure 22.

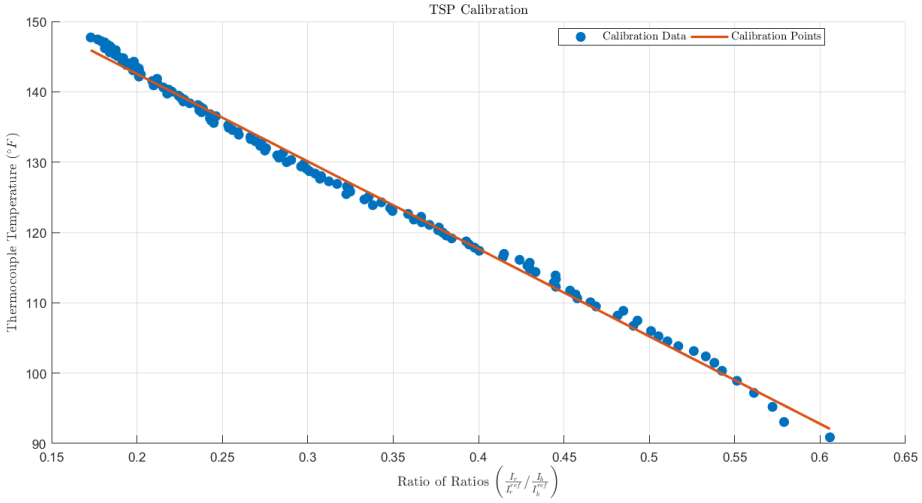

Figure 22: Example Calibration of Temperature vs. Ratio of Ratios Including a Linear Curve Fit Calibration

Once the ratio of ratios and coaxial thermocouple temperature are known, an in-situ calibration can be completed by fitting a first order polynomial to the data. The polynomial curve fit is done using a least-squares fit.

The least-squares fit was computed in MATLAB using the polyfit function. A higher order fit is possible and has been used in the past at Tunnel 9 to increase accuracy but was ignored in this case.

Calculation of Temperature

The temperature can be computed for TSP data by evaluating the calibration polynomial at the given values of ratio of ratios. Some slight modifications typically need to be made to ensure the heat transfer values will be correct when computed. TSP calibrations typically do not intersect with the pre-run reference temperature. This means that while temperature data during the heating of the test article matches well with the coaxial thermocouple, the reference temperature does not. This is shown in Figure 23, where the TSP reference temperature is nearly 30°F lower than the reference temperature recorded by the thermocouple.

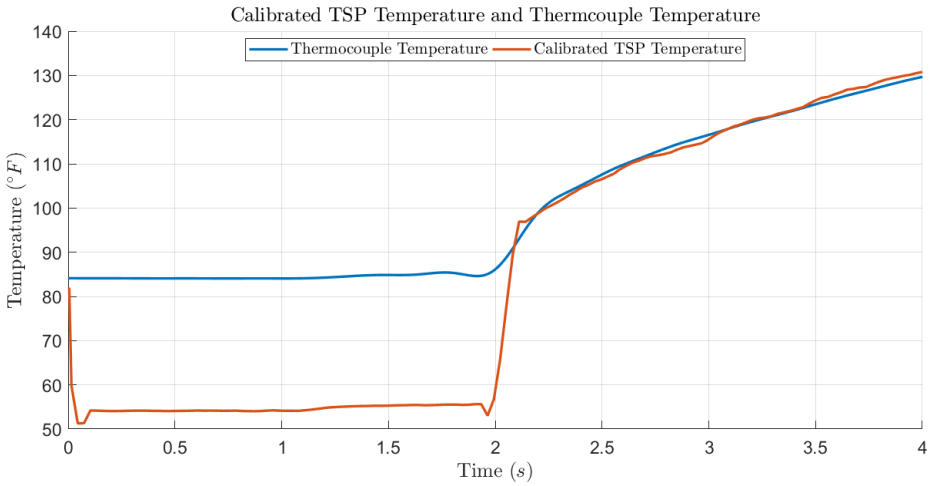

Figure 23: Example of Calibrated TSP Temperature Data vs. Coaxial Thermocouple Temperature Data

A difference of this magnitude would have an effect on the heat transfer calculation at the moment of initial heating. To remove the discrepancy, a series of TSP frames are selected to be forced to the reference temperature of the thermocouple.

Figure 24 shows the result of forcing the reference temperature for the first few frames of the run. The temperature history is a close match at the beginning of the run.

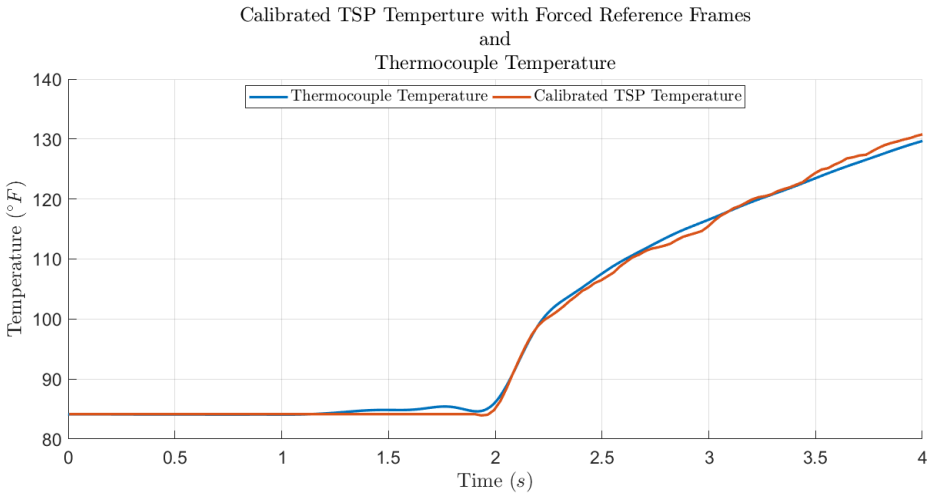

Figure 24: Example of Calibrated TSP Temperature Data with Forced Reference Frames vs. Coaxial Thermocouple Temperature Data

After the forced reference temperature frames, some frames are interpolated linearly between the reference temperature and the first calibrated temperature point to replace data corrupted by the tunnel startup.

Heat Flux Calculation

As the calibration is done using the temperature at the surface of the steel test article, the heat flux calculation is identical to the one used for the coaxial thermocouple in a previous chapter.

For a typical Tunnel 9 run, the heat transfer is computed at each pixel individually. For this experiment however, the data was averaged to create a single TSP value for each frame at the center of the test article inlet. For this experiment, the heat transfer for that single point is computed.

Because the temperature is assumed to be calibrated to the temperature of the steel surface, the material properties of steel are used for this calculation.

Uncertainty Calculations

Discrete Instrumentation Uncertainty

The discrete instrumentation used during this experiment was identical to the instrumentation used in Tunnel 9. A historic study of the Tunnel 9 discrete instrumentation was done and determined that the uncertainty of Tunnel 9 discrete heat transfer sensors was ±6%[18]. This was used as the bias for all discrete instrumentation.

TSP Uncertainty

The equations for the uncertainty of TSP was taken from the Tunnel 9 TSP alogorithm[16]. First, at every data point in a run the difference between the TSP calculated heat flux value and the thermocouple calculated heat flux value is computed.

$$\delta = abs(TC - TSP)$$

Then, the TSP addition of uncertainty can be found by taking the standard deviation of the heat flux difference, δ

$$\sigma_\delta = std(\delta)$$

Finally, that can be combined with the 6% bias term for discrete heat flux uncertainty to obtain the TSP uncertainty value for a single run. The general form of the uncertainty equations is[19],

$$UNC = \sqrt{UNC_{BIAS}^2 + UNC_{PRECISION}^2}$$

For Tunnel 9 TSP, this can be shown as:

$$UNC = \sqrt{(.06 \times \dot{q})^2 + (2 \times \sigma_\delta)^2}$$

Precision Calculation

For each case, multiple tests were run to develop statistics, and calculate the uncertainty based on the student-t distribution. For each value, the precision is calculated in the same way. First, the standard deviation is found where N is the number of samples, x is the heat flux and $\bar{x}$ is the mean n

$$\sigma = \sqrt{\frac{1}{N-1}\sum_{i=1}^{N}(x_i - \bar{x})^2}$$

Next, using the student-t inverse probability tables with the correct number of degrees of freedom, the precision value can be found.

$$p = \frac{\sigma}{\sqrt{N}}$$

Finally, the precision can be added to the bias to get the final uncertainty as shown above.

Chapter 4: Experimental Results

Testing was completed between June 29, 2018 and July 30, 2018. A total of 177 vitiated heater tests were completed. A full matrix of these tests can be found in Appendix A. The baseline testing was completed first, followed by 3 test series of samples with different thicknesses. Not all testing was completed in one entry due to facility availability, but all testing of a single series (paint thickness) was completed in one entry.

Testing resulted in two major findings which will both be discussed at length in this chapter. The first finding is that the application of TSP on a test article can create a bias in the discrete sensor measurements that is a function of the paint thickness and the magnitude of the heating input. The second finding is an alternate calibration method is defined that can greatly improve the accuracy and reduce the uncertainties of TSP heat transfer measurements in the case where a sudden drop in heat transfer occurs. This comes from an in-depth characterization of the measurements made using temperature sensitive paint with respect to the heating input and the paint thickness.

Baseline Testing

The baseline testing was completed first to fully define the three heating conditions used and investigate the repeatability of the vitiated heater facility. Baseline testing consisted of 36 tests, consisting of separate vitiated heater runs.

Baseline Testing Coaxial Thermocouple Results

First, we can look at the average heat flux response of the coaxial thermocouple to each heating condition. Figure 25 shows the coaxial thermocouple response to the baseline testing for all three conditions.

The three conditions are characterized by a sharp rise in heat transfer at the beginning of the test, followed by a section of nearly constant heat transfer, and finally a steep decline in heat transfer back to a near adiabatic behavior.

Figure 26 shows that the temperature change is characterized by a quick, steep rise in temperature followed by a rise in temperature of a near-constant slope. After the portion of constant temperature rise, another steeper section of temperature rise occurs, followed by an abrupt loss in temperature and a decay back to ambient temperature.

The total test time for each heating condition was determined by the facility temperature limit. Figure 26 shows that the total change in temperature was roughly the same for all three conditions. The higher heating conditions clearly do not reach a steady state condition in heat transfer before the facility is shut down, and the lower heating conditions are much steadier. This is because the facility temperature limit was reached very quickly for the higher heating conditions, and those conditions could not be run for a longer period to allow the heat flux to settle.

Figure 25 shows that for each condition there is a small spike in heat flux at the beginning and end of each test which is also seen in the slope of the temperature for each condition. This spike increases in relative magnitude as the overall heating increases. The spike is due to a small buildup of hydrogen combusting suddenly at the

beginning of the test, or it could be related to the relatively low cutoff frequency for the low pass filter. The spike seen does not affect the data we are most interested in, so it is largely ignored in this research.

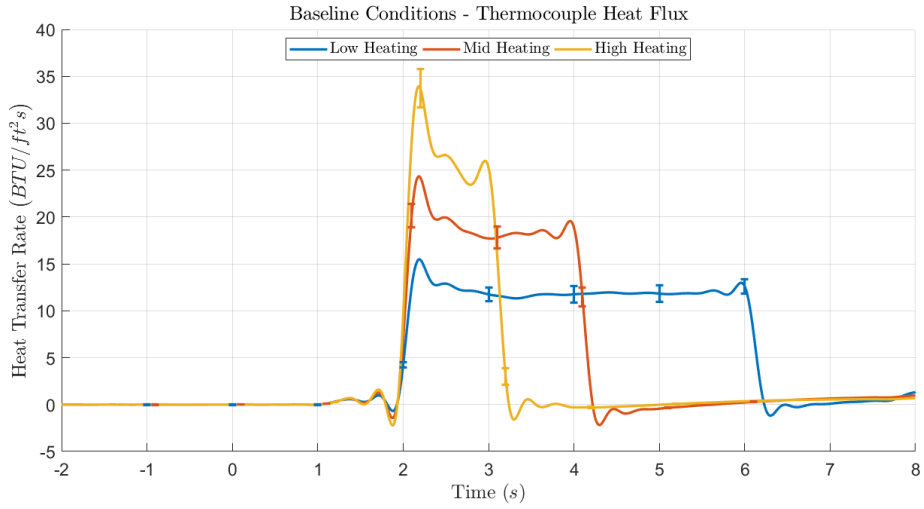

Figure 25: Thermocouple Heat Flux Response to Baseline Testing for all Three Heating Conditions

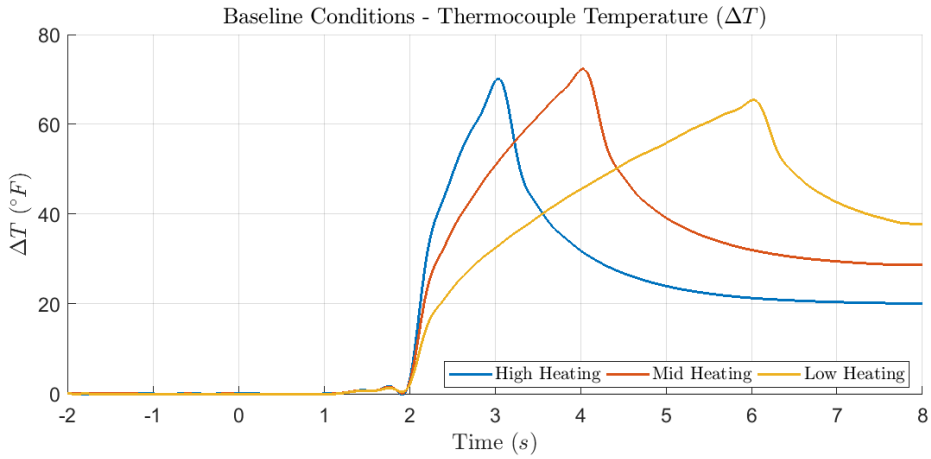

Figure 26: Coaxial Thermocouple Temperature Response to Baseline Testing for all Three Heating Conditions

The uncertainty in heat transfer rate shown in Figure 25 is a combination of the typical thermocouple uncertainty used at Tunnel 9 for coaxial thermocouples[18]

and the precision of the condition found using the standard deviation of the series of tests and the Student's t inverse cumulative distribution function.

Table 5 shows the number of runs used to characterize each condition, the average heat flux as measured by the coaxial thermocouple in the good flow region, and the precision of that good flow heat flux. The average heat flux for the three conditions roughly reflect the desired conditions of 10, 20 and 30 BTU/ft^2-s. The high heating condition does not quite get to 30 BTU/ft^2-s, but this was deemed the highest heat flux that could be generated in a near-steady fashion by the vitiated heater. It can already be seen that the high heating condition is the least steady of the three and increasing the heat flux would have decreased the test time, and likely raised the uncertainty. Because of this, the maximum heat flux was lowered to about 25 BTU/ft^2-s.

The precision of each condition is better than ±1.5% of the mean value. This is quite low considering the uncertainty assumed for heat flux measurements using coaxial thermocouples is 6%[18]. This uncertainty was much lower than expected.

The precision of the thermocouple for baseline testing improves as the heating condition increases. This trend was not consistent throughout the test, and is likely a coincidence here, but for all testing the precision was lower than ±5% and this was deemed low enough to facilitate good results.

Table 5: Baseline Testing Coaxial Thermocouple Average Results and Precision

Heating Condition	**# of Runs**	**Good Flow Time**	**Average Good Flow Heat Flux (BTU/ft^2-s)**	**Precision – 95%**

				Confidence Interval (% of mean)
Low Heating	5	2.3-5.9	11.9	1.21
Mid Heating	7	2.6-3.9	18.1	1.07
High Heating	11	2.3-2.9	25.4	0.47

Baseline Testing Schmidt-Boelter Results

As mentioned earlier, the Schmidt-Boelter sensors were not on the steel test article insert but were instead placed on either side and remained unpainted for every run. The Schmidt-Boelter sensors were used as reference to ensure that each testing series was done with the same condition (or nearly the same conditions) and were used to normalize the small differences between heating conditions for each testing series to facilitate data comparison.

Figure 27 shows the average heat flux response of the Schmidt-Boelter sensors for each heating condition. First, it can be noted that there are two sensors shown for the medium heating condition and the low heating condition, but only one sensor shown for the high heating case. One sensor needed to be dropped for the high heating case, and this will be discussed in more detail in the next section.

The general trends of the Schmidt-Boelter responses are nearly identical to that seen by the coaxial thermocouple. Each test is characterized by a steep rise in heat flux followed by a nearly steady section of heat flux, and then a steep decline

back to a near-adiabatic condition. In all cases, the spike at the beginning and end of the condition are nearly identical to the spikes shown by the coaxial thermocouple.

SB2 was placed upstream of the sample and SB1 was downstream. The placement explains the increase in measured value by SB2 for the low heating and mid heating case. This trend continues through all testing.

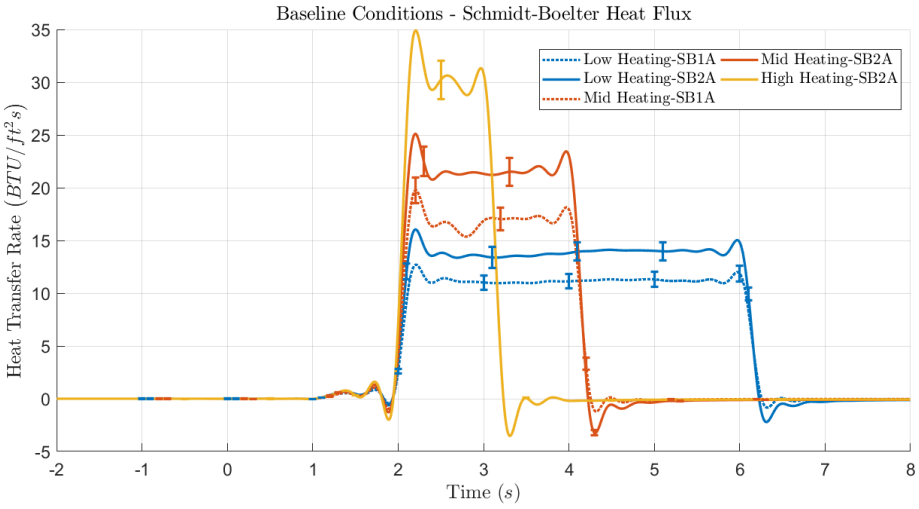

Figure 27: Schmidt-Boelter Heat Flux Response to Baseline Testing for all Three Heating Conditions

Table 5 shows the good flow average heat flux and precision as measured by the Schmidt-Boelter sensors. The precision is worse for the Schmidt-Boelter sensors than for the coaxial thermocouple. For all tests this is generally (but not always) the case. However, all precision is again under ±5%. These measurements are only used for comparing to previous data sets and some small normalizing and therefore this precision was deemed sufficient.

Table 6: Baseline Testing Schmidt-Boelter Average Results and Precision Compared to Thermocouples

Heating Condition	**Average Good Flow Heat Flux (BTU/ft^2-s)**	**Precision – 95% Confidence Interval (% of mean)**

Sensor	**SB1**	**TC**	**SB2**	**SB1**	**TC**	**SB2**
Low Heating	11.2	11.9	13.8	1.07	1.21	1.01
Mid Heating	16.9	18.1	21.3	2.48	1.07	1.64
High Heating	-	25.4	29.8	-	0.47	0.61

Schmidt-Boelter Data Inconsistency

For several heater runs, one or both Schmidt-Boelter sensors would behave in a manner that was inconsistent with the other sensors on the test article, or the general trends of the data. Figure 28 shows an example of this behavior.

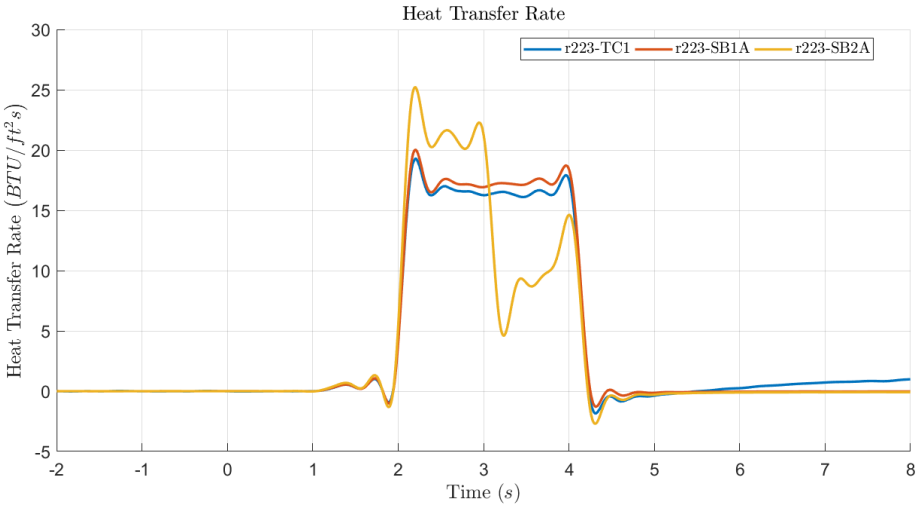

Figure 28: Example of Inconsistency in Schmidt-Boelter Data for a Mid Heating Case

Figure 28 shows an example where SB2 behaves erratically during a mid-heating run. This is a typical example of all cases where this behavior occurred. In all cases the behavior was characterized by a sudden sharp decrease in measured heat

flux. In some cases, the heat transfer measurement would rebound to a more reasonable level, but in most it would stay at a decreased value for the duration of the test.

It is clearly easy to identify sensors that act in this manner because the trends seen by the affected sensor are not mirrored by the other two sensors. In most cases, only one of the two Schmidt-Boelter sensors would be affected, but both sensors were affected at different times during the test. The coaxial thermocouple never showed behavior of this type.

All runs in which this behavior was seen were ignored in the analysis. For the low heating and mid heating condition there were still enough runs to fully define each condition and calculate statistics. For the high heating condition, too many runs resulted in this behavior for SB1 (the downstream Schmidt-Boelter) and therefore it was decided to drop the sensor from the analysis in lieu of dropping nearly all the high heating baseline runs.

Near the end of the baseline testing series it was determined that this issue could be mitigated by cleaning the Schmidt-Boelter sensors with alcohol. It is not fully understood why cleaning the sensors would result in improved performance in this way, but for all future tests the Schmidt-Boelter sensors were cleaned with isopropyl alcohol immediately before each run. This mitigation method was determined near the end of a testing window, and the decision was made to continue with the analysis and drop a sensor from the analysis of the high heating runs because time restrictions did not allow for the repeating of all high heating baseline tests.

The overall spoilage due to sensor inconsistency was 30%. All dropped runs are shown in Appendix A.

Corrections Applied to Data to Account for Varying Input Conditions

While the test setup was identical between baseline testing and all test with paint applied, there were some slight magnitude differences in the heating input. The heating input of the vitiated heater is ultimately set using a hand valve to increase and decrease the pressure of the main hydrogen fuel. This method is not the most accurate and could result in small differences within a test series.

Correction Method

The Schmidt-Boelter sensors were used to generate the correction term applied to reduce any error due to slight changes in input heating condition. For each testing series including the baseline testing series, the Schmidt-Boelter good flow average heat flux was calculated for all available sensors. The correction factor was then determined using the ratio of the series Schmidt-Boelter value, and the Schmidt-Boelter Value of the baseline testing set.

Correction Factors

Table 7: Correction Factors used in Comparing All Test Series with a Painted Sample to Baseline Results

Series	**100** **Baseline**	**200** **1.65 mil**	**300** **2.75 mil**	**400** **1.98 mil**
Low Heat	1	1.001	1.011	0.985
Mid Heat	1	0.983	1.004	0.965

High Heat	1	1.031	1.053	1.028

Table 7 shows the correction factors used for each series and each heating condition. As each test series was compared to the baseline testing series, the baseline series remains unchanged (shown by a correction factor of 1). All other tests had some slight variations. The largest variation was corrected by a factor of 1.053, or about 5.03% of the baseline mean value. This was deemed to be sufficiently small such that a simple correction factor like this could be used and would not cause an increase in uncertainty in the test results.

This correction was applied to all data sets uniformly. After applying the correction, all Schmidt-Boelter data collapsed.

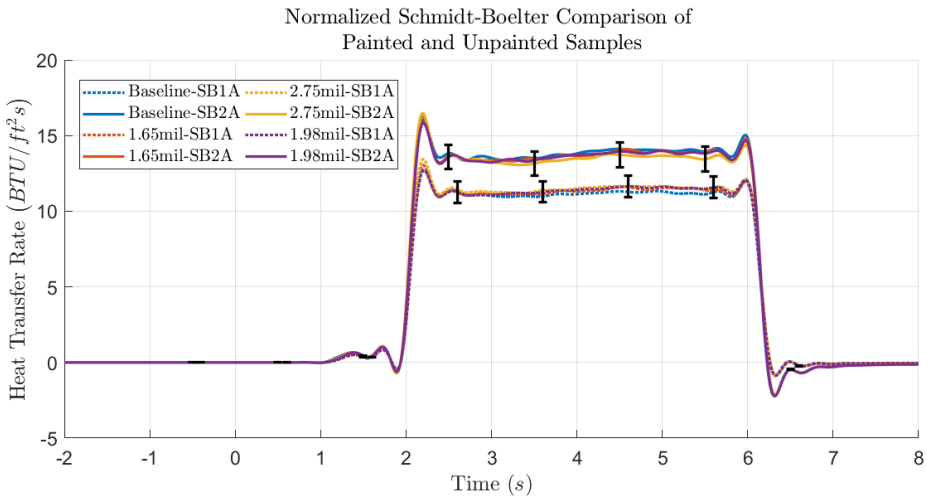

Figure 29: Schmidt-Boelter Data for a Low Heating Case After Correction Factor Has Been Applied

Figure 29 shows an example of Schmidt-Boelter Data for the low heating case. The data clearly collapses for both the upstream (SB2) and downstream (SB1) Schmidt-Boelter sensor. The correction method was also applied to the coaxial thermocouple.

Testing Results of Discrete Sensor Instrumentation with TSP Applied

For all heating inputs and paint thicknesses tested a bias was observed between data from a coaxial thermocouple covered in TSP, and a coaxial thermocouple from the baseline tests (not covered in TSP). Here, the results will be shown separately for each heating condition.

Low Heating Results

Figure 29 shows the Schmidt-Boelter heat transfer rate response for all paint thicknesses used in this test. It can be clearly seen that the two sensors agree within the uncertainty. Once again, the uncertainty reported here is the combination of a 6% uncertainty used for heat transfer sensors from Tunnel 9[18], and the precision determined using the standard deviation of each test series and the Student-t inverse cumulative distribution function.

Again, note that there are two sensors for this heating condition, one upstream of the test article insert and one downstream of the test article insert. For this heating condition both sensors agree well between test series.

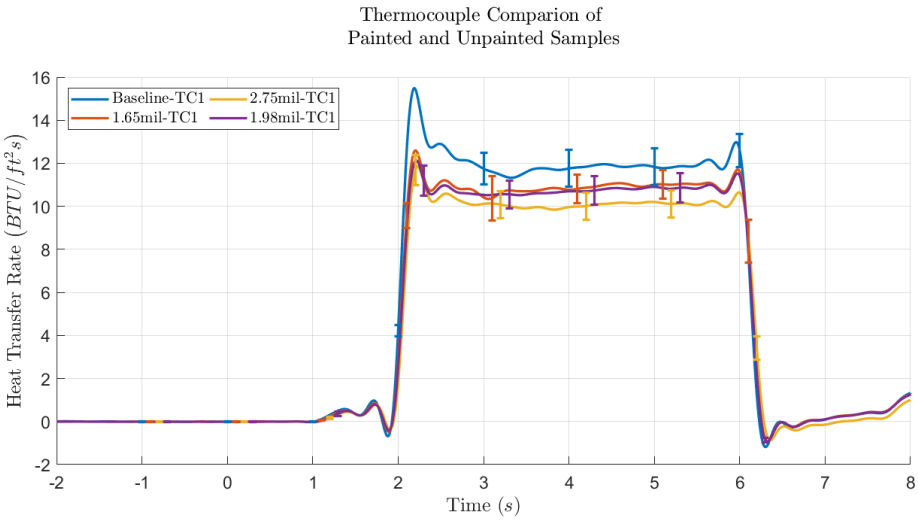

Figure 30:Coaxial Thermocouple Heat Flux Response for all Test Series at the Low Heating Condition

Table 8: TSP-Coated Coaxial Thermocouple Response vs. Baseline Uncoated Coaxial Thermocouple Response at the Low Heating Condition

Test Series	**Paint Thickness**	**Corrected Good Flow Heat Flux (BTU/ft^2-s)**	**Difference in Heat Flux from Baseline Results (%)**
100	-	11.9	0.00
200	1.65	11.0	-7.22
400	1.98	10.7	-9.98
300	2.75	10.2	-14.9

Figure 30 shows the calculated heat transfer rate using the measurements from the coaxial thermocouple underneath the paint. The baseline response from the sensor

is also shown for reference. A clear difference can be seen between runs with a coated thermocouple vs runs without a coated thermocouple. For runs with a lower paint thickness (200 series and 400 series) the data falls within the uncertainty of the sensor, but just barely. However, for high paint thicknesses, the difference falls far outside the uncertainty of the sensor and is a meaningful statistical difference.

Table 8 shows the values of the corrected heat transfer measured by each sensor and the percent difference from the baseline tests. A clear trend is seen, relating the bias introduced in the sensor to the paint thickness.

Mid Heating Results

Once again, Figure 31 shows the corrected Schmidt-Boelter response for each sensor. A small anomaly appeared in the measurements of the downstream Schmidt-Boelter in this case, but it is not believed to have made an effect on the analysis. Again, good agreement within the uncertainty of the sensor is seen for all testing series.

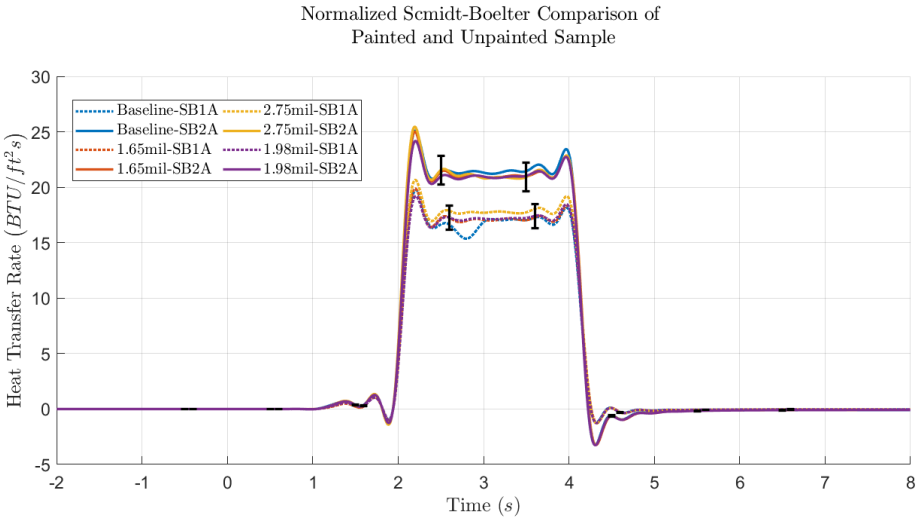

Figure 31: Schmidt-Boelter Heat Flux Response for all Test Series at the Mid Heating Condition

Figure 32 shows the thermocouple response of painted thermocouples at the mid heating condition with the baseline results for reference. Again, a similar trend is observed where the increase in paint thickness increases the bias in the measurement of heat transfer rate seen by the thermocouple. Table 9 shows the tabulated results for the mid-heating condition.

One interesting note is that the bias introduced by applying TSP to the sensor for the mid-heating case is on the same order as the bias seen in the low-heating case. It appears that the bias introduced is more a function of the paint thickness than the magnitude of the heat flux. This will be explored more further on in this section.

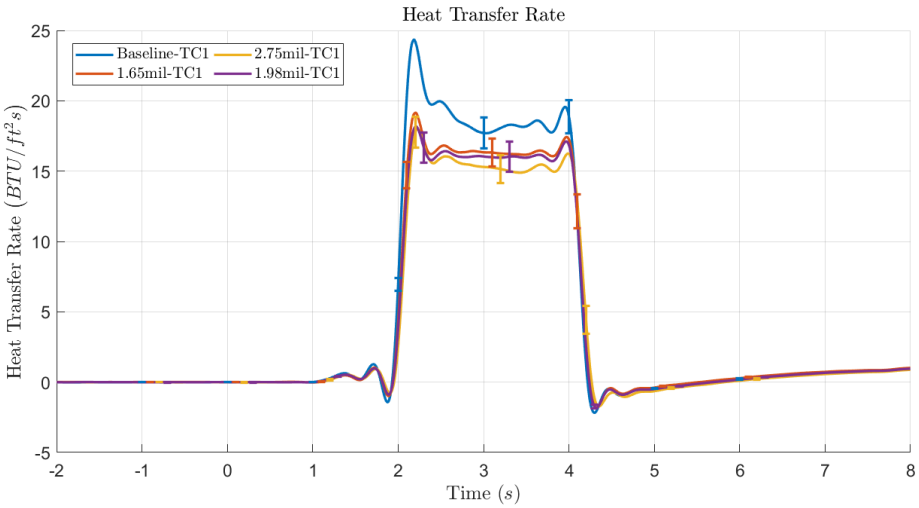

Figure 32:Coaxial Thermocouple Heat Flux Response for all Test Series at the Mid Heating Condition

Table 9: TSP-Coated Coaxial Thermocouple Response vs. Baseline Uncoated Coaxial Thermocouple Response at the Mid Heating Condition

Test Series	Paint Thickness	Corrected Good Flow Heat Flux (BTU/ft^2-s)	Difference in Heat Flux from Baseline Results (%)
100	-	18.1	0.00
200	1.65	16.6	-8.61
400	1.98	16.0	-11.7
300	2.75	15.2	-16.3

High Heating Results

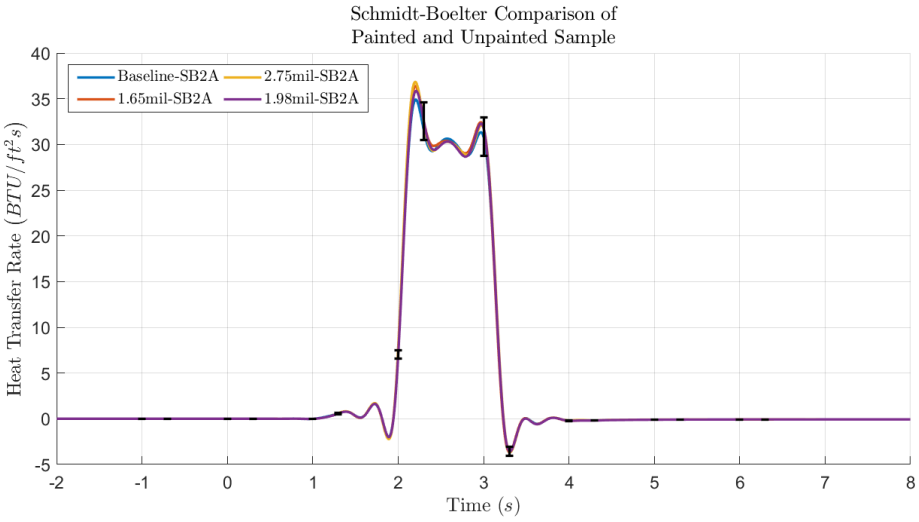

Figure 33: Schmidt-Boelter Heat Flux Response for all Test Series at the High Heating Condition

Figure 33 shows the corrected Schmidt-Boelter response for all cases. Recall that the downstream Schmidt-Boelter sensor was removed from the analysis. No correction factor was higher than 5% for the high heating case, and all general trends agree on the corrected data

Figure 34 shows the coaxial thermocouple response at the high heating condition. And again, shows a similar trend that as paint thickness increases, the bias also increases.

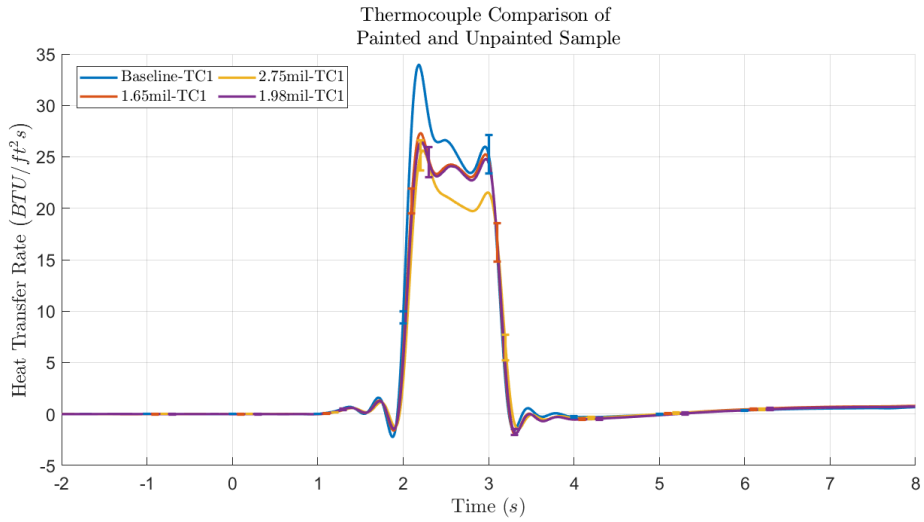

Figure 34:Coaxial Thermocouple Heat Flux Response for all Test Series at the High Heating Condition

Table 10 shows the tabulated data for high heating set of runs. One thing to note here is that bias is slightly different than that seen in the mid-heating and low-heating case. In the high-heating case, the bias is lower for the two thinner paint thicknesses than it was for the mid-heating and low-heating case. However, the bias is higher for the largest paint thickness than it was for the lower heating conditions.

Table 10: TSP-Coated Coaxial Thermocouple Response vs. Baseline Uncoated Coaxial Thermocouple Response at the High Heating Condition

Test Series	**Paint Thickness**	**Corrected Good Flow Heat Flux (BTU/ft^2-s)**	**Difference in Heat Flux from Baseline Results (%)**
100	-	25.4	0.00
200	1.65	24.1	-5.20

400	1.98	23.5	-7.74
300	2.75	21.0	-17.5

Trends in Bias Created by Applying TSP to Coaxial Thermocouple

Table 11: Bias Created by Applying TSP to Coaxial Thermocouple for all Paint Thicknesses and Heating Inputs in Percent of Baseline Mean Value

Paint Thickness	**1.65 mil**	**1.98 mil**	**2.75 mil**
Low Heating	-7.22	-9.98	-14.9
Mid Heating	-8.61	-11.7	-16.3
High Heating	-5.20	-7.74	-17.5

Data gathered from painted and unpainted samples will be used to analyze the thermocouple bias trends.

For all heating conditions the bias increases as a function of the paint thickness, as can be seen in Table 11. For the highest paint thickness (2.75 mil), the bias is also a clear function of the heating input, but this trend does not continue for the 2 thinner paint thicknesses. It is worth noting that the high heating case was the least steady case tested, and the bias seen in the thinner paint thicknesses is within the uncertainty, and therefore may not be meaningful.

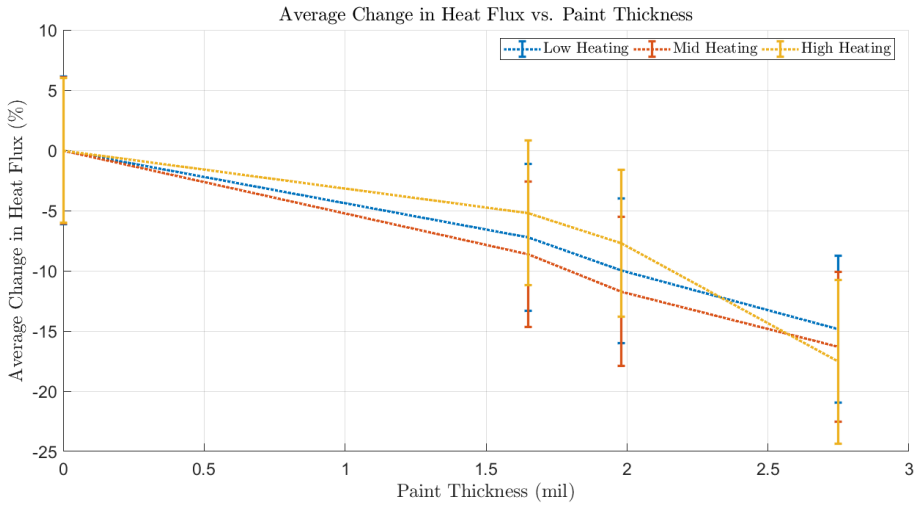

Figure 35: Percent Change in Measured Heat Flux vs. Thickness of Paint Applied to Coaxial Thermocouple

Again, in Figure 35 we can see that the bias seen in measured heat flux is clearly a function mainly of paint thickness. For the low-heating and mid-heating cases, the change in heating condition seems to make almost a negligible difference, especially when looking at uncertainties. Even adding the high heating case, it can be noted that all uncertainties at a certain paint thickness are within the uncertainties of other heating conditions at the same paint thickness.

The contribution of bias due to paint thickness however does not fall within the uncertainty of the sensor for higher paint thicknesses. For paint thicknesses of 1.65 mil and 1.98 mil, while at the edge of the uncertainty, the bias still falls within the uncertainty of the sensor. The test series with 2.75 mil paint thickness however falls significantly under the baseline value, outside the value we could reasonably expect with 95% confidence.

One other interesting note, when looking at Figure 30, Figure 32 or Figure 34 we can see that the response of the painted coaxial thermocouple does not approach the response of the unpainted coaxial thermocouple during baseline testing.

It was assumed that the application of TSP onto the coaxial thermocouple would cause a "time lag", and that with enough time the response of the painted thermocouple would approach the same steady state value as the unpainted thermocouple. However, in Figure 30 the total run time is roughly four seconds, and the TSP-coated thermocouple does not appear to ever approach the baseline result. After the heating stops however, the coated and uncoated thermocouple measure the same value again.

This result was unexpected and is the driving factor behind calling this result a "bias" as it seems to be constant, and not simply the results of a "time lag".

Temperature Sensitive Paint Characterization

To begin characterizing TSP as it is used in Tunnel 9, the data will be reduced using a modified version of the standard form of data reduction currently used in Tunnel 9 to reduce TSP data as described in the previous chapter. This includes using an in-situ calibration of all data points during heating to create a linear calibration curve and forcing the first few frames to be equal to the reference temperature to obtain the correct temperature vs. time curves. The calibration information for all 3 heating conditions are shown in Table 12.

Table 12: Calibration Setting for Standard TSP Calibration

Heating Condition	**Calibration Time (sec)**	**Reference Temperature Frames (sec)**	**Linear Temperature Gradient Frames (sec)**

Low Heating	-2-6	0-1.9	1.9-2.1
Mid Heating	-2-4	0-1.9	1.9-2.1
High Heating	-2-3	0-1.9	1.9-2.1

Standard TSP Heat Flux Characteristics

TSP heat flux reduced using a modified version of the standard TSP data reduction method all follow a similar trend. An example of reduced TSP data is shown in Figure 36.

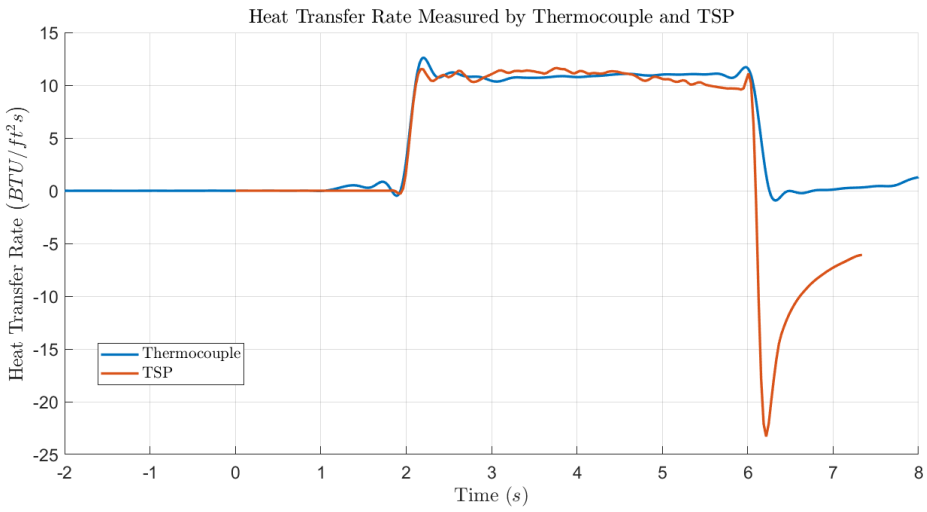

Figure 36: Example Comparison of Standard TSP Heat Flux Measurement and Coaxial Thermocouple Measurement

All TSP heat flux responses reduced with the standard TSP data reduction methods are characterized similarly. For the first 4 seconds (-2 to 2 seconds), all cases match the initial adiabatic case, as they are forced to the reference temperature at this point. TSP then does a decent job matching the initial spike in heat transfer seen when the hydrogen begins flowing in the vitiated heater. During the steady state portion, the

TSP agrees well with the thermocouple until about halfway through the steady portion.

About halfway through the steady portion, the TSP data begins to decrease, but the error between TSP and the coaxial thermocouple is within the stated coaxial thermocouple data reduction uncertainty. As the thermocouple spikes back down to the near-adiabatic condition at the end of the run, the TSP far overshoots the adiabatic condition and displays large negative heat flux. After the initial overshoot, the TSP data very slowly approaches the adiabatic response shown by the thermocouple. In this experiment, data was not taken long enough to see at what point the TSP agrees with the thermocouple again, but it would be on the order of seconds.

A noteworthy difference between the response of the thermocouple and the response of the TSP is the slope of the heat flux decline. In all cases, the TSP has a much steeper slope than the thermocouple. This behavior is often seen in Tunnel 9. While such steep drop in heat transfer typically doesn't occur in Tunnel 9, the overall behavior for heat transfer drops of a lower slope are often seen.

TSP Characterization for Different Paint Thicknesses

We will now look at the response of the TSP for different paint thicknesses at a single heating condition to determine the effect of paint thickness on TSP heat flux response.

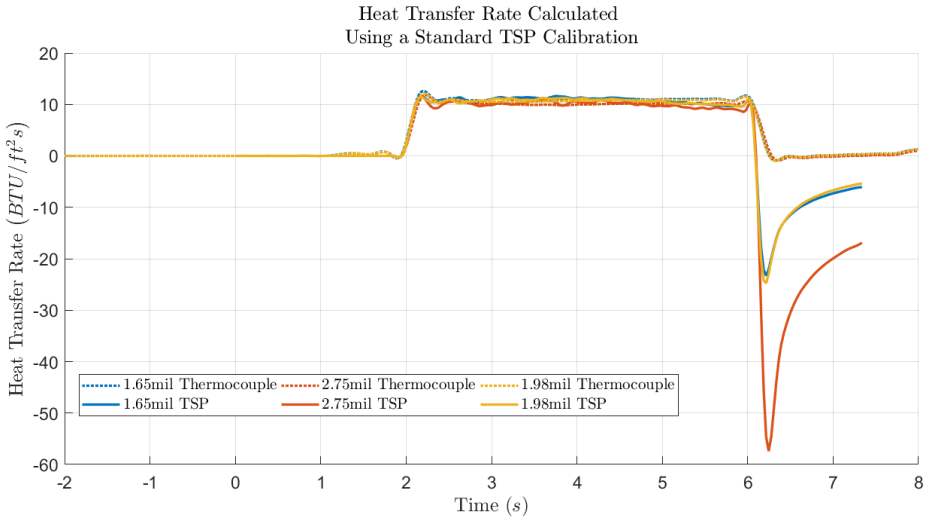

Figure 37: TSP Heat Flux Response for Different Paint Thicknesses at the Low Heating Condition

First, we will look at the low-heating condition with all three paint thicknesses tested. Figure 37 shows the response of the TSP for the entire test, and Figure 38 shows a cropped version of Figure 37, focusing only on the last 3 seconds of the run.

The overshoot is a function of the paint thickness, but this behavior does not appear to be linear. For the lower paint thicknesses (1.65 mil and 1.98 mil) the overshoot and subsequent TSP error appears nearly identical. However, at the 2.75 mil paint thickness the maximum value of the overshoot increases over 100%. These trends continue for the mid-heating and high-heating case as well, with different magnitudes.

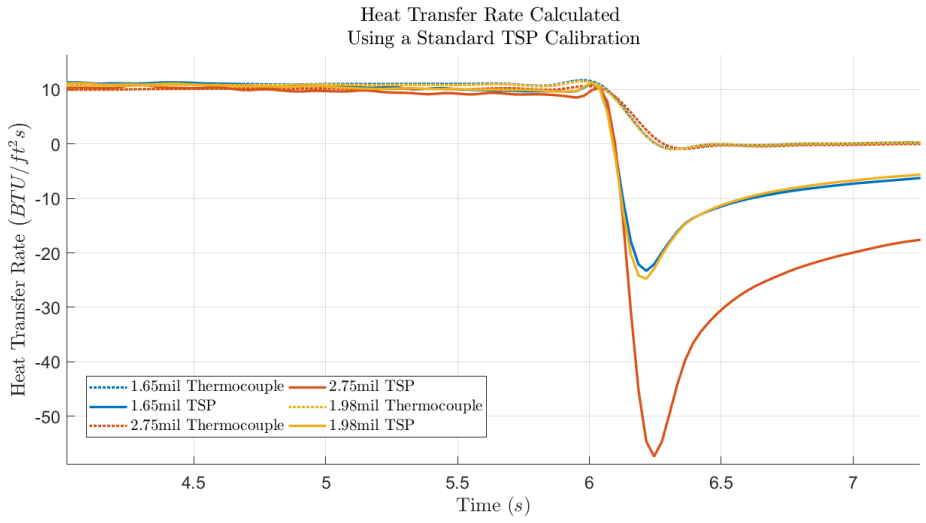

Figure 38: TSP Heat Flux Response for Different Paint Thicknesses at the end of the Low Heating Condition

TSP Characterization for Different Heating Conditions

Now, we can look at the response of TSP when related to different heating conditions, which is shown for the 1.65 mil paint thickness in Figure 39.

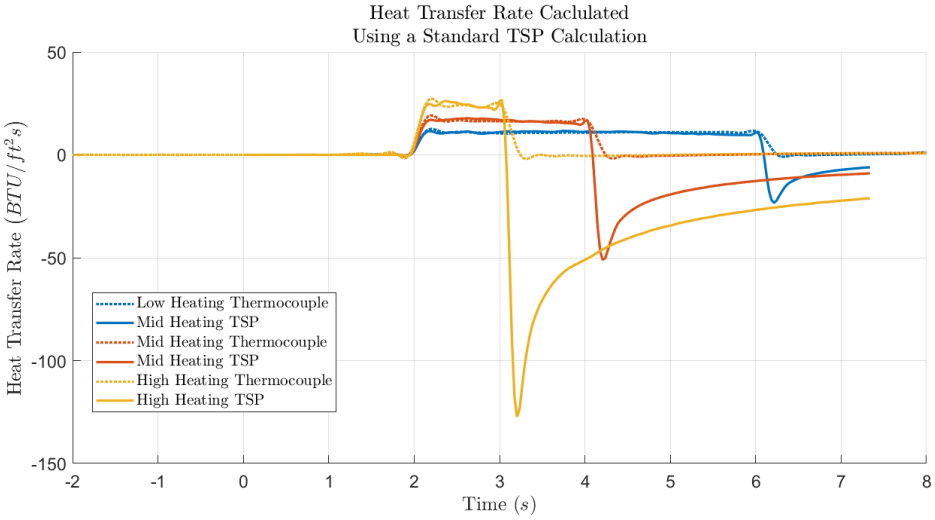

Figure 39: TSP Heat Flux Response for Different Heating Conditions at 1.65 mil Paint Thickness

Figure 39 shows that the overshoot is strongly a function of the input heating condition. The overshoot seen at the end of an individual run increases as the heating conditions increases. Also, the time it takes for the TSP measurement to reach the

adiabatic steady state at the end of the run appears to increase as the heating input increases.

This result implies that the accuracy of TSP in situations where there is a sharp reversal in heat flux is related to the magnitude of the heating input.

Again, as was the case with the error due to the paint thickness, the general trends of the error for different magnitudes agree. However, in this case the magnitude increases greatly for the largest paint thickness similar to the large jump in error seen for that paint thickness as seen in Figure 38.

TSP Characterization Summary for Standard TSP Data Reduction

Now, collecting all data, we can make more statements on the trends of the data. First, we can look at the maximum overshoot seen in the TSP response as a function of the paint thickness and the heating input. Table 13 shows the data for all cases.

It is clearly seen that the overshoot is a function of the paint thickness, with a large jump coming in all cases between the 1.98 mil cases and the 2.75 mil cases. This suggests that there is some paint thickness between 1.98 mil and 2.75 mil that could be considered a cutoff value because of the large jump in overshoot that occurs. It can also be noted that as the behavior of the overshoot is not linear with respect to paint thickness more research is necessary to define the overshoot at lower paint thicknesses as there are not enough points in this analysis to define a curve. They could be significantly less than the overshoot values seen here.

Table 13: Maximum overshoot for TSP Reduced with Standard TSP Data Reduction in percent of mean good flow input heat flux (%)

Paint Thickness	**1.65 mil**	**1.98 mil**	**2.75 mil**
Low Heating	190	200	460
Mid Heating	240	270	670
High Heating	340	430	860

Next, we can look at the TSP uncertainty, calculated as described in the previous chapter. Table 14 shows the uncertainty values calculated using this method. Note that while the beginning half of each run appears to have low uncertainty, the overshoot at the end of the runs is so large that the uncertainty values are high.

Table 14: Uncertainty of TSP Reduced with Standard TSP Data Reduction in percent of mean good flow input heat flux (%)

Paint Thickness	**1.65 mil**	**1.98 mil**	**2.75 mil**
Low Heating	36	38	88
Mid Heating	63	56	160
High Heating	106	79	210

The uncertainty shown in Table 14 follows the same basic trends as the magnitude of the overshoot shown in Table 13. The one exception is the mid heating condition which has slightly less uncertainty at 1.98 mil than 1.65 mil. This is the only one that does not follow the trend, and the difference seems insignificant. To look at this a different way, Figure 40 shows the uncertainty data for each paint thickness plotted vs. the input heating condition.

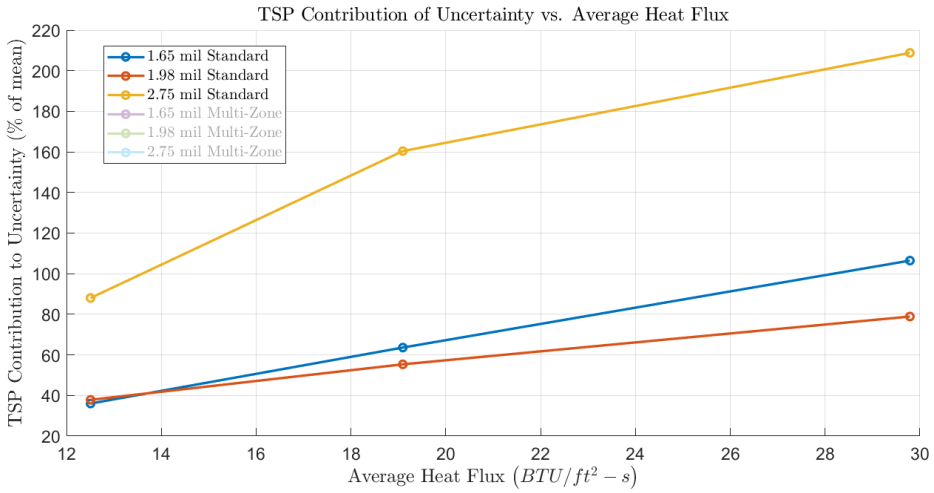

Figure 40: Uncertainty of TSP Reduced with Standard TSP Data Reduction

Again, Figure 40 shows similar trends to Table 13. The uncertainty is a function of the paint thickness and the heating magnitude. Just like the overshoot, at lower paint thicknesses, the effect of paint thickness is insignificant to the effect of the increased heating input. At a certain point, the paint thickness becomes the driving factor behind uncertainty, and that is seen in the 2.75 mil case.

Similar to the characterization of the bias in painted vs. unpainted coaxial thermocouples, more points are needed to fully define the curves describing the uncertainty as a function of paint thickness and heating input.

Temperature Sensitive Paint Calibration Analysis

To understand better the behavior of temperature sensitive paint when measuring steep drops in heat transfer rate, like the ones examined in this research, we need to look at the calibration used to convert the calculated ratio of ratios into temperature using the calibration method described in the previous chapter.

TSP Calibration Hysteresis

The reason behind the large overshoot seen in the TSP heat transfer response for all heating inputs and paint thicknesses is a hysteresis seen in the TSP calibration.

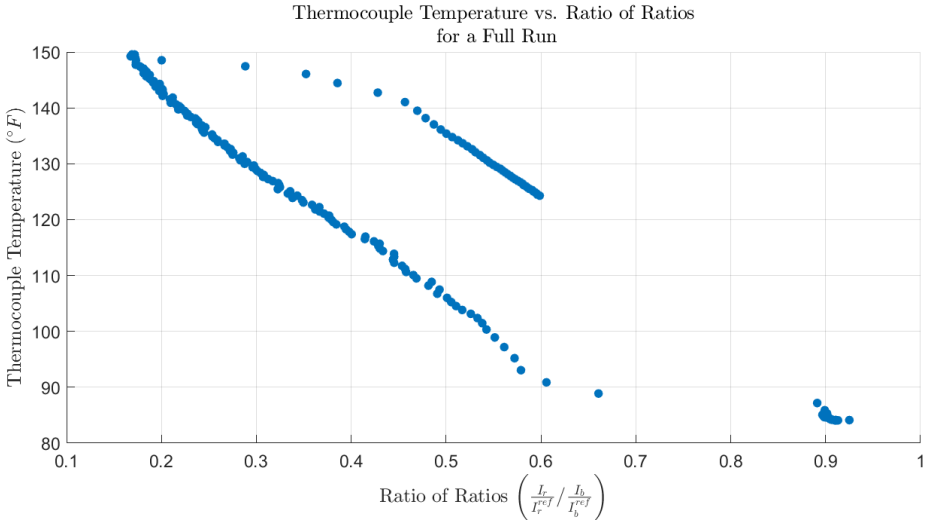

Figure 41: Example TSP Calibration for a Low Heating Condition and 1.65 mil Paint Thickness

Figure 41 shows a calibration of a low-heating run with 1.65 mil paint thickness for reference. All calibrations show similar trends as the one shown. As mentioned in the previous chapter, the calibration for TSP should ideally be linear in shape. The calibration shown in Figure 41 is clearly non-linear, and a non-linear calibration will inherently introduce error into a measurement.

There are 3 sections that develop in the calibrations in this case,

1. The initial points grouped up around a ratioed value of 0.9 and the ambient temperature, around 80°F.
2. A heating curve, creating a long near-linear section stretching from ambient temperature to the maximum temperature, around 150°F.
3. A cooling curve, creating another linear section with similar ratio values as the heating curve, but much higher temperatures.

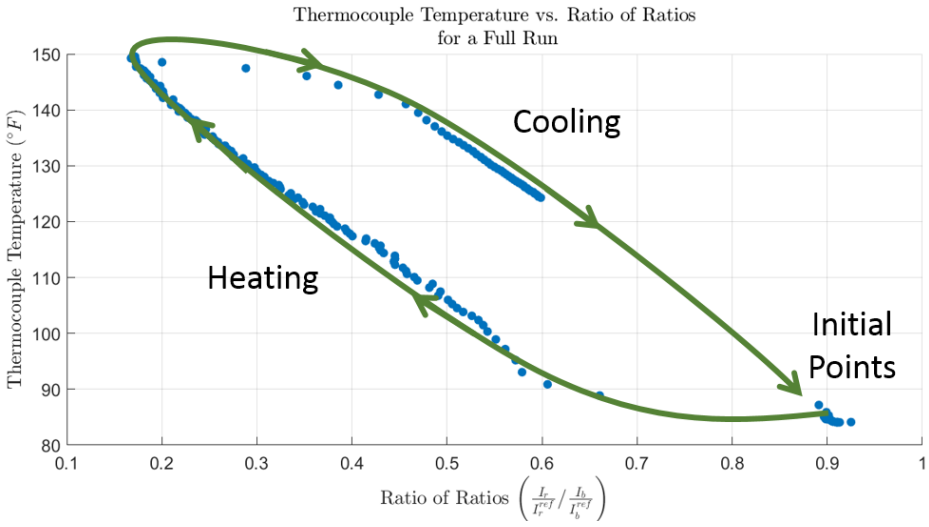

Figure 42: Annotated Example Calibration Showing Hysteresis of TSP Calibration during Vitiated Heater Runs

Figure 42 shows the hysteresis curve that develops during a typical vitiated heater run. The initial points are seen in the bottom right of the calibration, and the curve follows the green path as the run progresses. The issue here is clearly that using the heating hearting curve to reduce the cooling data will yield inaccurate results because the cooling curve and heating curve are not co-linear. However, both curves are still linear during a significant region themselves, and that allows us to use the typical Tunnel 9 calibration procedure on each section of the curve separately.

To investigate the error in TSP measurements further and to investigate possible mitigation methods, we can look at calibrations using different sets of data to create different calibration curves.

TSP Calibration Using Heating Data

First, we will look at a calibration created using the standard TSP method, which uses data from the heating section of the calibration curve.

Table 15: TSP Calibration Settings Using Data from the Heating Section of the Calibration Curve

Heating Condition	**Calibration Time (sec)**	**Reference Temperature Frames (sec)**	**Linear Temperature Gradient Frames (sec)**
Low Heating	-2-6	0-1.9	1.9-2.1
Mid Heating	-2-4	0-1.9	1.9-2.1
High Heating	-2-3	0-1.9	1.9-2.1

Table 15 shows the settings used in this calibration. It can be noted that this is the same table as Table 12 because a calibration using the data on the heating section of the curve is the standard method of calibration used for TSP in Tunnel 9.

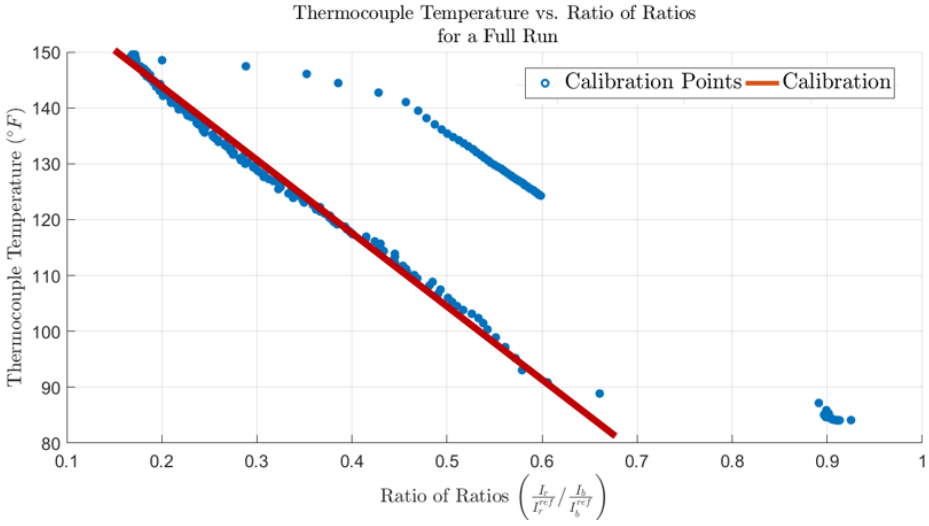

Figure 43: TSP Calibration Using Data from the Heating Section of the Calibration Curve

Figure 43 shows the calibration method used for all data discussed in the previous section. The calibration is clearly linear with respect to the points that fall in the heating section of the calibration curve. All initial points and points on the cooling section of the calibration curve are ignored.

To look at how well the TSP matches the coaxial thermocouple under the paint using the given calibration, we will examine the temperature response of both the coaxial thermocouple and the TSP. Figure 44 shows the temperature response of the TSP and the coaxial thermocouple for the given calibration.

Before heating begins, the TSP shows the reference temperature, because the calibration settings forced this value. After the rise in temperature is seen, the TSP matches decently with the coaxial thermocouple, up until the top of the temperature rise (around 6 sec.). Towards the maximum value of temperature, the TSP begins to drift away from the value shown by the coaxial thermocouple, but not appreciably.

After the heating stops, the TSP does not agree with the coaxial thermocouple. The temperature response of the TSP drops far quicker than the temperature response of the thermocouple. This different negative slope causes the large overshoot discussed in the previous section.

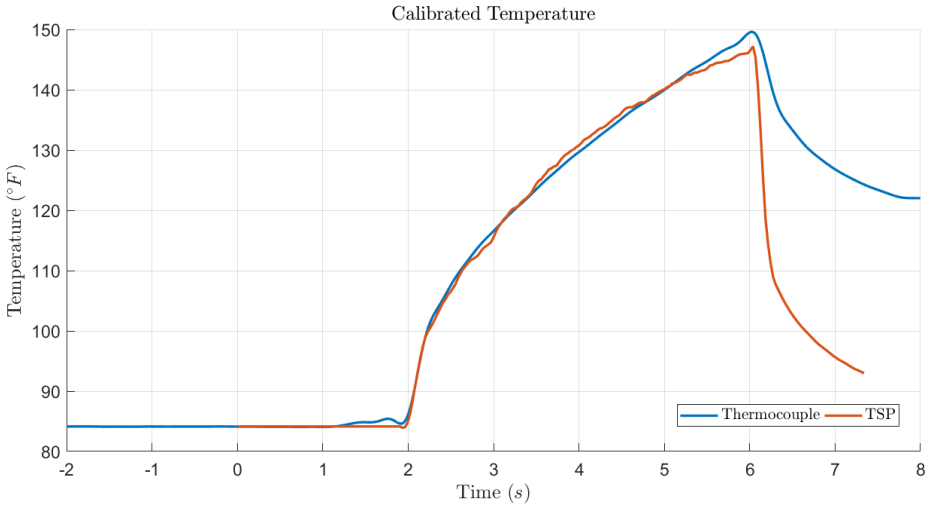

Figure 44: Temperature Response of TSP and the Painted Coaxial Thermocouple Using a Standard TSP Calibration Method

TSP Calibration Using Cooling Data

Next, we will look at a TSP calibration that utilizes points from the cooling section of the calibration curve. Table 16 shows the calibration settings used for this analysis. It can be noted that the reference temperature frames and linear temperature gradient frames do not change. Those settings are relating to the startup of the vitiated heater, and not the frames with which the data is calibrated.

Table 16: TSP Calibration Settings Using Data from the Cooling Section of the Calibration Curve

Heating Condition	**Calibration Time (sec)**	**Reference Temperature Frames (sec)**	**Linear Temperature Gradient Frames (sec)**
Low Heating	6-7.5	0-1.9	1.9-2.1
Mid Heating	4-7.5	0-1.9	1.9-2.1
High Heating	3-7.5	0-1.9	1.9-2.1

Figure 45 shows the calibration created when using the points on the cooling side of the calibration curve. The plot clearly has a different y-intercept and possibly slope than the calibration in Figure 43.

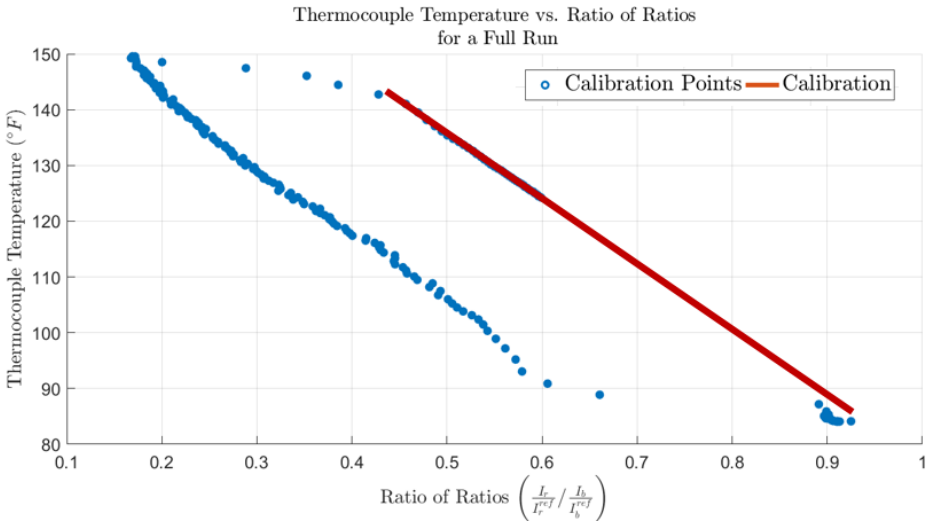

Figure 45: TSP Calibration Using Data from the Cooling Section of the Calibration Curve

Figure 46 shows the temperature response of the thermocouple and the TSP for a single run. Unlike the data obtained using a standard calibration, shown in Figure 44, the data during heating does not match. This makes sense when looking at the calibration, as the calibration using the data on the cooling side of the curve results in a shift in the y-intercept of the calibration. This would cause a constant change in temperature, which appears here.

However, this calibration does show much improved performance on the cooling section of the data. The temperature response of the thermocouple and the TSP show good agreement for all points between 6.25 and 7.5 seconds.

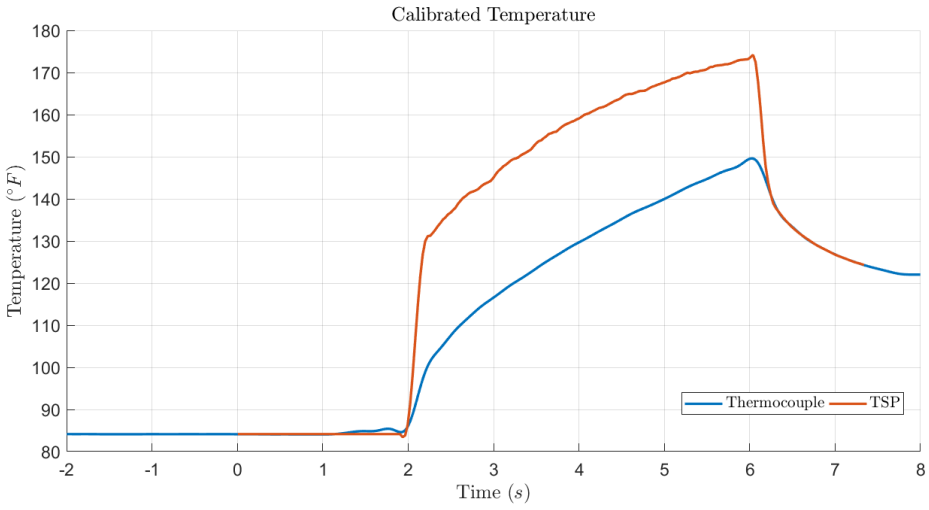

Figure 46: Temperature Response of TSP and the Painted Coaxial Thermocouple Using a TSP Calibration of the Cooling TSP Sample

TSP Calibration Using All Data

Now, we can quickly look at TSP results using all available data to create a calibration. The calibration settings for this can be found in Table 17. Once again, the reference temperature frames and linear temperature gradient frames do not change.

Table 17: TSP Calibration Settings Using All Available Data

Heating Condition	**Calibration Time (sec)**	**Reference Temperature Frames (sec)**	**Linear Temperature Gradient Frames (sec)**
Low Heating	-2-7.5	0-1.9	1.9-2.1
Mid Heating	-2-7.5	0-1.9	1.9-2.1
High Heating	-2-7.5	0-1.9	1.9-2.1

Figure 47 shows the calibration using all data points, which cuts through the center of the data. Figure 48 shows the temperature response of the thermocouple and the TSP for an example run. Clearly, using all points in a calibration does not average out the error creating from using a heating curve or a cooling curve, but instead adds error to both the heating and cooling sections of the data.

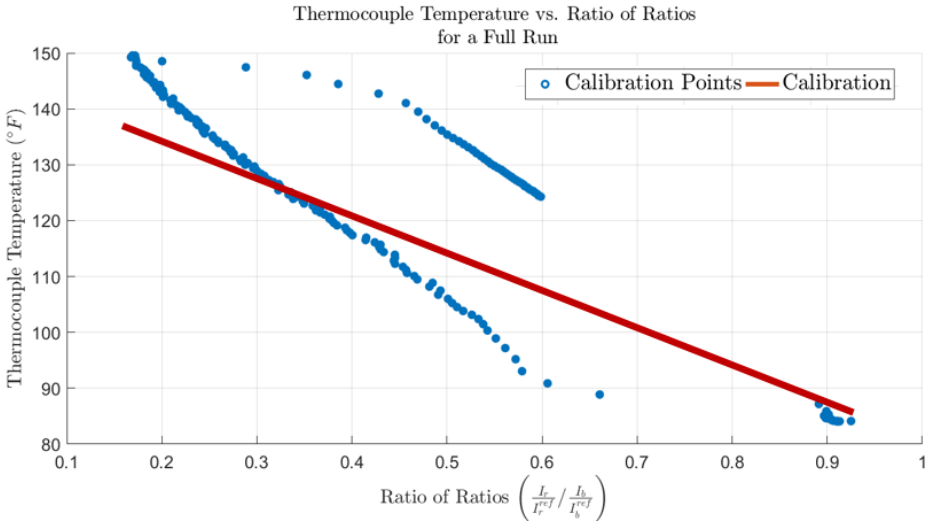

Figure 47: TSP Data Using All Available Data

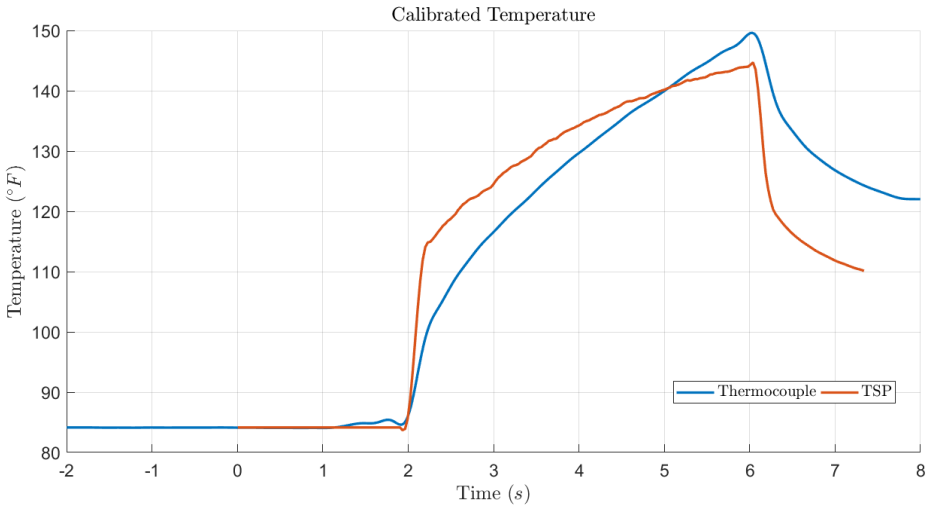

Figure 48: Temperature Response of TSP and the Painted Coaxial Thermocouple Using Calibration from All Available Data

TSP Dual-Calibration Method

By looking at Figure 44 and Figure 46, it becomes clear that in this instance, the highest accuracy can be obtained by combining two calibrations. This dual-calibration method would utilize a standard TSP calibration with points from the heating side of the calibration curve for the first section of the data and then switch to a different calibration when the sample abruptly starts cooling. For the example case shown in Figure 44, the calibration switch would occur at roughly 6 seconds. The calibration settings for the two calibrations can be found in Table 15 and Table 16 as they are the data from the heating and cooling calibration.

When switching between calibrations, some intermediate points need to be defined to create a smooth transition from data calculated with one calibration to data calculated with another calibration. To do this, intermediate points were linearly assigned between the final temperature point from the first section of data to the initial point from the second set of data.

Temperature Response using Dual-Calibration Method

Figure 49 shows the two calibrations that will be used in this example case to demonstrate the dual-calibration method. The lower curve is the heating curve and will be used for the first section of the data. The upper curve is the cooling data and will be used after the abrupt change in heat transfer rate.

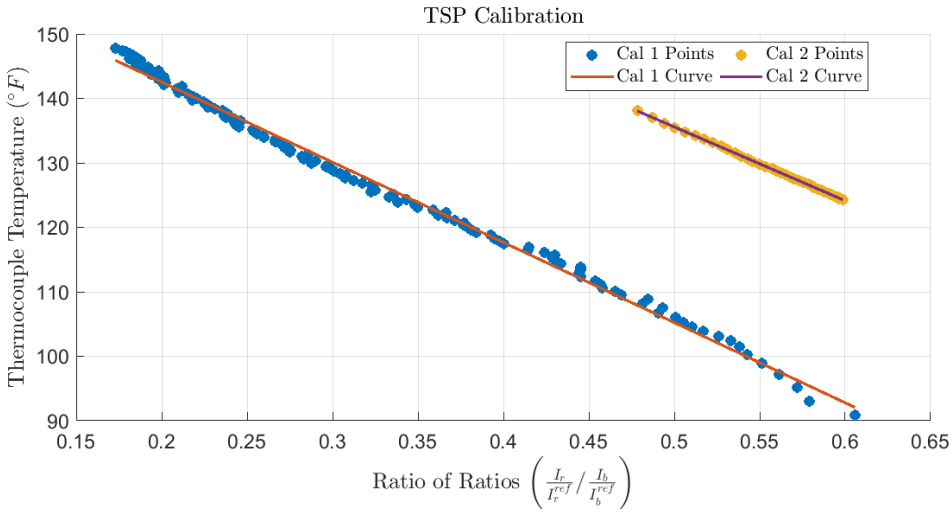

Figure 49: Two Calibrations from One Data Set, Used to Compute Temperature for a Vitiated Heater Run Using a Dual-Calibration Method

Figure 50 shows the temperature response comparison of the two methods of TSP calibration, with reference to the thermocouple response. The dual-calibration method has better agreement with the thermocouple. There is still an area near the maximum temperature where the dual calibration method does not show good agreement, but the standard calibration does not have good agreement at that point either, and therefore the dual-calibration method will not have better agreement.

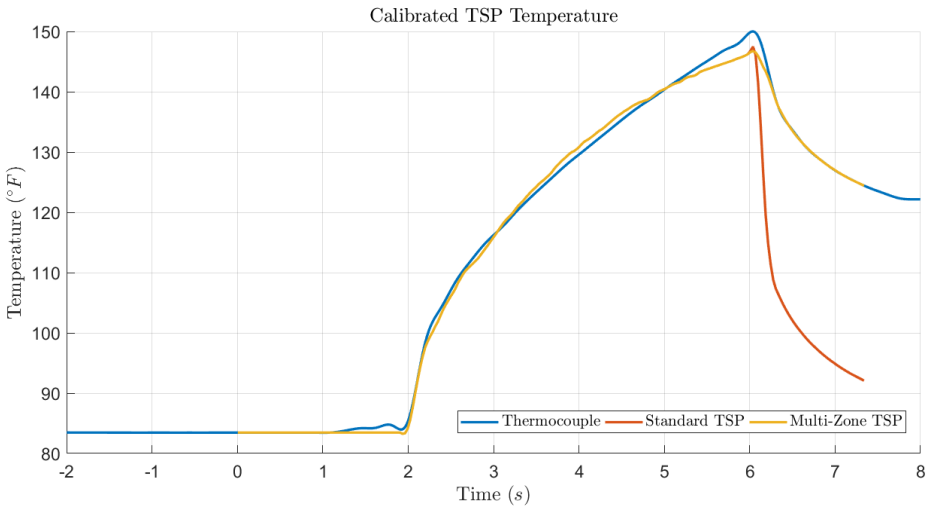

Figure 50: Temperature Response of Coaxial Thermocouple and TSP using a Standard Calibration and a Dual-Calibration

Heat Flux Response Using Dual-Calibration Method

Figure 51 shows the heat transfer response of TSP calculated using the dual-calibration method for 1.65 mil paint thickness. The trends seen in Figure 51 are similar for all paint thickness.

The dual-calibration method has much better agreement than the standard calibration, shown in Figure 39. The characteristic overshoot at the moment of abrupt cooling is no longer there. In fact, the TSP shows no overshoot of the near-adiabatic condition in most cases, where the thermocouple typically shows some minor overshoot.

The response using the dual-calibration method no longer shows a steeper change in heat transfer rate than the thermocouple. The two sensors show much better agreement during the heat flux drop.

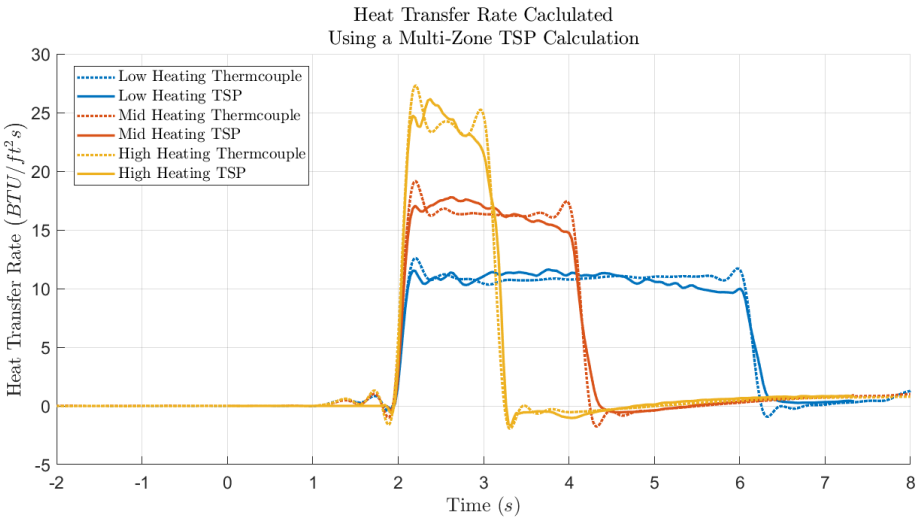

Figure 51: Heat Transfer Rate Response of Thermocouple and TSP Computed Using Dual-Calibration Method for 1.65 mil Paint Thickness

We will now, investigate the heat flux drop at the end of the run for different paint thicknesses, for the low-heating condition in Figure 52. Again, similar to the discrepancy in temperature in Figure 50 we see relatively poor agreement as we approach the heat flux drop. This is typical for all cases. However, during the heat transfer drop the agreement between TSP and coaxial thermocouple is great, with a much better agreement in slope and overshoot.

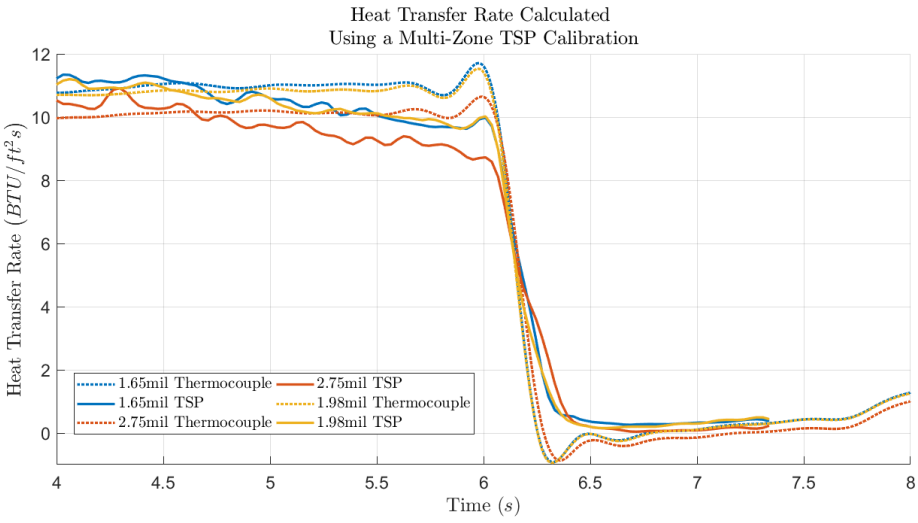

Figure 52: Heat Transfer Rate Response of Thermocouple and TSP Computed Using Dual-Calibration Method for Low-Heating Condition

Figure 53 shows the computed uncertainty for the dual-calibration method, and Table 18 shows the data in a tabulated form. The trends seen are very similar to the trends seen for the uncertainty with the standard calibration shown in Figure 40. At lower paint thicknesses, the heat flux input has a larger influence on the uncertainty than the paint thickness, but at higher paint thicknesses the paint thickness itself has a larger influence on uncertainty.

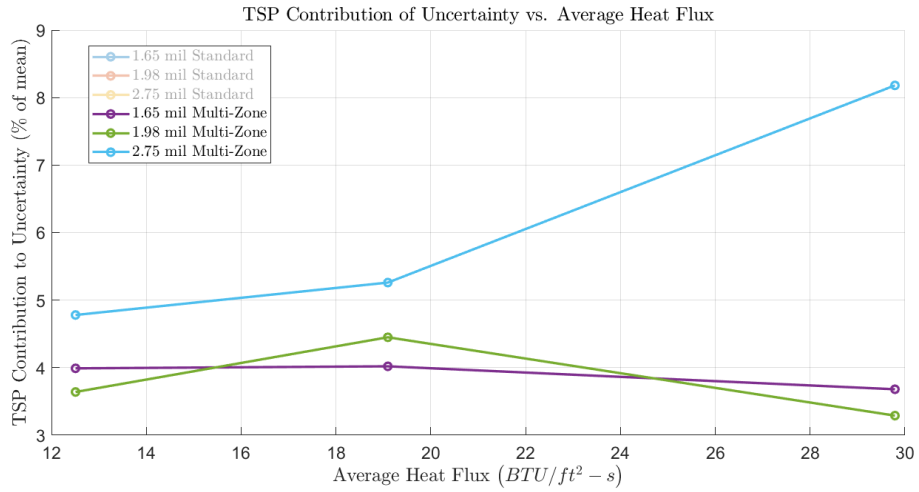

Figure 53: Uncertainty of TSP Reduced with Dual-Calibration TSP Data Reduction

Table 18: Uncertainty of TSP Reduced with Dual-Calibration TSP Data Reduction in percent of mean good flow input heat flux

Paint Thickness	**1.65 mil**	**1.98 mil**	**2.75 mil**
Low Heating	4.0	3.6	4.8
Mid Heating	4.0	4.5	5.2
High Heating	3.7	3.3	8.1

The largest difference between the uncertainty of the standard calibration method and the dual calibration method are the magnitudes of the uncertainty. Figure 54 shows the percent change in magnitude of uncertainty between standard calibration and dual-calibration.

The uncertainty drops for all cases roughly 89-95%. It should be noted that while this number is quite large, it is because of the nature of the experiment designed. The experiment was designed because it was a known case where TSP does not show good accuracy. Therefore, for a typical Tunnel 9 run we cannot expect a 90% drop in uncertainty, but for situations where a sudden drop in heat flux is seen, we should expect a significant decrease in TSP uncertainty.

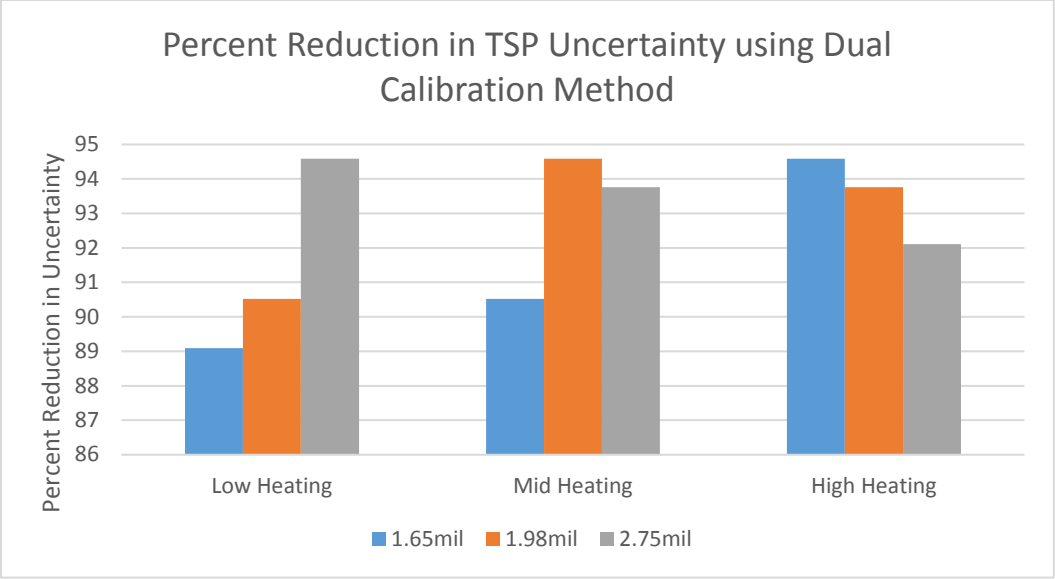

Figure 54: Percent Reduction in TSP Uncertainty using Dual-Calibration Method vs. Standard Calibration Method

Chapter 5: Conclusions and Future Work

Heat Transfer Measurement Bias as a Function of Paint Thickness

From the results of this research, we can conclude that there is a bias in heat flux measurements measured with coaxial thermocouples flush mounted on a wind tunnel test article due to the application of temperature sensitive paint to the thermocouple.

The data shown in Figure 35 shows that for thick paint thicknesses, a bias is created by applying TSP that is greater than the uncertainty of the sensor. For thinner paint thicknesses the bias appears to be dependent on paint thickness, however for most cases it falls in the uncertainty of the sensor.

There has been limited testing for a bias in heat flux sensors in Tunnel 9. No significant effect on the surface heat flux sensors has been seen in this testing, but this is a difficult phenomenon to study in Tunnel 9 for several reasons. One major reason is that the surface roughness of a test article typically affects the transition location during a Tunnel 9 test, and having a single thermocouple painted (or left unpainted) would likely trip the boundary layer and cause a higher heat flux at that area.

Some testing for this type of discrepancy was attempted at Tunnel 9 by Kurits et. Al. However, the results of the experiment did not yield significant results due to similar reasons to those listed above[15].

The identification of this issue was not one of the main goals of this research, but now that the effect is known it can be further researched to gain a better

understanding, and further improve the accuracy or heat transfer rate measurements in Tunnel 9.

While limited testing for this discrepancy has been largely inconclusive at Tunnel 9, test articles in Tunnel 9 typically have a maximum paint allowable paint thickness, which is enforced to ensure any bias seen by the surface heat flux sensors is low.

To make in-depth conclusions on this phenomenon we would need more data points. Again, as this wasn't the focus of the research the experiment was not specifically planned to study this. There still are some things that we can comment on including the convective heat transfer effects and the effect this may have on Tunnel 9 measurements.

Bias in Coaxial Thermocouple Measurements Typically Collected in Tunnel 9

While the sensors, data acquisition, data reduction methods, and temperature sensitive paint formulation were identical to those used in Tunnel 9, the paint thicknesses were not entirely representative of what would be seen.

Over the past decade, engineers at Tunnel 9 have identified the best operating range in terms of paint thickness. A minimum paint thickness was determined using the minimum signal output of the paint. The signal output of the paint is directly related to the paint thickness and a minimum was determined to ensure usable signal to noise ratio. A maximum paint thickness is enforced to ensure little effect on surface heat transfer sensors. Again, the effect has not been thoroughly studied or quantified until now, and more work is needed to better quantify it.

Looking again at Figure 35, we can attempt to estimate the bias that will be seen in Tunnel 9, remembering that all heating conditions are representative of heating conditions typically seen in Tunnel 9. We can estimate that Tunnel 9 will only see up to 10% error, but it could be much lower.

Again, due to the low number of points, drawing conclusions on the shape of the bias curve is difficult. Figure 56 shows that the best curve fit for the low-heating case was a linear fit, estimating the bias seen at Tunnel 9 paint thicknesses as between 5 and 7%. For the high heating condition however, as shown in Figure 55, a quadratic curve fit is best. And depending on the curve fit, the error could decrease. If the bias behaves quadratically, the bias seen at Tunnel 9 would be closer to 3-5%. Again, more research is necessary to fully define the curves and gain a better understanding of the accuracy of Tunnel 9 measurements, but it is more likely than not that the bias due to paint in Tunnel 9 is below 5%.

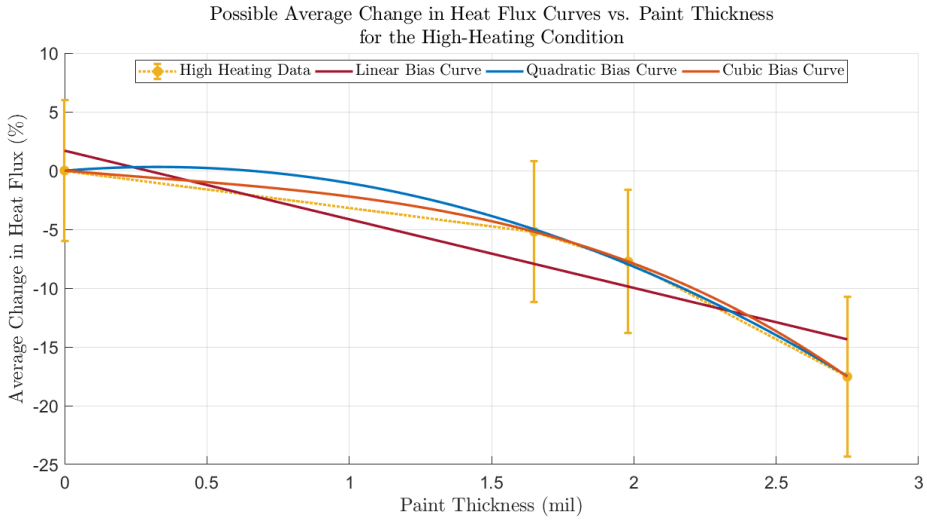

Figure 55: Possible Curves of Different Order of Coaxial Heat Transfer Bias vs. Paint Thickness for the High-Heating Condition

Convective Heat Transfer Effects

One major effect that was not quantified in this analysis was the convective heat transfer coefficient difference between the steel sample with and without paint. As mentioned previously, it is assumed in Tunnel 9 that the convective heating input at the wall is equal to the one-dimensional conductive heat transfer at the surface of the test article[8]. Further, it is assumed that the temperature gradient through the paint layer is linear and therefore has little effect on the heat transfer[13].

However, it may not be a valid to assume that the convective heat transfer rate is identical for steel and TSP. We can conclude that the paint layer influences the heat transfer measurement, but we cannot say what portion of that effect is due to convective heat transfer differences.

Figure 56 shows the error curve for the low-heating condition from Figure 35. It also shows three different possible curves that could be generated using the data and uncertainty values at each point. It's clearly seen that the data collected during this experiment is not enough to make any assumptions on the convective heat transfer effect. In fact, linear curves could be drawn showing a 5% increase or decrease in heat transfer with an infinitesimally thin paint layer. More testing would be needed in order to better define these curves and allow for more conclusions to be drawn.

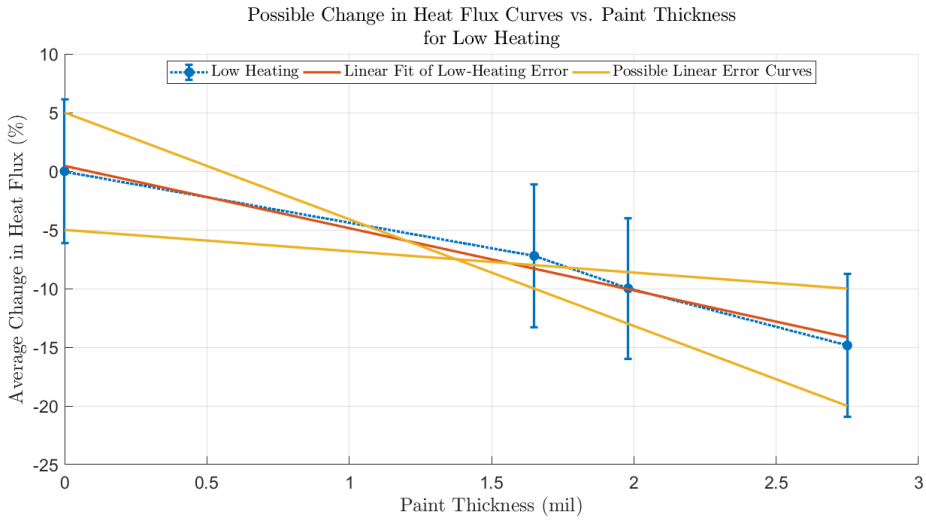

Figure 56: Possible Linear Curves of Coaxial Heat Transfer Bias vs. Paint Thickness for the Low-Heating Condition

Future testing could improve the understanding of this issue by testing thinner paint layers. The curves in Figure 35 are shown to converge to 0% bias at 0 mil paint thickness, but this may not be the case. Adding data points by testing more paint thicknesses would improve our understanding of this effect.

Some work was done as part of the 177-run test matrix to determine if surface roughness had any effect on the heat transfer measurement. These were done by lightly sanding the test article to alter the surface roughness but not alter the paint thickness. Timing did not permit more testing like this, and the results were inconclusive.

TSP Characterization when Measuring Abrupt Heat Flux Drops

TSP Uncertainty Trends

As shown in Figure 40 the uncertainty in TSP measurements is a function of the magnitude of the heating input, and the paint thickness. For the two lower paint

thicknesses tested the uncertainty was similar, and the uncertainty scaled linearly with the input heating condition. For the larger paint thickness (2.75 mil), the uncertainty was not similar to that of the lower two paint thicknesses, but also scaled linearly with the input heating condition.

The change in uncertainty due to the change in paint thickness does not appear to be linear. There is a large different between the uncertainty at 1.98 mil paint thickness, and the uncertainty at 2.75 mil paint thickness. To make more conclusions about the uncertainty at thinner paint thicknesses, more testing would be needed using a thinner paint layer. However, the uncertainty would more than likely decrease from the uncertainty found in this research. Note again that the uncertainty values are extremely high in this case as the experiment was designed as a situation where TSP was known to show poor performance.

TSP Standard Calibration and Reasons for Poor Performance

The experiment was designed to have a steep heat flux drop to create an exaggerated scenario similar to one seen in Tunnel 9 when a test article pitches through an angle of attack sweep. Some parts of the test article start on the wind-side, and during pitching, move to the leeside of the test article which causes a large drop in heat transfer.

This experiment accomplished a large sudden drop in heat transfer by closing the valve for the main hydrogen fuel, stopping all heating into the test section in a very short amount of time.

In all cases, TSP cannot accurately measure the abrupt change in heat flux at the end of the test. This is shown in Figure 37 and Figure 39. The behavior was characterized as a larger overshoot than measured by the thermocouple and then a slow climb back to the correct adiabatic condition.

For an ideal TSP measurement, the slope of the temperature vs. ratio of ratios is constant for all temperatures. In this way, for each temperature, there should only be one value of ratio of ratios that can be assigned. For the example shown in Figure 57, all temperatures above 125°F have 2 values of ratio of ratios that can be assigned. One value is from the heating section of the curve, and one is from the cooling section of the curve.

In this example, the difference between each point is large, and the slope and y-intercept of a linear curve from the data on the heating section of the calibration curve is very different from the slope and y-intercept of the curve using the cooling side of the curve. As discussed earlier, this discrepancy is the reason for the poor agreement in the TSP data.

An explanation for this behavior can be found in the calibration curves for the TSP for these runs. Figure 57 shows the behavior of an example run of the low heating condition with each change in heating marked. Figure 58 shows the corresponding change in heating. The slope of the ratio of ratios calibration changes at each change in heating. At point 2, and 4 there is a significant change in the slope of the calibration. One explanation for this behavior could be the high heat capacity of the TSP. The paint layer can store heat, causing the temperature recorded at the base of the paint layer to change much slower than the temperature of the paint layer.

Because the ratio of ratios is only dependent on the temperature of the paint layer, a difference is seen here.

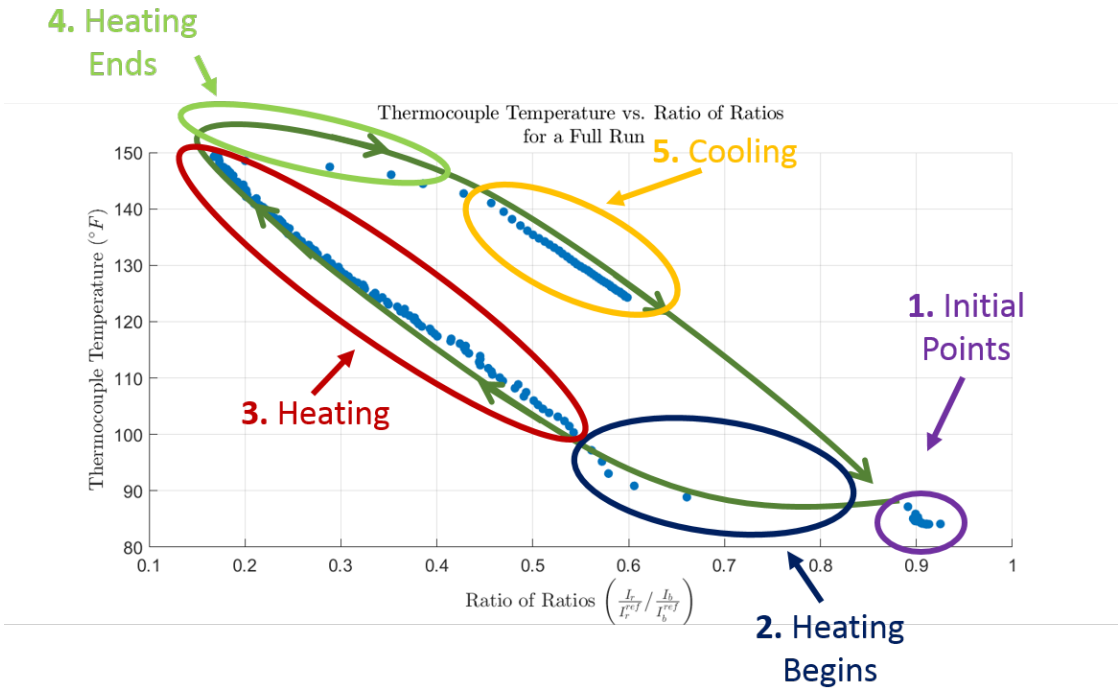

Figure 57: Annotated Calibration Curve Showing Heating, Cooling and Both Heating Changes

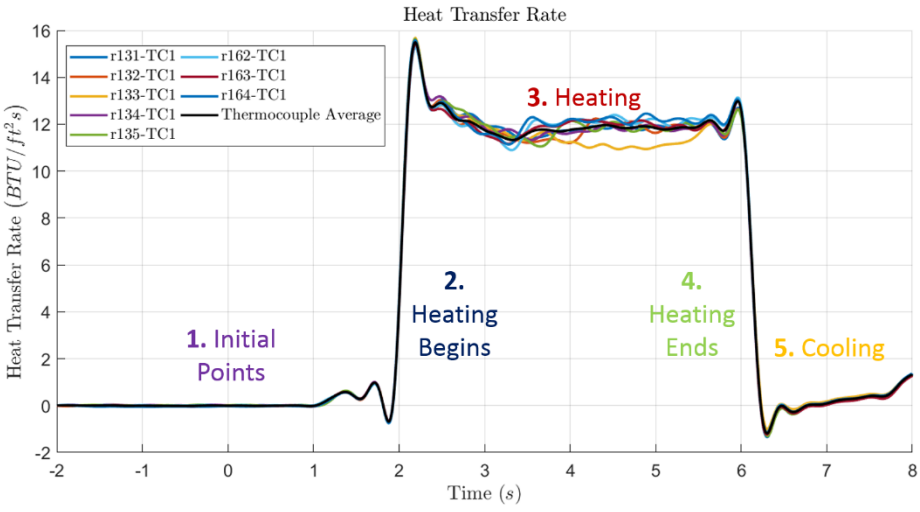

Figure 58: Example Heat Transfer from Vitiated Heater with Marked Sections

Very quickly during constant heating, the system reaches a constant heating rate and the calibration curve returns to a linear state. This is seen for the remainder of the heating portion of the data. When heating ends, we again see a major change in the calibration slope which may be due to the heat capacity of the paint. This time, the paint cools much faster than the steel sample it is painted onto. Because the paint is cooling faster than the steel (and therefore the thermocouple), the curve of the calibration is different than during heating.

It is assumed that with enough time the system would again reach equilibrium, and a similar slope as seen in the heating curve before again matching the initial points. Data was not taken long enough to investigate this further.

The non-uniform heating and cooling of the TSP-steel sample thermal system results in a drastic change in calibration intercept and to some degree the slope between heating and cooling data for abrupt changes in heat flux. For less abrupt changes in heat flux, the system would have more time to stabilize, and less of a difference would be seen.

Dual-Calibration Method

This research proves that a dual-calibration method can be used to increase the accuracy of TSP measurements when compared to a standard calibration method. This research showed that in the case of a sudden drop in heat flux, shown here when the main hydrogen fuel is turned off, a dual-calibration method can be used to obtain better agreement of the temperature and heat flux measurements of the flush-mounted coaxial thermocouple and the TSP.

The calibration shown in Figure 49 proves that after a sudden drop in heat flux a TSP calibration is still linear. This linear calibration can be used to create a temperature history that agrees well with the temperature history recorded by the coaxial thermocouple mounted in the test article.

A single calibration cannot be used in situations where a sharp heat flux change is seen due to the dynamic response of TSP. However, a combination of two calibrations can be used to accurately measure the temperature history. A calibration using data while the test article is heated is needed to record the temperature while heating, and a calibration using data while the test article cools is needed to record the temperature history while the test article cools.

Dual-Calibration Effectiveness

Figure 54 shows that for this case, a reduction of roughly 89-95% in TSP uncertainty can be seen. This improvement is extraordinarily large due to the test designed here. The test designed here was chosen as a "worst case" scenario. While a sudden slope change in input heat flux is seen on test articles in Tunnel 9, they do not resemble step changes in slope as this example does.

In practice, the improvement would not be nearly this high, and improvement would only be seen in cases where as slope reversal in heat transfer exists. More work is needed to assess the practical improvement in the accuracy of heat transfer measurements using dual-calibrated TSP.

Thermocouple Bias and TSP

In the standard calibration method, and the dual-calibration method, the TSP is calibrated to the temperature under the surface of the paint at the location of the coaxial thermocouple. This means that any bias seen in the thermocouple measurement due to the application of TSP onto the sample will also be seen in the TSP data.

Again, for Tunnel 9 the bias may be quite low, and more research is needed to understand this phenomenon further for smaller paint thicknesses. Because the method to compute TSP uncertainty is based on the difference between the thermocouple value and the TSP value, this bias will not appear in the TSP uncertainty value.

Dual Calibration Tunnel 9 Application

While this experiment used current Tunnel 9 hardware and data reduction methods, it was a simplified version of a typical Tunnel 9 test. The experiment used averaging to create a single point TSP measurement for each run. This creates a single temperature-time history to compare to a coaxial thermocouple at the same location.

In a typical Tunnel 9 test article, there can be dozens of coaxial thermocouples installed on a test article, and TSP data is taken over most of the test article's surface and mapped to a 3-D grid of the test article. This essentially allows TSP data to be analyzed at each camera pixel, on each camera system that is employed for a test. In

total, millions of points can be analyzed for each test. This does not allow for the one to one comparison of TSP data to coaxial thermocouple data as used here.

Further, to successfully employ a dual-calibration method a time at which the calibration switch occurs must be input. For this experiment that was manually input and remained constant for all tests at a certain heating condition. For a Tunnel 9 test this would not be possible because every point on the test article would not see a slope change in heat flux at the same time as it does in this case.

Tunnel 9 test articles are subject to a change in the slope of the heat flux while dynamically pitching during a run. This means that the time at which the slope change occurs will be different for each point on the test article based on the angle of attack of the test article, as well as the local surface angle relative to the test article axis. A method will have to be defined to programmatically find the time at which the calibrations will switch.

Future Work

The primary focus of future work, as discussed previously, will be to further investigate the response of TSP and a coaxial thermocouple to sudden changes in heating loads using a thinner paint layer than was used in this test. More data points are needed to examine the effect of a paint layer on a coaxial thermocouple.

Current predictions are that the typical paint thickness utilized on Tunnel 9 test articles is not thick enough to cause a substantial bias in the thermocouple heat transfer measurements. However, more data points are needed to investigate this

theory propose any possible corrections. The behavior of the bias caused by the addition of a paint layer is not known due to the lack of data points.

While investigating the effect of thinner paint thicknesses, the effect of convective heat transfer can also be investigated. This would cause a similar bias in the heat transfer due to a change in the convective heat transfer coefficient. The thermal properties of Tunnel 9 TSP are largely unknown, and while difficult to investigate, the convective heat transfer effect could be extremely important. This testing could also be supplemented with more simulation of this phenomenon. A one-dimensional and two-dimensional simulation of the coaxial thermocouple, steel substrate and temperature sensitive paint layer could give more insight into the physical reason behind the bias created in measure heat flux by a painted coaxial thermocouple and may also shed more light on the calibration hysteresis seen during this experiment.

Finally, future research will include the application of the dual-calibration method to Tunnel 9 data sets. There are several TSP data sets in Tunnel 9 that have recorded a change in heat flux slope as was investigated in this research. The raw data is still available for many of these cases. As the dual-calibration method does not alter the experimental setup for TSP in any way, the method can be applied to existing data sets.

The application has several challenges, discussed earlier, including the application to a 3D test article, and the programmatic switching of calibrations after a change in heat flux. All of these will have to be investigated, and a new data

reduction method will need to be validated to successfully apply a dual-calibration method to Tunnel 9 in the future.

Appendices

Appendix A: Full Test Matrix

Table 19: Full Test Matrix

	Run Number	Main Fuel Pressure (psig)	Main Fuel Timing		Test Description	Good Run
			Start	Duration		
100 Series - No Paint - Baseline Tests	5-Jun-18					
	101	200	2	1	HH	Yes
	102	200	2	1	HH	Yes
	103	200	2	1	HH	Good
	104	200	2	1	HH	Bad
	105	200	2	1	HH	Good
	106	200	2	1	HH	Good
	107	200	2	1	HH	Good
	108	200	2	1	HH	Good
	109	200	2	1	HH	Good
	110	200	2	1	HH	Good
	111	200	2	1	HH	Bad
	112	200	2	1	HH	Good
	113	200	2	1	HH	Bad
	114	200	2	1	HH	Bad
	115	200	2	1	HH	Good
	116	146	2	2	MH	Good
	117	146	2	2	MH	Good
	118	146	2	2	MH	Good
	119	146	2	2	MH	Bad
	120	146	2	2	MH	Good
	121	146	2	2	MH	Good
	122	146	2	2	MH	Good
	123	146	2	2	MH	Bad
	124	146	2	2	MH	Bad
	125	146	2	2	MH	Bad
	126	146	2	2	MH	Good
	6-Jun-18					
	127	92	2	4	LH	Bad

	128	92	2	4	LH	Bad
	129	92	2	4	LH	Bad
	130	92	2	4	LH	Bad
	131	92	2	4	LH	Good
	132	92	2	4	LH	Good
	133	92	2	4	LH	Good
	134	92	2	4	LH	Good
	135	92	2	4	LH	Good
	136	92	2	4	LH	Bad
200 Series - 1.65 mil	2-Jul-18					
	201	200	2	1	HH	Bad
	202	200	2	1	HH	Good
	203	200	2	1	HH	Bad
	204	200	2	1	HH	Good
	205	200	2	1	HH	Good
	206	200	2	1	HH	Bad
	207	200	2	1	HH	Good
	208	200	2	1	HH	Bad
	209	200	2	1	HH	Good
	210	200	2	1	HH	Good
	3-Jul-18					
	211	146	2	2	MH	Bad
	212	146	2	2	MH	Bad
	213	146	2	2	MH	Bad
	214	146	2	2	MH	Good
	215	146	2	2	MH	Good
	216	146	2	2	MH	Good
	217	146	2	2	MH	Good
	218	146	2	2	MH	Good
	219	146	2	2	MH	Bad
	220	146	2	2	MH	Good
	221	146	2	2	MH	Good
	222	146	2	2	MH	Good
	223	146	2	2	MH	Bad
	224	92	2	4	LH	Good
	225	92	2	4	LH	Bad
	226	92	2	4	LH	Good
	227	92	2	4	LH	Good
	228	92	2	4	LH	Good
	229	92	2	4	LH	Good

	230	92	2	4	LH	Good
	231	92	2	4	LH	Good
	232	92	2	4	LH	Good
	233	92	2	4	LH	Good
150 Series - Baseline Check Case	5-Jul-18					
	151	200	2	1	HH	Bad
	152	200	2	1	HH	Good
	153	200	2	1	HH	Bad
	154	200	2	1	HH	Bad
	155	200	2	1	HH	Bad
	156	200	2	1	HH	Good
	157	200	2	1	HH	Good
	158	146	2	2	MH	Good
	159	146	2	2	MH	Good
	160	146	2	2	MH	Bad
	161	146	2	2	MH	Good
	162	92	2	4	LH	Good
	163	92	2	4	LH	Good
	164	92	2	4	LH	Good
300 Series - 2.75 mil	20-Jul-18					
	301	200	2	1	HH	Good
	302	200	2	1	HH	Good
	303	200	2	1	HH	Good
	304	200	2	1	HH	Good
	305	200	2	1	HH	Good
	306	200	2	1	HH	Good
	307	200	2	1	HH	Good
	308	200	2	1	HH	Good
	309	200	2	1	HH	Good
	310	200	2	1	HH	Good
	311	146	2	2	MH	Good
	312	146	2	2	MH	Good
	313	146	2	2	MH	Good
	314	146	2	2	MH	Good
	315	146	2	2	MH	Good
	316	146	2	2	MH	Good
	317	146	2	2	MH	Bad
	318	146	2	2	MH	Good
	319	146	2	2	MH	Bad
	320	146	2	2	MH	Good

	321	92	2	4	LH	Good
	322	92	2	4	LH	Good
	323	92	2	4	LH	Good
	324	92	2	4	LH	Good
	325	92	2	4	LH	Good
	326	92	2	4	LH	Good
	327	92	2	4	LH	Good
	328	92	2	4	LH	Good
	329	92	2	4	LH	Good
	330	92	2	4	LH	Good
	331	92	2	4	LH	Good
	332	92	2	4	LH	Bad
400 Series - 1.98 mil	30-Jul-18					
	401	200	2	1	HH	Bad
	402	200	2	1	HH	Good
	403	200	2	1	HH	Bad
	404	200	2	1	HH	Bad
	405	200	2	1	HH	Good
	406	200	2	1	HH	Good
	407	200	2	1	HH	Bad
	408	200	2	1	HH	Good
	409	200	2	1	HH	Bad
	410	200	2	1	HH	Bad
	411	200	2	1	HH	Bad
	412	200	2	1	HH	Bad
	413	146	2	2	MH	Bad
	414	146	2	2	MH	Good
	415	146	2	2	MH	Bad
	416	146	2	2	MH	Bad
	417	146	2	2	MH	Bad
	418	146	2	2	MH	Bad
	419	146	2	2	MH	Good
	420	146	2	2	MH	Good
	421	146	2	2	MH	Bad
	422	146	2	2	MH	Good
	423	146	2	2	MH	Good
	424	92	2	4	LH	Good
	425	92	2	4	LH	Good
	426	92	2	4	LH	Good

	427	92	2	4	LH	Good
	428	92	2	4	LH	Good
	429	92	2	4	LH	Good
	430	92	2	4	LH	Good
	431	92	2	4	LH	Bad
	432	92	2	4	LH	Good
	433	92	2	4	LH	Good

Bibliography

[1] Lafferty, J. F., Coblish, J. J., Marineau, E., Norris, J. D., Kurits, I., Lewis, D. R., Smith, M., and Marana, M., "The Hypervelocity Wind Tunnel No. 9; Continued Excellence Through Improvement and Modernization," American Institute of Aeronautics and Astronautics, 2015.

[2] Anderson, J. D., *Hypersonic and high-temperature gas dynamics*, Reston, Va: American Institute of Aeronautics and Astronautics, 2006.

[3] Hamner, M., "Use of Temperature Sensitive Paint in the AEDC Hypervelocity Wind Tunnel 9," American Institute of Aeronautics and Astronautics, 2003.

[4] Horvath, T., "Experimental Aerothermodynamics in Support of the Columbia Accident Investigation," Reno, Nevada: 2004.

[5] Kurits, I., "Quantitative Global Heat-Transfer Measurements using Temperature-Sensitive Paint on a Blunt Body in Hypersonic Flows," University of Maryland, 2008.

[6] Kurits, I., Lewis, M., and Hamner, M., "Global Heat-Transfer Measurements on the NASA Crew Exploration Vehicle at AEDC Tunnel 9," American Institute of Aeronautics and Astronautics, 2008.

[7] Kurits, I., and Norris, J., "Hypersonic Global Heat-Transfer Measurements During Continuous Pitch Sweeps at AEDC Tunnel 9," American Institute of Aeronautics and Astronautics, 2010.

[8] Coblish, J., Coulter, S., and Norris, J., "Aerothermal Measurement Improvements using Coaxial Thermocouples at AEDC Hypervelocity Wind Tunnel No. 9," American Institute of Aeronautics and Astronautics, 2007.

[9] Merski, N. R., "Global Aeroheating Wind-Tunnel Measurements Using Improved Two-Color Phosphor Thermography Method," *Journal of Spacecraft and Rockets*, vol. 36, Mar. 1999, pp. 160–170.

[10] Berridge, D. C., McKiernan, G. R., Wadhams, T. P., Holden, M. S., Wheaton, B. M., Wolf, T. D., and Schneider, S. P., "Hypersonic Ground Tests In Support of the Boundary Layer Transition (BOLT) Flight Experiment," Atlanta, Georgia: AIAA, 2018.

[11] Liu, T., and Sullivan, J. P., *Pressure and temperature sensitive paints*, Berlin ; New York: Springer, 2005.

[12] Kurits, I., Norris, J., and Bhandari, P., "Temperature-Sensitive Paint Calibration Methodology Developed at AEDC Tunnel 9," American Institute of Aeronautics and Astronautics, 2011.

[13] Kurits, I., and Lewis, M. J., "Global Temperature-Sensitive Paint System for Heat Transfer Measurements in Long-Duration Hypersonic Flows," *Journal of Thermophysics and Heat Transfer*, vol. 23, Apr. 2009, pp. 256–266.

[14] Aguilera Munoz, C., and Yu, K. H., "Effect of Fin-Guided Fuel Injection on Dual Mode Scramjet Operation," American Institute of Aeronautics and Astronautics, 2014.

[15] Kurits, I., Lewis, M. J., Hamner, M. P., and Norris, J. D., "Development of a Global Heat Transfer Measurement System at AEDC Hypervelocity Wind Tunnel 9," IEEE, 2007, pp. 1–16.

[16] Marana, M., Butcher, C., and Juliano, J., *Test Data Processing at AEDC Hypervelocity Wind Tunnel 9*, AEDC Hypervelocity Wind Tunnel 9: 2017.

[17] "Tables of Thermoelectric Voltages and Coefficients for Download," *National Institue of Standards and Technology* Available: https://srdata.nist.gov/its90/download/download.html.

[18] Kammeyer, M., *Reassessment of Precision Errors in Coax Thermocouple Heat Transfer Data*, AEDC Hypervelocity Wind Tunnel 9, 1994.

[19] Coleman, H. W., and Steele, W. G., *Experimentation and uncertainty analysis for engineers*, New York: Wiley, 1989.